Installation of a dynamic power cable for a floating offshore wind turbine

A comparative study

M.A. Beerens

Master of Science Thesis

TU Delft Delft University of Technology

VBMS

Installation of a dynamic power cable for a floating offshore wind turbine: a comparative study

by

M.A. Beerens

in partial fulfillment of the requirements for the degree of

Master of Science
in Offshore & Dredging Engineering

at the Delft University of Technology,
to be defended publicly on Monday February 1, 2016 at 15:00 AM.

Student number: 4091701		
Supervisor:	Prof. dr. A.V. Metrikine	
Thesis committee:	Ir. P. van der Male	TU Delft
	Dr. ir. K.N. van Dalen	TU Delft
	Ir. L. van Baalen	VBMS

This thesis is confidential and cannot be made public until February 1, 2021.

TU Delft Delft University of Technology

VBMS

The work in this thesis was supported by VBMS. Their cooperation is hereby gratefully acknowledged.

Background picture: VBMS´ CLV Ndurance at a project location. Company picture of VBMS.

Note: This document has been designed for full colour double-sided printing.

'Tell me and I forget,
teach me and I may remember,
involve me and I learn.'

— Benjamin Franklin

Abstract

The latest Conference of Parties at Paris resulted in an important agreement that 27 percent of the total European energy consumption has to come from renewable energy in 2030. Offshore wind energy is an important resource for renewable energy. The shortage of shallow water areas pushed offshore wind farms into deeper waters. Floating Offshore Wind Turbines (FOWTs) become more economically viable in deeper waters than bottom founded wind turbines.

The goal of this research is to explore multiple installation methods for the pull-in of a dynamic power cable into a FOWT and to compare them with respect to workability determined by different limitations.

The FOWTs transfer its energy using dynamic power cables. The dynamic cable configuration used in this research is a pliant wave supported by distributed buoyancy modules (DBMs). The properties of the dynamic cable and the configuration have been chosen in cooperation with cable supplier JDR. For the FOWT a design of a vertical axis wind turbine combined with a tri-pod substructure is used. VBMS´ Ndurance is chosen as reference cable lay vessel (CLV) for the installation.

The first method is pull-in of the dynamic cable in a pre-installed FOWT. A CLV performs the pull-in directly after laying of the dynamic cable towards the FOWT, with the tether supporting the dynamic cable configuration being installed afterwards. The second method is a post-lay pull-in of the dynamic cable into the FOWT with aid of the CLV. The third method is a post-lay pull-in of the dynamic cable from the FOWT only. In the last two methods, the dynamic cable is picked after wet storage on the seabed. The difference between these methods lies in the shape in which the dynamic cable is wet-stored. The DBMs and tether are already installed during the wet storage period of method two and three. In addition, free lay of the dynamic cable and overboarding of it prior to the pull-in operation is modelled as a reference case.

In the first two pull-in method the dynamic cable transfers from the CLV towards the FOWT using a winch control system. The system controls the pay-out and pull-in rates of the winches on the CLV and FOWT, respectively. The system ensures a minimum seabed clearance and avoids that the cable configuration becomes too tight.

Ansys AQWA and OrcaFlex are used to model every aspect of the different methods and operations. In addition, an external Python script is used to control the rates of the winches. All dynamic cable analysis are performed using a regular wave approach with three different wave heights and periods for every direction, distributed uniformly in 30 degree bins.

The results show that all pull-in methods are suitable to install the dynamic cable into the FOWT. Based on these results the third pull-in has the highest workability. This is explained by the fact that the pull-in is performed by using the FOWT only. Therefore only the FOWT influences the cable motions, whereas in the other methods also the CLV adds to the dynamic cable behaviour. The FOWT has a more stable motion behaviour in environmental conditions compared to the

CLV. For this reason the interaction of the cable with the seabed is reduced and a higher workability is obtained.

Cable compression is a limitation which is a common issue in cable installation analyses. In this research it is the most common failure mechanism for all methods in environmental conditions. A correlation between compression and large vertical cable accelerations is found in the free lay model and the pull-in method 1. These vertical accelerations are mainly caused by the buoyant cable section which lies in the splash zone. Compression in the two post-lay methods is caused by interaction with the seabed during recovery of the cable.

The buoyant part of the cable is modelled with the DBMs uniformly distributed. At the transition point, where the cable diameter changes due to the DBMs, problems with exceeding of the maximum curvature are found, since the cable has no contact with the chute. Avoiding of exceeding of this maximum curvature is possible by introducing a structure which supports the DBMs at the stern of the vessel.

Preface

This M.Sc. thesis is submitted in partial fulfillment of the requirements for the degree of Master of Science in Offshore & Dredging Engineering at Delft University of Technology. The work is carried out in close cooperation with the Support department of VBMS.

Prior to the thesis I had limited knowledge of subsea power cable installation, the simulation programs OrcaFlex and Ansys AQWA or the programming language Python. A large amount of time has therefore been spent to acquire this knowledge. The modelling, pre- and post-processing of the results have been a demanding and time consuming process, but the results have been worth it.

This thesis would not have been possible without the support of all the people around me. I would like to thank everyone by name, but a few people deserve a particular mention.

Firstly, I would like to thank my daily supervisor Ir. Lennart van Baalen of VBMS, for giving me several opportunities to expand my knowledge and providing support during the whole process. I also would like to thank Prof. dr. Andrei Metrikine for chairing the graduation committee. Special thanks to Ir. Pim van der Male for his day-to-day supervision, support and useful comments during the process. Thanks to Dr.ir. K.N. van Daalen for being part of the thesis committee.

Furthermore, I would like to thank VBMS for giving me the opportunity to perform my M.Sc. thesis within their company and to cooperate with highly skilled engineers. Many thanks to Ir. Paul van der Ham, who taught me the "tips and tricks" of both OrcaFlex and Python. In addition, checking the models and the useful comments on the rapport are greatly appreciated. Besides that, I would like to thank Ir. Ruud Beindorff and Ir. Parag Shanbhag for learning me the basics of Ansys AQWA. Without these colleagues it would not be possible achieve this amount of progression in such a short period of time. Thanks to all the other colleagues of VBMS who have contributed to this M.Sc. thesis.

In addition to this, I would like to thank Wouter van Straalen for our great time at Delft University of Technology. From the first day of the Bachelor of Science in Civil Engineering, until the last day of the Master of Science in Offshore Engineering, we have worked and shared everything together. Without him it would not be possible to successfully accomplish all the courses.

Last but not least, I would also thank my girlfriend Christel, my parents, family and friends for their unconditional support, faith and trust in me over the years.

Maarten Beerens
Papendrecht, January 2016

Contents

List of Figures

List of Tables

Nomenclature

Notation	Description	Units
A	Reference area	m^2
A_{ij}	Hydrodynamic mass or inertia coefficient	$-$
a	Particle accelerations	m^2/s
$COG_{x,y,z}$	Centre of gravity in x, y, z direction	m
C_{ij}	Retardation function	$-$
C_a	Added mass coefficient	$-$
C_d	Drag coefficient	$-$
C_{max}	Maximum curvature	m^{-1}
D_f	Buoy diameter	mm
D_p	Cable diameter	mm
$E(f)$	Variance density spectrum	m^2/Hz
EA	Axial stiffness	MN
EI	Bending stiffness	kNm^2
F	Wave force	kN
$\vec{F}$	Resulting external force	kN
f	3-Parameter Weibull probability density function	$-$
g	Gravitational acceleration	m/s^2
H	Wave height	m
H_{max}	Maximum wave height	m
H_s	Significant wave height	m
$\vec{H}$	Instantaneous angular momentum	Nm
h	Waterdepth	m
h_{max}	Maximum height above seabed	m
h_{min}	Minimum height above seabed	m
I_{ij}	Solid mass moment of inertia of a floating structure	m^4
KC	Keulegan-Carpenter	$-$
K_{ij}	Hydrodynamic spring coefficient	$-$
$K_{xx,yy,zz}$	Radius of Gyration in x, y, z direction	m
k	Wave number	rad/m
L	Length	m
L_f	Buoy length	mm
L_{min}	Minimum line length	m
M	External moment	Nm
MBR	Minimum Bend Radius	m
M_{ij}	Solid mass or inertia coefficient	$-$
$\vec{M}$	Resulting external moment	Nm
m	Solid mass of mass moment of inertia	kg
m_n	n^{th}-order moment of the variance density spectrum	m^2
N	Total number of waves	$-$

n	Sum	$-$
$p(H)$	Probability density function	$-$
r	Peak enhancement exponent	$-$
Re	Reynolds number	$-$
$S_F(\mu)$	Spectral density of the low frequency part of the wave drift force	m^2/Hz
S_f	Centre-to-centre spacing buoys	m
$S_r(\omega)$	Response spectrum	m^2/Hz
$S_\zeta(\omega)$	Spectral density	m^2/Hz
T	Tension	kN
T	Wave period	s
T_{max}	Safe Working Load	kN
T_{min}	Maximum allowable compression	kN
T_p	Spectrum peak period	s
T_s	Significant wave period	s
T_z	Significant wave period	s
T_η	Average time interval between successive up or down crossings through level	s
$\vec{U}$	Instantaneous velocity	m/s
u_{max}	Amplitude of the flow velocity oscillation	m/s
u_t	Flow velocity	m/s
V	Cylinder volume per unit cylinder length	m^3/m
v	Winch rate	m/s
v	Particle velocity	m/s
v_t	Body velocity	m/s
W_{air}	Weight in air	kg/m
W_{sea}	Weight in seawater	kg/m
X	Surge	m
x	Horizontal position relative to the neutral position	m
$x(t)$	Displacement at time t	m
$\dot{x}(t)$	Velocity at time t	m/s
$\ddot{x}(t)$	Acceleration at time t	m/s^2
Y	Sway	m
Z	Heave	m
α	Angle of the winch wire	$^\circ$
η	Wave elevation	m
θ	Pitch	$^\circ$
γ	Peak enhancement factor	$-$
ε	Phase angle	rad
ζ	Surface elevation	m
ζ_a	Wave amplitude	m
λ	Wave length	m
ρ	Density	kg/m^3
σ_ζ	Variance of the water surface elevation	m^2
ϕ	Roll	$^\circ$
ψ	Yaw	$^\circ$
ω	Angular wave frequency	rad/s
ω_0	Natural frequency	rad/s
ω_p	Circular frequency at spectral peak	rad/s
∇	Volume of displacement of a floating structure	m^3

Abbreviations

Abbreviation	Meaning
CLV	Cable Lay Vessel
COB	Centre of Buoyancy
COG	Centre of Gravity
CPS	Cable Protection System
DBMs	Distributed Buoyancy Modules
DP	Dynamic Positioning
DNV	Det Norske Veritas
FOWT	Floating Offshore Wind Turbine
GPS	Global Position System
HAWT	Horizontal Axis Wind Turbines
HDD	Horizontal Directional Drilled
IMCA	International Marine Contractors Association
JONSWAP	Joint North Sea Wave Observation Project
LCE	Linear Cable Engine
MBR	Minimum Bending Radius
POB	Persons On Board
RAO	Response Amplitude Operator
ROV	Remotely Operated Vehicle
SWL	Safe Working Load
TDP	Touch Down Point
VAWT	Vertical Axis Wind Turbines
VBMS	VolkerWessels Boskalis Marine Solutions
WTs	Wind Turbines

CHAPTER 1

Introduction

1.1 Background

The latest Conference of Parties resulted in an important agreement that 27 percent of the total energy consumption in the European Union has to come from renewable energy in 2030 [19]. Offshore wind energy is an important resource for that. People have been using wind energy for over 1000 years, resulting in a huge amount of knowledge about this renewable energy source. For this reason several countries choose to use wind energy to meet the energy agreement. Figure 1.1 presents the prospective growth in time of global cumulative wind power capacity, investigated by Global Wind Energy Counsil [1].

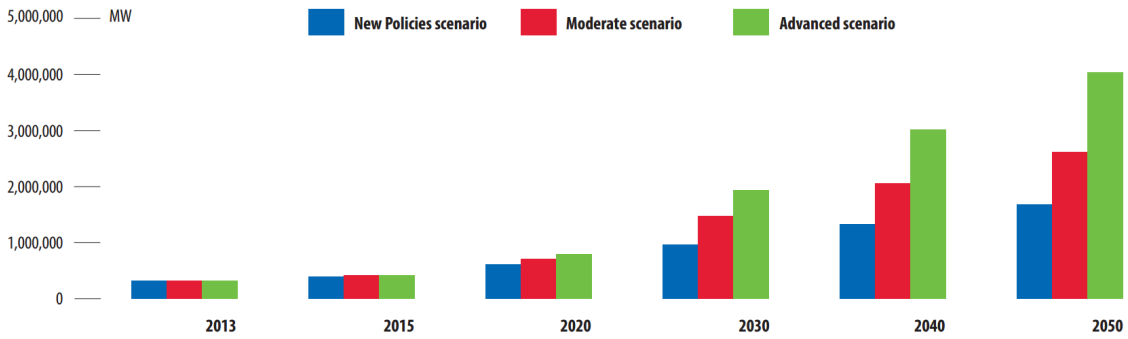

Figure 1.1: Global cumulative wind power capacity [1]

Placement of wind turbines (WTs) for wind energy started onshore. Limitations like absence of unused land area, landscape pollution, noise nuisance and higher wind speeds offshore have moved WTs offshore. Two decades have been passed since the first bottom-mounted offshore WTs were installed in Europe and many large-scale commercial projects are in operation now. Current fixed-bottom technology has seen deployment to water depths of roughly 30 m [20]. The shortage of shallow water areas, however, pushed offshore wind farms into deeper waters.

Collu, Kolios, Chahardehi and Brennan [2] showed that FOWTs become more economically viable in deeper waters than bottom founded wind turbines, presented in Figure 1.2. FOWTs have not yet been commercially implemented on a large scale, but recent developments and prototyping have shown that FOWTs have a high potential.

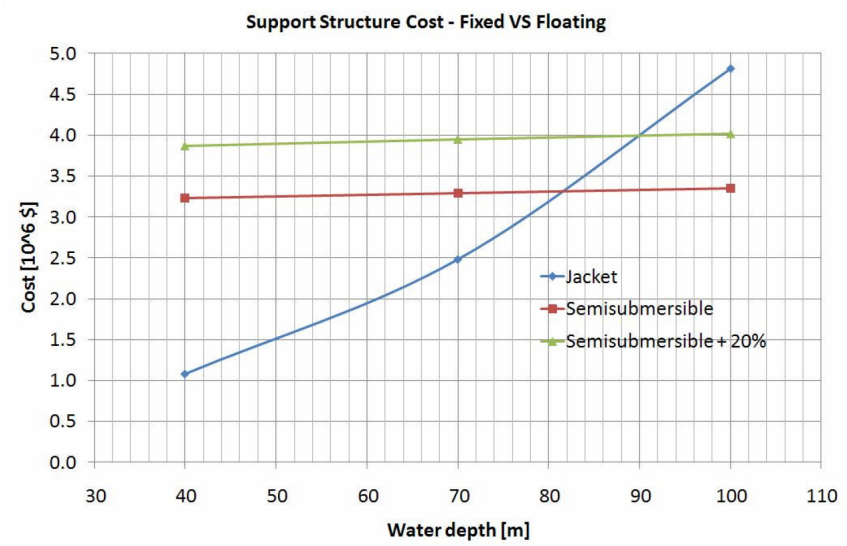

Figure 1.2: Fixed and floating support structure cost versus water depth [2]

The FOWTs are connected by dynamic power cables, which transport the produced electricity towards shore. Installation of these dynamic cables is a specialised operation since theses cables are vulnerable products. A CLV is used to perform the installation of these dynamic cables. CLVs have a significant day-rate, so decreasing installation time of a dynamic cable is important for both cable contractors and wind farm developers. Integrity of the cable is the main priority for cable contractors.

Research on different installation methods for connecting the FOWT with a dynamic cable is necessary to determine limitations for the different installation methods, in order to ensure integrity of the cable. The results of this research could be used during the design phase of new FOWTs.

Cost reduction for production, installation, maintenance and decommissioning of wind farms is of utmost importance for the wind energy industry, since it could make wind energy competitive with energy form other sources.

Research on installation of dynamic cables for FOWTs is especially interesting for cable contractors. For this reason this research is performed in cooperation with VBMS (VolkerWessels Boskalis Marine Solutions). VBMS has established a trusted and experienced position as an international submarine power cable installation contractor. Typical clients of VBMS are electrical power companies, grid operators and companies in the oil and gas industry. The company provides a full package for installation of cables. Activities executed by VBMS are:

- Installation and burial of export and inter array cables
- Inspection, repair and maintenance of cables
- Construction of land- & outfalls
- Construction of offshore cable crossings
- Oil and gas umbilicals

1.2 Problem definition

Deployment of FOWTs on a large scale is a high potential new market. VBMS wants to be part of this market and distinguish oneself with the specialised dynamic cable installations into FOWTs. For this reason exploring different cable installation methods and the suitability of their CLVs performing these installations, is required to turn this vision into reality.

1.3 Objective

The goal of this research is to explore multiple installation methods for the pull-in of a dynamic power cable into a FOWT and to compare them with respect to workability determined by different limitations.

1.4 Outline of the report

The first part of this research consists of the theoretical background for the research, followed by the methodology. This part describes the installation methods, a description of the system and finally how the system is modelled.

Results obtained from the time-domain simulations of the models are given and discussed subsequently and followed by recommendations for further research.

CHAPTER 2

Theoretical background

This Chapter describes the theoretical background of the linear wave theory, the second order wave drift forces and the wave statistics. The response of a floating structure in waves is described afterwards followed by the drag and added mass coefficients. Finally, the used software packages used in this research are described.

2.1 Linear wave theory

Ocean waves can be described using the linear wave theory. The long-crested propagating harmonic wave theory is the most interesting result of the linear wave theory. Many wave characteristics can be derived from this theory. Wind driven surface waves combined with a current are generally the main source of dynamic environmental loads on a product during installation. The sea state can be presented by either regular or irregular waves. A design wave (deterministic) approach represents a methods in which design loads are determined based on regular wave analysis of the wave expected to give the largest response. A design spectra (stochastic) approach is a method in which design loads are determined based on irregular wave analysis of a maximum sea state. For the main simulations regular waves are used and for some research irregular waves are used. The main principles of both wave approaches are described in this Section.

2.1.1 Regular waves

In this research, the airy wave theory [4] is applied as a basic description of regular waves. This is a fundamental theory which defines the waves as a sinusoidal function. The water surface slope is assumed very small applying this theory. The surface slope is defined by the ratio of the wave height H to the wave length λ. This assumption is valid for floating structures in deep waters. The water is considered to be deep if the water depth h is more than half the wave length λ, so: $h/\lambda > 1/2$. These (relatively) short waves do not 'feel' the sea floor. [4]

Airy wave theory describes the motion of water particles dependent of vertical and horizontal position and time. These wave particles are described to move in a circular orbital motion in which the wave period and length are related through the dispersion relation, presented in Equation 2.1.

$$\omega^2 = k\ g \cdot \tanh kh \tag{2.1}$$

Here ω is the angular wave frequency ($\frac{2\pi}{T}$), g is the gravitational acceleration, k is the wave number, h the water depth and T is the wave period. The wave number can be derived for a wave with a prescribed period-water depth relation using Equation 2.1. In deep water ($\lim kh \to \infty \tanh kh =$

1), so Equation 2.1 can be simplified as:

$$\omega^2 = k\ g \quad \text{(deep water)} \tag{2.2}$$

The surface elevation (ζ) is described by Equation 2.3, in which ζ_a is the wave amplitude ($\zeta_a = \frac{H}{2}$) and x is the horizontal position relative to the neutral position.

$$\zeta = \zeta_a \cos(\omega t - kx) \tag{2.3}$$

Figure 2.1 represents an example of a regular wave prescribed by the airy wave theory, with a amplitude ζ_a of 1.5 m, a period T of 6 s and at position $x = 0$.

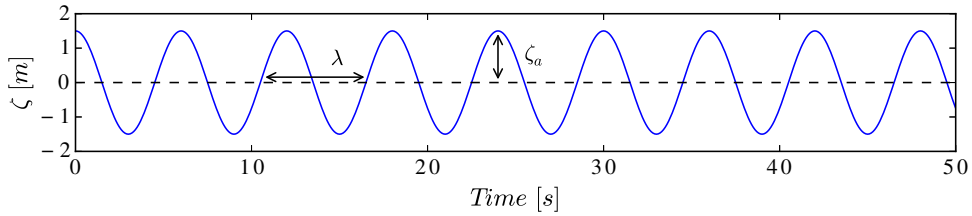

Figure 2.1: Regular wave

2.1.2 Irregular waves

Realistic ocean waves can be presented using a linear superposition of many wave components with random amplitudes, frequencies and phases [3]. The principle of superposition is presented in Figure 2.2.

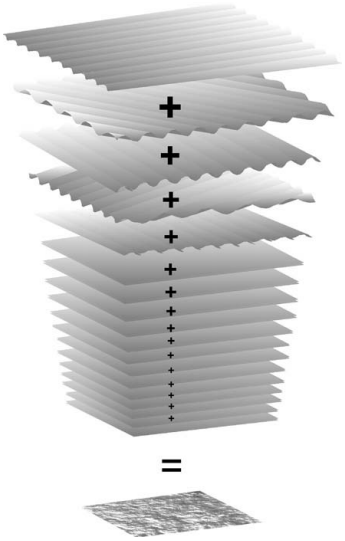

Figure 2.2: Superposition principle [3]

The relation between the wave frequency and amplitude in these superpositions of regular waves are characterised by a wave spectrum. This wave spectrum defines the distribution of wave energy over frequency which is representative for a certain sea-state.

A wave spectrum often used in the North Sea area is the JONSWAP spectrum. After analysing

data collected during the Joint North Sea Wave Observation Project JONSWAP, Hasselmann et al [21] found that the wave spectrum is never fully developed. It continues to develop through non-linear, wave-wave interactions even for very long times and distances. Hence an extra factor was added to the existed Pierson-Moskowitz spectrum in order to improve the fit to their measurements.

The JONSWAP spectrum is thus a Pierson-Moskowitz spectrum multiplied by an extra peak enhancement factor γ^r, presented in Equation 2.4 for fetch limited situations. Equations 2.5 through 2.8 present the factors determined during the JONSWAP experiment.

$$S_\zeta(\omega) = \underbrace{\frac{320 \cdot H_s^2}{T_p^4 \cdot \omega^5} \exp\left[-\frac{-1950}{T_p^4 \cdot \omega^4}\right]}_{\text{Pierson-Moskowitz}} \gamma^r \tag{2.4}$$

Where:

$$r = \exp\left[-\left(\frac{\frac{\omega}{\omega_p} - 1}{\sigma_\zeta \sqrt{2}}\right)^2\right] \tag{2.5}$$

$$\omega_p = \frac{2\pi}{T_p} \tag{2.6}$$

$$\gamma = 3.3 \text{ (peakedness factor)} \tag{2.7}$$

$$\sigma_\zeta = \begin{cases} 0.07 & \omega \leq \omega_p \\ 0.09 & \omega > \omega_p \end{cases} \tag{2.8}$$

Where ω_p is the circular frequency at spectral peak, H_s the significant wave height and T_p spectrum peak period. Sometimes, a third free parameter is introduced in the JONSWAP wave spectrum by varying the peakedness factor γ, which makes the JONSWAP spectrum applicable in other locations in the world.

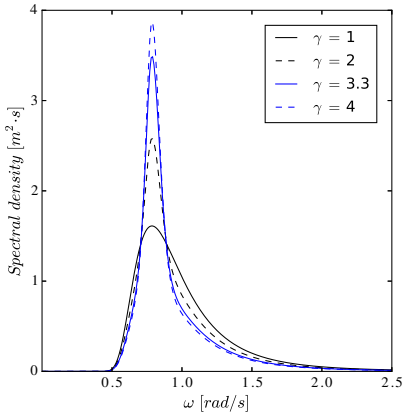

Figure 2.3: JONSWAP spectrum

Figure 2.3 presents a JONSWAP spectrum with a H_s of 1.5 meters, a period T_p of 8 seconds and varying peakedness factor γ. The JONSWAP spectrum can be used in the development of a wave elevation time series. This time series consists of the sum, n, of many regular waves of different frequency (ω_n) and amplitude (ζ_{an}), which is performed by the inverse Fourier transformation of the wave spectrum. This transformation is performed in Equation 2.9 , by application of the harmonic series method [3]. In Equation 2.9 ε_n forms a random phase angle between 0 and

2π. The wave numbers, k_n, can be computed from the chosen frequency ω_n using the dispersion relationship presented in Equation 2.1.

$$\zeta(t) = \sum_{n=1}^{N} \zeta_{an} \cos(\omega_n t - k_n x - +\varepsilon_n) \tag{2.9}$$

The amplitudes, ζ_{an}, can be determined knowing that the area under the associated segment of the spectrum $S_\zeta(\omega) \cdot d\omega$ is equal to the variance of the wave component, presented in Equation 2.9.

$$\zeta_{an} = \sqrt{2 \cdot S_\zeta(\omega) \cdot d\omega} \tag{2.10}$$

By applying Equations 2.9 and 2.10 to the JONSWAP spectrum, defined in Equation 2.4, a time series of surface elevation can be created.

2.2 Wave statistics

The theory corresponding to wave statistics is described in this Section.

2.2.1 Significant wave height

Holthuijsen [3] described that for waves with narrow spectrum in deep water, the height of the wave is practically equal to twice the height of the crest:

$$H \approx 2\zeta_a \tag{2.11}$$

The significant wave height, H_s, is defined as the mean value of the highest one-third of wave heights. This fraction of the waves can be identified in the Rayleigh distribution, so H_s can be determined from that distribution. The H_s that are involved in this definition are located in the highest third of the Rayleigh distribution, presented in Figure 2.4, i.e., where $H > H^*$, with H^* defined by:

$$\int_{H^*}^{\infty} p(H)dH = \frac{1}{3} \tag{2.12}$$

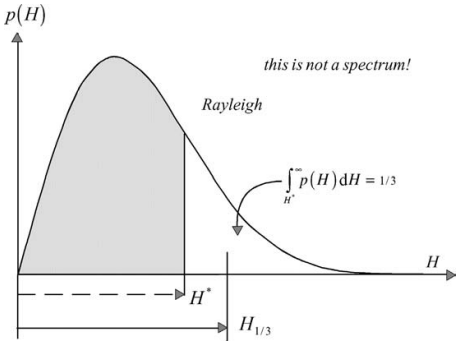

Figure 2.4: The significant wave height in the Rayleigh probability density function [3]

An analytical expression for the Rayleigh distribution defines the significant wave height H_s as:

$$H_s \approx 4\sqrt{m_0} \tag{2.13}$$

where m_0 is the zeroth-order moment of the variance density spectrum $E(f)$, expressed as:

$$m_n = \int_0^\infty \omega^2 S(\omega) d\omega \qquad \text{with: } n = 0,1,2,... \tag{2.14}$$

2.2.2 Maximum wave height

A maximum wave height, H_{max} is used in a regular wave design approach. The maximum wave height, H_{max}, is determined with a statistical approach related to H_s.

$$H_{max} = H_s \sqrt{\frac{1}{2} \ln N} \tag{2.15}$$

Using a 1 in 1000 wave occurrence of H_{max} in Equation 2.15 results in a multiplication factor for H_s:

$$H_{max} \approx 1.86 \cdot H_s \tag{2.16}$$

2.2.3 Wave period

The period of a wave is the time between a successive crossing of the wave through the mean level. There a several wave periods which are described in this Section.

The average time interval between successive up or down crossings through level T_η can be expressed as:

$$T_\eta = \frac{\sqrt{\frac{m_0}{m_2}}}{e^{-\frac{\eta^2}{2m_0}}} \tag{2.17}$$

A special case is the mean zero-crossing period T_z which can be obtained with $\eta = 0$.

$$T_z = \sqrt{\frac{m_0}{m_1}} \tag{2.18}$$

The period of a wave energy spectrum with the highest energy value is called the peak period, T_p. The T_p is determine based on a experimental relation, presented in Equation 4.2, of T_z and the peak enhancement factor, γ, presented by DNV [22]:

$$\frac{T_z}{T_p} = 0.6673 + 0.05037\gamma - 0.006230\gamma^2 + 0.0003341\gamma^3 \tag{2.19}$$

Another characteristic wave period is the significant wave period T_s. For waves with a narrow spectrum, is practically equal to the peak period of the spectrum:

$$T_s \approx T_p \quad \text{(for swell dominated seas)} \tag{2.20}$$

For wind-sea spectrum, this is not the case, but it has been found empirically that the average period of the higher waves is:

$$T_s \approx 0.95 \cdot T_p \quad \text{(for wind dominated seas)} \tag{2.21}$$

2.2.4 Wave Scatter diagram

A wave scatter gives a prediction about the sea states at a certain location. There are several statistical approaches to determine a wave scatter. A 3-parameter Weibull probability density function f is used in this research, expresses in Equation 2.22 according to DNV [22]:

$$f_{H_s}(h) = \frac{\beta_{H_s}}{\alpha_{H_s}} \left(\frac{h - \gamma_{H_s}}{\alpha_{H_s}} \right)^{\beta_{H_s}-1} \exp - \left(\frac{h - \gamma_{H_s}}{\alpha_{H_s}} \right)^{\beta_{H_s}} \tag{2.22}$$

in which T_z conditional is on H_s, modelled by a lognormal distribution:

$$f_{T_z|H_s}(t \mid h) = \frac{1}{\sigma t\sqrt{2\pi}} \exp - \left(\frac{(\ln t - \mu)^2}{2\sigma^2} \right) \tag{2.23}$$

Where the distribution parameters μ and σ are functions of H_s. Experience shows that the following model often gives good fit to the data:

$$\begin{array}{rcccl} \mu & = & E[\ln T_z] & = & \alpha_0 + \alpha_1 h^{a_2} \\ \sigma & = & std[\ln T_z] & = & \beta_0 + \beta_1 \exp^{b_2 h} \end{array} \tag{2.24}$$

The coefficients a_i, b_i, $i = 0, 1, 2$ are estimated from actual data.

2.3 Second order wave drift forces

The irregular wave spectrum as described in Section 2.1.2 includes a second order wave spectrum as a result of sum frequencies in the energy spectrum. In moored systems these second order wave drift forces result in deflection with a large amplitude and period.

An expression for the second order wave drift force, $F_1^{(2)}$, is given by Pinkster [23].

$$\begin{aligned} F_1^{(2)}(t) = &\sum_{i=1}^{N}\sum_{j=1}^{N} \zeta_i^{(1)}\zeta_j^{(1)} P_{ij} \cdot \cos\left\{(\omega_i - \omega_j)t + (\tilde{\varepsilon_i} - \tilde{\varepsilon_j})\right\} \\ &+ \sum_{i=1}^{N}\sum_{j=1}^{N} \zeta_i^{(1)}\zeta_j^{(1)} Q_{ij} \cdot \sin\left\{(\omega_i - \omega_j)t + (\tilde{\varepsilon_i} - \tilde{\varepsilon_j})\right\} \end{aligned} \tag{2.25}$$

Where P_{ij} and Q_{ij} are transfer functions that give the part of the wave drift force which is in-phase and out-of-phase with the low frequency of the square of the incident waves, respectively. The frequency of the low frequency part of the wave drift force is equal to the difference between the frequencies of the regular wave components. This is the frequency of the regular wave group which is the result of superposition of two regular waves. It is noted that the constant part of the wave drift force is the sum of the constant parts of each of the wave components. The amplitude of the quadratic transfer function is:

$$\mid T_{ij} \mid = \sqrt{P_{ij}^2 + Q_{ij}^2} \tag{2.26}$$

Since P_{ij} and Q_{ij} never occur in isolation, it can be arranged so that certain symmetry relations are valid:

$$\begin{array}{rcl} P_{ij} & = & P_{ji} \\ Q_{ij} & = & -Q_{ji} \\ \mid T_{ij} \mid & = & \mid T_{ji} \mid \end{array} \tag{2.27}$$

Figure 2.5 visualises the transformation from a $x - function$ to a $y - function$ via the transfer-function H.

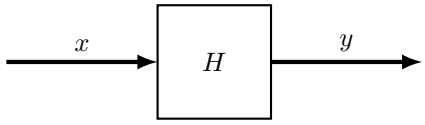

Figure 2.5: Quadratic transfer function

The quadratic transfer function belonging to Figure 2.5 is presented in Equation 2.28:

$$S_y(\mu) = \int_0^\infty \mid T(\omega, \omega + \mu) \mid^2 S_x(\omega) S_x(\omega + \mu) d\omega \tag{2.28}$$

The mean drift force in irregular waves with spectral density $S_{\zeta\zeta}(\omega)$ is found by rephrasing all j by i in Equation 2.25:

$$F_{1_{mean}}^{(2)} = \sum_{i=1}^{N} {\zeta_i^{(1)}}^2 \cdot P_{ii} \tag{2.29}$$

which, using Equation 2.10 for the expression of ${\zeta_i^{(1)}}^2$:

$${\zeta_i^{(1)}}^2 = 2S_\zeta(\omega_i) \cdot d\omega_i \tag{2.30}$$

results in:

$$F_{1_{mean}}^{(2)} = 2\sum_{i=1}^{N} S_\zeta(\omega_i) \cdot P(\omega_i, \omega_i) \tag{2.31}$$

where $P(\omega_i, \omega_i)$ is known as the mean drift force coefficient in regular waves and given as:

$$P(\omega_i, \omega_i) = \frac{F_1}{\zeta_i^2}(\omega_i) \tag{2.32}$$

Pinkster [23] found that the spectral density of the low frequency part of the wave drift force, $S_F(\omega)$, is:

$$S_F(\mu) = 8\int_0^\infty S_\zeta(\omega + \mu) \cdot S_\zeta(\omega) \cdot \mid T(\omega + \mu, \omega) \mid^2 \cdot d\omega \tag{2.33}$$

Figure 2.6 presents the $S_F(\omega)$ for a JONSWAP spectrum with a H_s of 1.5 m and a T_p of 8 s. $T(\omega + \mu, \omega)$ is assumed to be 1.0 here, in order to show where the energy is located.

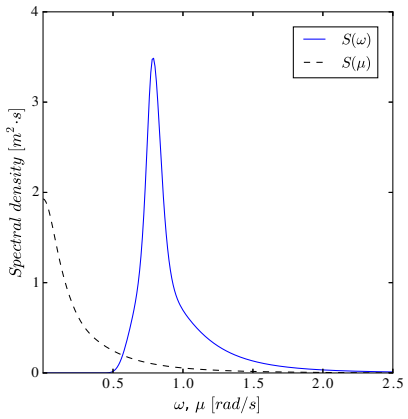

Figure 2.6: Low-frequency spectrum of a JONSWAP spectrum

2.4 Floating structures in waves

This Section describes the theory of floating structures in waves.

2.4.1 Definition of Motions

A free floating structure in a three-dimensional reference frame has six degrees of freedom. Three translations of the structures centre of gravity (COG) in the direction of the $x-$, $y-$, $z-$axes

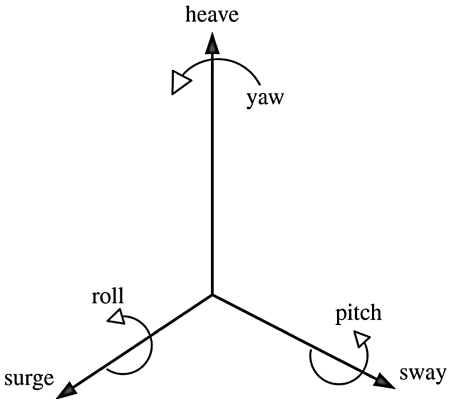

Figure 2.7: Coordination system floating structures [4]

and three rotations around these axes. Figure 2.7 presents these translations and rotations for a floating structure.
The waves acting on the structure are assumed to be harmonic, therefore the motions of the structure are harmonic as well. When the motions of the COG are known, the motions in any point on the structure can be calculated applying the superposition principle. Journée and Massie [4] described the motions of the floating structures COG by the following equations:

$$\begin{array}{lcll} \text{Surge} & : & X & = & X_a \cos(\omega t + \varepsilon_{x\zeta}) \\ \text{Sway} & : & Y & = & Y_a \cos(\omega t + \varepsilon_{y\zeta}) \\ \text{Heave} & : & Z & = & Z_a \cos(\omega t + \varepsilon_{z\zeta}) \\ \text{Roll} & : & \phi & = & \phi_a \cos(\omega t + \varepsilon_{\phi\zeta}) \\ \text{Pitch} & : & \theta & = & \theta_a \cos(\omega t + \varepsilon_{\theta\zeta}) \\ \text{Yaw} & : & \psi & = & \psi_a \cos(\omega t + \varepsilon_{\psi\zeta}) \end{array} \tag{2.34}$$

The coordinate system used during the research is visualised in Figure 2.8.

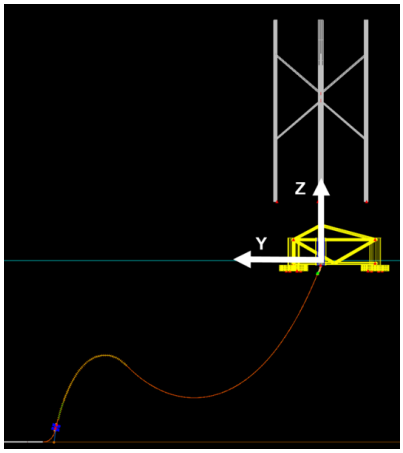

(a) Side orientation

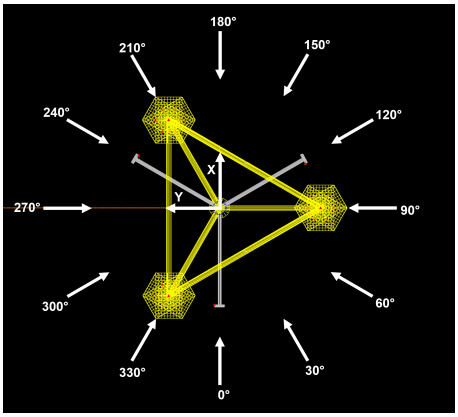

(b) Wave directions

Figure 2.8: System orientation

2.4.2 Response in regular waves

The equations of motion of a rigid body in a space fixed coordinate system follows from Newton's second law. The vector equations for the translation of and the rotations about the COG are given

in Equation 2.35 in which $\vec{F}$ is the resulting external force, $\vec{U}$ the instantaneous velocity acting in the COG and m the mass. Resulting external moment $\vec{M}$ and instantaneous angular momentum $\vec{H}$ on the COG complete the parameters in Equation 2.35.

$$\vec{F} = \frac{d}{dt}(m\vec{U}) \quad \text{and} \quad \vec{M} = \frac{d}{dt}(\vec{H}) \tag{2.35}$$

The response of free floating structures can be assumed linear. Assuming that a free floating structure is a linear system, superposition of the oscillations of the structure in still water and the forces acting on the restrained structure in waves can be applied in order to derive the resulting motions of the structure, presented in Figure 2.9.

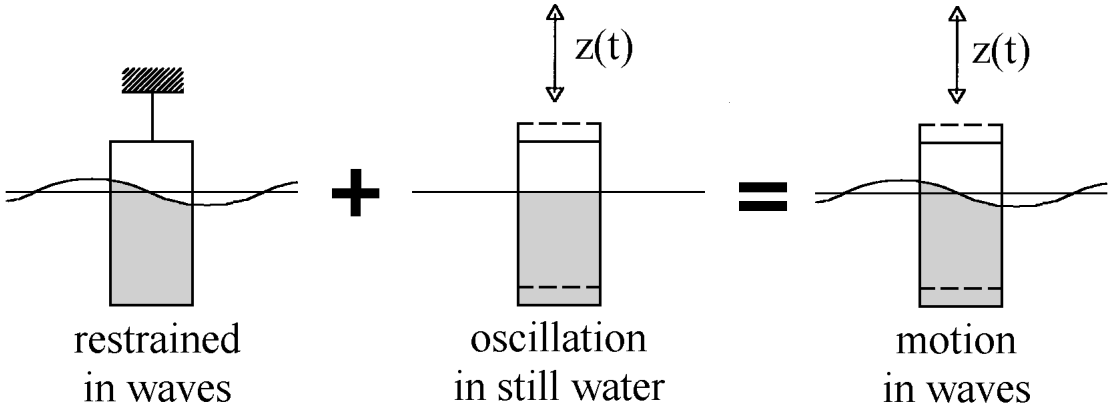

Figure 2.9: Superposition of hydromechanical and wave loads [4]

Two important assumptions are made for the loads on the right hand side of Equation 2.35 for this superposition:

- The hydromechanical forces and moments are assumed to be induced by the harmonic oscillations of the floating structure, moving in the undisturbed surface of the fluid.
- The wave exciting forces and moments are assumed to be produced by waves coming in on the floating structure.

The hydromechanical forces and moments acting on the oscillation floating structure in still water are the linear hydrodynamic reaction forces and moments, damping- and spring forces. The coupled EoM in six degrees of freedom in waves is given in Equation 2.36.

$$M_{i,j} \cdot \ddot{\vec{x}_j} = \vec{F_i} \quad \text{for: } i = 1,...6 \text{ and } j = 1,...6 \tag{2.36}$$

in which $M_{i,j}$ is the solid mass or inertia coefficient. $\ddot{x}_j$ the acceleration of the structure in direction j is and F_i sum of the forces of moments action in direction i.

Sum of the forces F_i consists of three components:

1. Harmonic wave exciting forces and moments, $\vec{F_i}$
2. Linear hydrodynamic damping force, $C_{i,j}\dot{\vec{x}}$
3. Linear hydrostatic spring force, $K_{i,j}\vec{x}$

Combining Equation 2.36 with sum of the forces as explained above results in a coupled system of second order differential equations, with six degrees of freedom:

$$(M_{i,j} + A_{i,j})\ddot{\vec{x}} + C_{i,j}\dot{\vec{x}} + K_{i,j}\vec{x} = \vec{F_i} \tag{2.37}$$

in which $A_{i,j}$ is the hydrodynamic mass or inertia coefficient, $C_{i,j}$ the retardation function and $K_{i,j}$ the spring coefficient.

2.4.3 Response in irregular waves

The wave energy spectrum as defined in Equation 2.10 can be written as:

$$S_\zeta(\omega) \cdot d\omega = \frac{1}{2}\zeta_a^2(\omega) \tag{2.38}$$

Analogous to this, the energy spectrum of a motion (or response, r) can be defined by:

$$\begin{aligned} S_r(\omega) \cdot d\omega &= \tfrac{1}{2} r_a^2(\omega) \\ &= \left|\tfrac{r_a}{\zeta_a}(\omega)\right|^2 \cdot \tfrac{1}{2}\zeta_a^2(\omega) \\ &= \left|\tfrac{r_a}{\zeta_a}(\omega)\right|^2 \cdot S_\zeta(\omega) \cdot d\omega \end{aligned} \tag{2.39}$$

Thus, the response spectrum of a motion can be found by using the transfer function of the motion and the wave spectrum:

$$S_r(\omega) = \left|\frac{r_a}{\zeta_a}(\omega)\right|^2 \cdot S_\zeta(\omega) \tag{2.40}$$

The principle of this transformation of wave energy to response energy is presented in Figure 2.10 for the heave motion ($r = z$).

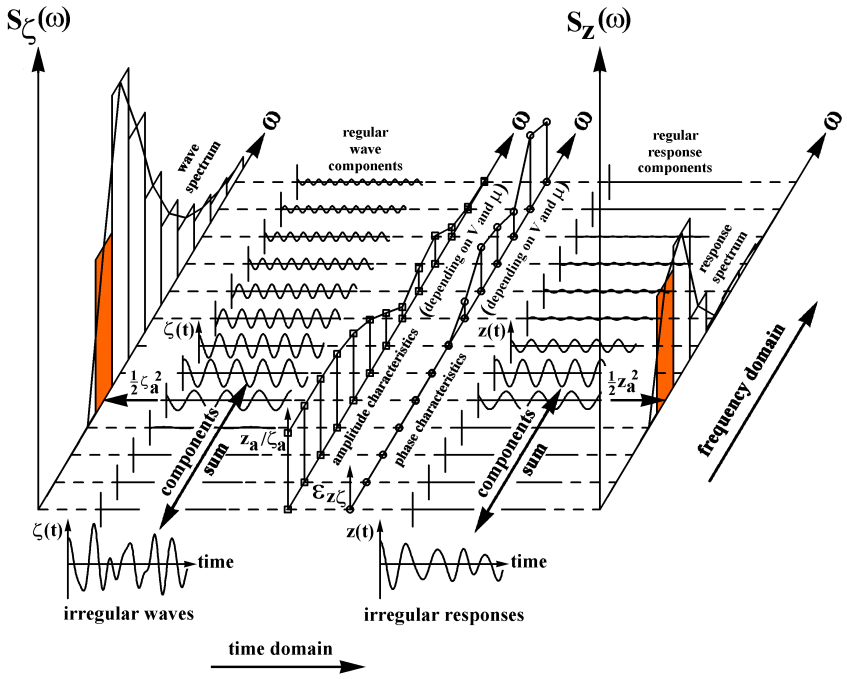

Figure 2.10: Principle of transfer of waves into response [4]

From the response spectrum of a degree of freedom in Equation 2.40, the moments of a degree of freedom response spectrum are given by:

$$m_{nr} = \int_0^\infty S_r(\omega) \cdot \omega^n \cdot d\omega \qquad \text{with: } n = 0,1,2,... \tag{2.41}$$

2.4.4 Response Amplitude Operator

Motions of floating structures in waves can be defined by Response Amplitude Operators (RAOs), as presented in Equation 2.42. The RAO transfer function is only defined if the ship motions are assumed to be linear.

$$S_r(\omega) = \left| \underbrace{\frac{r_a}{\zeta_a}(\omega)}_{\text{RAO}} \right|^2 \cdot S_\zeta(\omega) \tag{2.42}$$

There are two types of RAOs and each type of RAO consist of an amplitude and a phase:

1. Displacement RAOs: Amplitude = $\frac{r_a}{\zeta_a}(\omega)$ Phase = $\varepsilon_{r\zeta}(\omega)$
2. Wave load RAOs: Amplitude = $\frac{F_a}{\zeta_a}(\omega)$ Phase = $\varepsilon_{F\zeta}(\omega)$

The amplitude of a displacement RAO relates the motion amplitude to the amplitude of the waves, and the phase defines the timing of the motion relative to the wave.

Wave load RAOs do not completely define the motions of the floating structures as do displacement RAOs. They merely define the force and moment with a wave exerts on the floating structure. These forces and moments, together with any other loads on the floating structure and properties on the mass and inertia of it, are used to determine the motions of the floating structure.

Each of the six degrees of freedom as defined in Figure 2.7 has an RAO for each wave period and direction. RAOs can be obtained from model tests or from specialist diffraction programs, such as Ansys AQWA, which is described in Section 2.6.1.

2.5 Drag and added mass

The cable in the water is subject to forces due to waves and currents. These forces can be described by Morison type formulations. The Morison equation is the sum of two force components: an inertia force in phase with the local flow acceleration and a drag force proportional to the square of the instantaneous flow velocity. In an oscillatory flow with flow velocity $u(t)$, with a moving body with velocity, $v(t)$, the Morison equation becomes:

$$F(t) = \underbrace{\rho V \dot{u(t)}}_{\text{Froude-Krylov force}} + \underbrace{\rho C_a V(\dot{u}(t) - \dot{v}(t))}_{\text{Hydrodynamic mass force}} + \underbrace{\frac{1}{2}\rho C_d A(u(t) - v(t)) \mid u(t) - v(t) \mid}_{\text{Drag force}} \tag{2.43}$$

in which $F(t)$ is the total in-line force on the object, ρ the mass density of the fluid, V the cylinder volume per unit cylinder length, $\dot{u}(t)$ the flow acceleration, $\dot{v}(t)$ body acceleration, A the reference area. The Morison equation contains two empirical hydrodynamic coefficients, an added mass coefficient C_a and a drag coefficient C_d. Both coefficients are determined from experimental data. Sarpkaya [24] showed that these coefficients depend in general on the Reynolds number, Re, Keulegan-Carpenter number, KC and surface roughness.

The Reynolds number Re is expressed as:

$$Re = \frac{(u(t) - v(t)) \cdot D}{\nu} \tag{2.44}$$

in which D is obstacle diameter and ν the kinematic viscosity. The Reynolds number dependency of the drag coefficient is presented in Figure 2.11.
The Keulegan-Carpenter number, KC, is expressed as:

$$KC = \frac{u_{max} \cdot T}{D} \tag{2.45}$$

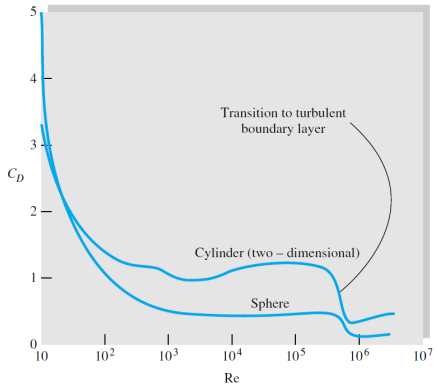

Figure 2.11: Reynolds number dependent drag coefficients [5]

in which u_{max} is the amplitude and T the period of the flow velocity oscillation. The Keulegan-Carpenter dependency of the drag coefficient is presented in Figure 2.12.

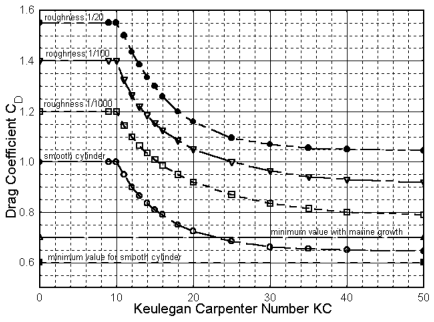

Figure 2.12: Keulegan-Carpenter number dependent drag coefficients [4]

2.6 Software packages

The software packages used in this research are described in this Section.

2.6.1 Ansys AQWA

Ansys AQWA Suite version 15 is used for the motion analysis the FOWT and CLV.

ANSYS AQWA [25] provides an engineering toolset for the investigation of the effects of wave, wind and current on floating and fixed offshore and marine structures, including semi-submersibles which will be the basis of a design.

AQWA Hydrodynamic Diffraction provides an integrated environment for developing the primary hydrodynamic parameters required for undertaking complex motions and response analyses. Model creation is performed through a connection with ANSYS Design Modeler software, with new hydrodynamic diffraction analysis system in ANSYS Workbench. Three-dimensional linear radiation and diffraction analysis may be undertaken with multiple bodies, taking full account of hydrodynamic interaction effects that occur between bodies. Computation of the second-order wave forces via the full quadratic transfer function matrices permits use over a wide range of water depths.

AQWA Hydrodynamic Time Response provides dynamic analysis capabilities for undertaking global performance assessments of floating structures in the time domain. In addition, sea-keeping simulations may be undertaken with the inclusion of forward speed effects. Slow-drift effects and extreme-wave conditions may be investigated.

The calculation of RAOs for floating structures is possible using equation of motions as defined in Equation 2.37. The analysis approach calculating the RAOs using Ansys AQWA is presented in Figure 2.13.

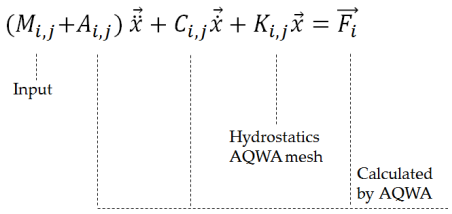

Figure 2.13: RAO calculation using Ansys AQWA

The distribution of mass within the structure determines the inertia and is input of the model. Ansys AQWA is capable creating a mesh of a geometry. The hydrostatics of a structure can be calculated using this mesh. The AQWA line module of Ansys AQWA calculates RAOs combining the input with a mesh and diffraction theory.

2.6.2 OrcaFlex

OrcaFlex is a time domain finite element program developed by Orcina and commonly used within the offshore industry. OrcaFlex is used for static and dynamic analysis of marine risers, mooring systems, installations and towed systems. It is highly suitable for the modelling of cable operations, such as cable overboarding and cable pull-in operations.

In OrcaFlex a line, which can represent multiple objects, like a cable, pipe, mooring line, etc., is the main aspect of the model. A finite element line model is a schematisation of these objects, presented in Figure 2.14.

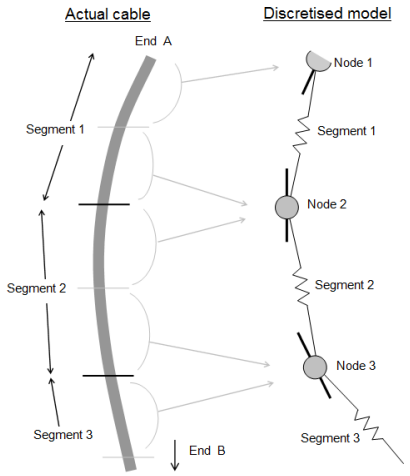

Figure 2.14: Line model schematisation [6]

The schematisation in Figure 2.14 shows three nodes. Each node represents half of the length of

segment one and segment two. Except for the nodes at the line ends, which represents only one half segment length. The segments in the discretised model are massless, straight and are only of importance for axial and torsional properties. All other properties are lumped to the nodes, e.g. bending stiffness, mass, buoyancy, etc. The segment length can be defined in OrcaFlex which means that the accuracy of the model can be defined. It must be noted however that a smaller segmentation results in a longer simulation time, so a optimum between accuracy and simulation time must be found.

External forces from environmental loads and/or other sources are transferred to the nodes. Besides lines, other objects like buoys and vessels can be implemented in OrcaFlex models.

OrcaFlex has been validated in-house by Orcina and by external organisations against other finite element software, model tests, and direct offshore installation experience and observations. For further and more detailed information and descriptions please refer to the OrcaFlex user manual [6].

CHAPTER 3

System description

This Chapter contains a general approach of cable installation and a description of the total system. The system starts with a dynamic cable with a certain configuration rising from the seabed towards the FOWT. A subsea tether arrangement connects the cable with the seabed, whereupon buoys create a buoyant cable part. A dynamic bend stiffener supports the connection of the cable with the FOWT. A CLV is used for the installation and pull-in of the cable. This Section describes the properties of these different objects.

3.1 Cable installation procedure

The procedure to install a dynamic cable transporting the electricity generated by FOWTs towards shore is described in this Section. The installation procedure consists of three different phases:

- Onshore connection
- Laying export cable
- Connection of the cable to the FOWT

A schematic impression of the FOWT connected with a mooring system and a dynamic cable is presented in Figure 3.1.

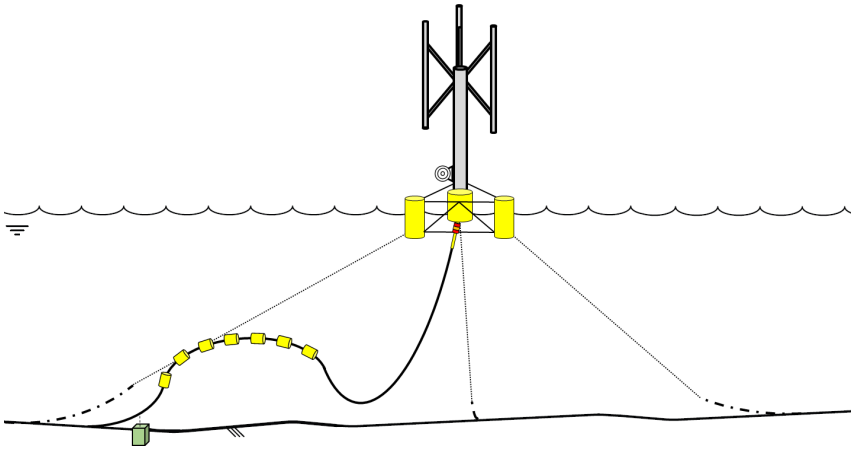

Figure 3.1: Schematic overview of the final configuration

3.1.1 Onshore connection

The power generated by the offshore wind farm is exported to an onshore electrical grid. A location onshore is determined where the connecting with this electrical grid can be made. A horizontal directional drilling (HDD) duct is used to connect the cable from offshore to onshore without excavation in a sea defence. The CLV moves towards the HDD duct to pull the cable

Figure 3.2: CLV beached [7]

trough the duct. VBMS' CLVs have the possibility to beach themselves, which makes it possible to sail closer to shore. In deep water a Dynamic Positioning (DP) system is used to keep the CLV at the same locations. A DP system cannot operate in shallow water depths, so an anchor system is used to pull the CLV closer to the beach. The CLV grounds with the flat keel on seabed, when it is close enough to shore, presented in Figure 3.2. The possibility to beach depends on weather and soil conditions, the CLV will stay float further away from shore if beaching is not possible. After moving in, the CLV starts releasing cable to shore using either floats, bottom pull, roller supports or another solution. Figure 3.3 shows the cable pulled through the landfall.

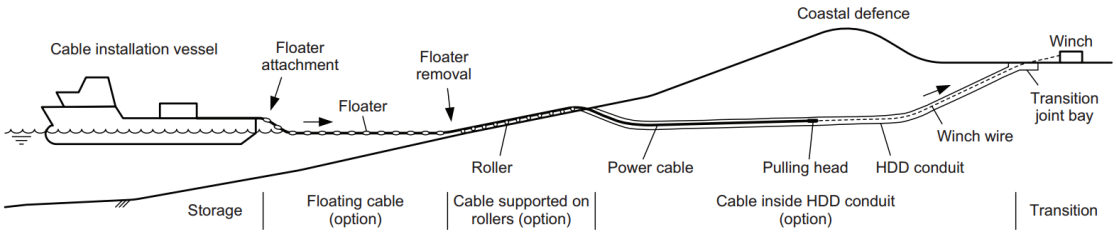

Figure 3.3: Export cable shore end pull in from CLV to shore [8]

3.1.2 Free lay of the export cable

The CLV starts laying export cable when the connection with shore has been made. The export cable transfers the power of the total wind farm towards shore. For this reason this cable is generally bigger and heavier related to the cable in between the turbines. An offshore wind farm is often equipped with two export cables, for redundancy purpose. Figure 3.4a shows a CLV laying cable and the terminology related to the laying process. The touch down point (TDP) is the point where the cable touches the ground and is varying during surface laying.

Failure of cables due to fishery, dropped anchors or dropped cargo is a real treat. Hence, the CLV buries the export cable into the seabed up to 3 m, in order to protect the cable against this treat. There are several means of burying cables, of which one is the use of a submarine cable plough. The cable plough is placed on the seabed during beaching operation as described in Section 3.1.1 and pulled behind the CLV during cable laying. A detailed drawing of a typical subsea cable plough is presented in Figure 3.4b. Cable ploughing is possible if the bottom tension of the cable with the seabed is not higher than approximately 20 kN. The cable has been laid

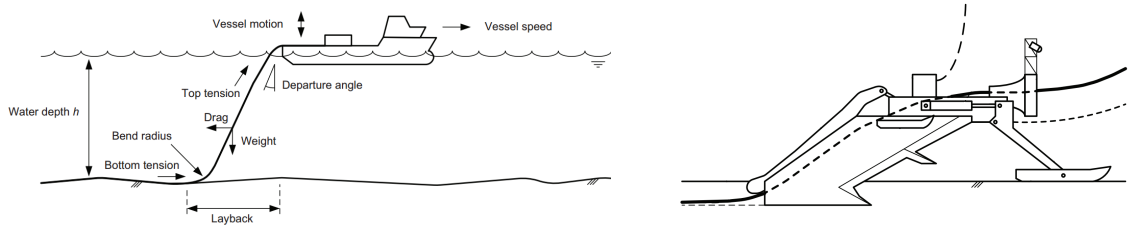

(a) Cable laying process

(b) Subsea cable plough

Figure 3.4: Free lay of the export cablle[8]

near the pre-determined centre line. A cable offset of approximately 5 m from the centre line is allowed.

3.1.3 Connection with the FOWT

The export cable is now connected to shore and buried towards the FOWT. A dynamic power cable is used to connect the export cable to the FOWT. A dynamic cable is capable to withstand more motions compared to traditional power cables. The connection of the dynamic cable is made performing a pull-in of the dynamic cable into the FOWT. Three different methods performing the pull-in are conceived and described in this Section.

3.1.3.1 Method 1: Pull-in in pre-installed FOWT

The first pull-in method is pull-in of the dynamic cable in a pre-installed FOWT. The CLV performs the pull-in directly after laying of the dynamic cable towards the FOWT. This is the conventional pull-in method used in the industry for bottom founded turbines.

In this method the FOWT is installed prior to arrival of the CLV on the location. The CLV makes a turn of ninety degrees in order to move sideways towards the FOWT. This is necessary to come closely with the CLV to the FOWT. Figure 3.5a gives an impression of this turn.

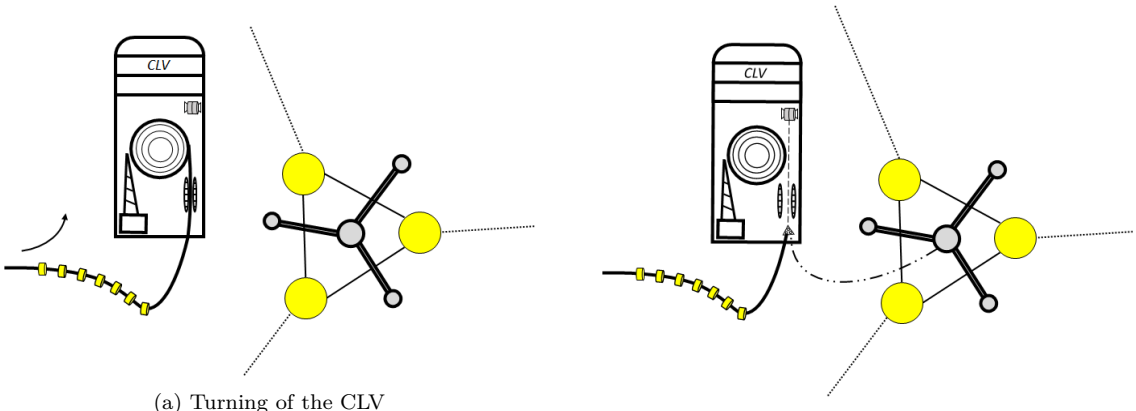

(a) Turning of the CLV

(b) Cable releasing

Figure 3.5: Movement of the CLV before pull-in

The FOWT releases a messenger wire towards the CLV to make a connection between the FOWT and the dynamic cable. This messenger wire is connected to a pull-in winch, which has been placed on the FOWT. Laying of a cable is only possible if the CLV ensures enough tension on the cable

in order to not exceed the maximum curvature of the dynamic cable. The CLV is equipped with a Linear Cable Engine (LCE), which is a two track tensioner. The LCE generates the required tension during surface laying of the cable. The tensioner is opened to release the last part of the cable in the water. A pay-out winch is used to take over the tension if the LCE is opened and to overboard the cable, presented in Figure 3.5b.

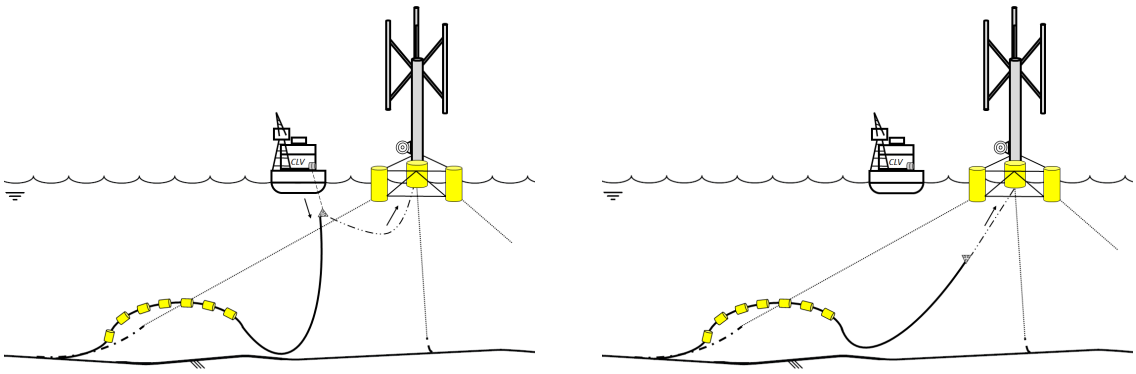

(a) Lowering the connection

(b) Disconnected from CLV

Figure 3.6: Side view lowering operation

Figure 3.6a shows a side view of lowering of the pullhead. The pullhead is rigging equipment placed on the cable end to connect the pull-in and pay-out wires to the cable. The pull-in winch at the FOWT starts the pull-in and takes over the tension of the pay-out winch. The pay-out winch is disconnected using a Remotely Operated Vehicle (ROV) when the total tension is taken by the pull-in winch. The pull-in winch continues until the cable reaches the hang-off point. The hang-off point is a location on the FOWT used to fix, strip and connect the cable to the turbine.

3.1.3.2 Method 2: Post-lay pull-in via CLV

The second pull-in method is a post-lay pull-in of the dynamic cable to the FOWT with aid of the CLV. The pull-in is performed after wet storage of the dynamic cable on the seabed. This means that the entire project location can be provided with power cables prior to the installation of the FOWTs. As a result of this method installation of the cable is divided into two periods for the cable contractor, lay-down and recovery, respectively. The different phases of pull-in method 2 are presented in Figure 3.7.

The CLV lies the cable on the seabed following a determined lay-down path, presented in Figure 3.7a. The dynamic cable is stored on the seabed for the period between cable lay and pull-in, presented in Figure 3.7b. There are multiple options to store the cable on the seabed. Storage of the cable in a favourable direction is used in pull-in method 2, presented in Figure 3.7c. The benefit of this storage method is the possibility to choose a storage direction, based on the weather data of the location and accessibility in the field.

The presence of a current with influence near the seabed determines if measurements are necessary to keep the cable on the preferred spot during storage. Typical measurements are:

- Placement of an anchor at the cable end
- Placement of rockbags on and next to the cable

A temporary anchor line is used to pick-up the cable from the seabed after the storage period. The CLV pulls the anchor line in using a pay-out winch and the CLV moves simultaneous slowly towards the lay orientation of the dynamic cable. This temporary equipment attached to the cable

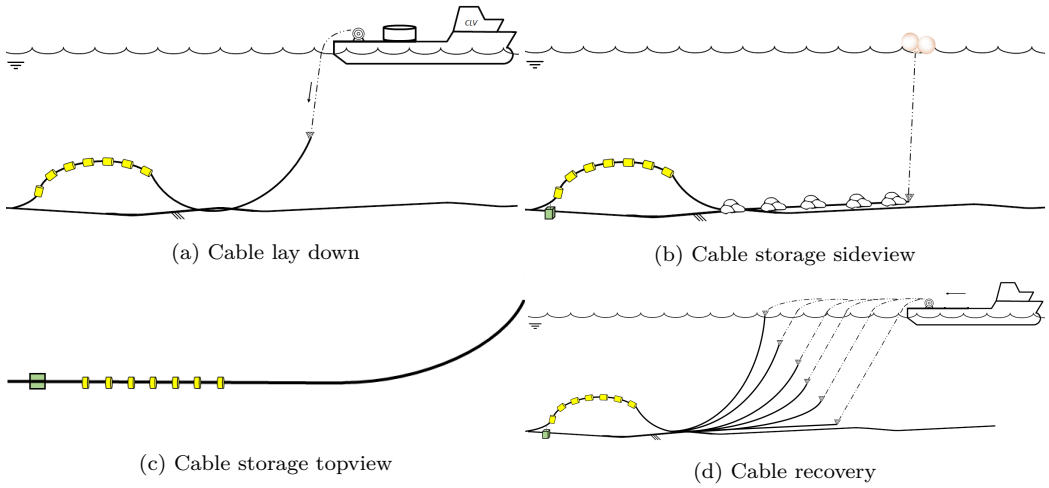

(a) Cable lay down

(b) Cable storage sideview

(c) Cable storage topview

(d) Cable recovery

Figure 3.7: Cable stages during pull-in method 2

is removed when the pullhead is on deck of the CLV. The cable is connected with a messenger wire which has been released from the FOWT. The pull-in of the dynamic cable in the FOWT starts afterwards. The pay-out winch on the CLV releases the cable. The pull-in winch on the FOWT starts pull-in simultaneously. The difference between pull-in method 1 and 2 is the position of the pullhead at the start of the pull-in.

3.1.3.3 Method 3: Post-lay pull-in via FOWT

The third pull-in method is a post-lay pull-in of the cable after a storage period from the FOWT only. Pull-in method 3 is similar to pull-in method 2, however in pull-in method 2 there is no CLV necessary to perform the pull-in.

In addition, the difference between pull-in method 2 and 3 is the shape in which the dynamic cable is wet-stored on the seabed. In pull-in method 3 the pullhead is located on the seabed under the entrance point of the FOWT, presented in Figure 3.8a. The dynamic cable is stored in a s-shape on the seabed in this pull-in method, presented in Figure 3.9. This storage method is also used for bottom founded turbines if the cable is stored on the seabed prior to the pull-in.

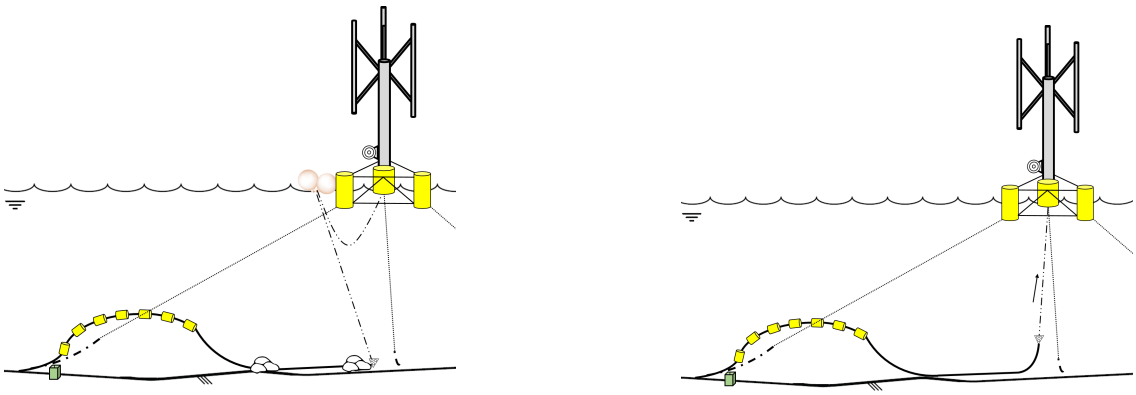

(a) Connection of a messenger wire after storage period

(b) Pull-in of the cable in the FOWT

Figure 3.8: Side view pull-in operations via FOWT

Figure 3.9: S-lay storage method

The FOWT is placed after the storing period and performs the pull-in. A small assistance vessel connects an anchor line, which is connected to the pullhead, with the FOWT. The FOWT starts pull-in using a pull-in winch and the s-shape is pulled out slowly. The pull-in continues until the cable reaches the hang-off platform.

3.2 Dynamic power cable

As already mentioned, a dynamic cable is used to create a dynamic catenary from the seabed towards the FOWT. Traditional cables are not able to resist the environmental conditions for 30 years when they are free-hanging in the water. For this reason dynamic cables are designed with different properties according to traditional power cables and are unique for every location in the world. The properties of the dynamic cable are described in Section 3.2.1. An assessment of the cable configuration to ensure integrity of the cable is described in Section 3.2.3.

3.2.1 Cable properties

Figure 3.10 presents a cable cross section of the dynamic power cable used in this research, supplied by cable manufacture JDR [9]. The cross section is optimised to achieve bend stiffness, weight and drag characteristics to match project specific challenges. This is required to operate in dynamic applications for the design lifetime. The properties of the dynamic cable used in this research are presented in Table 3.1.

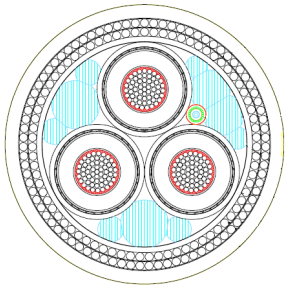

Figure 3.10: Cable cross section[9]

Symbols	Properties	Values	Units
D_p	Outside diameter	150 ± 3	mm
W_{air}	Weight in air	50	kg/m
W_{sea}	Weight in seawater	25	kg/m
EA	Axial stiffness	250	MN
EI	Bending stiffness	15	kNm^2
MBR	Minimum Bend Radius (MBR)	3	m
C_{max}	Maximum curvature	0.33	$1/m$
T_{max}	Safe Working Load (SWL)	300	kN
T_{min}	Maximum allowable compression	0	kN

Table 3.1: Cable properties [9]

Exceeding of the maximum curvature and tension of the cable is not allowed during the installation. Also, cable compression is prohibited. Cables are in-homogeneous products, which makes it difficult to ensure the same properties over the cable length. For this reason some safety is added by the cable supplier on the cable properties.

3.2.2 Validation cable properties

Cable properties are unique for every project, so validation of these properties is required to check if they are reliable. The graphs in Figure **??** present the values of the used cable according to the cable database of VBMS, which are highly confidential. Therefore, they are only presented to the thesis committee. No significant differences are found thus it is assumed that the used properties in this research are reliable.

3.2.3 Cable configuration

The configuration of dynamic cables rising from the seabed towards the FOWT determines the behaviour of the cable in the water. Fatigue and exceeding of the maximum allowable tension are typical failure mechanisms of dynamic cables. Thies, Johanning and Smith [10] compared two solutions to configure the dynamic cable hanging under a floating structure:

- Free-hanging catenary set-up
- Lazy wave configuration

Their research showed better cable performance in the lazy wave configuration; lower effective tension and longer fatigue lifetime of the cable. The lazy wave configuration as investigated can be constructed by adding buoys to the cable or using a floating mid-water arch, Figure 3.11a and 3.11b, respectively.

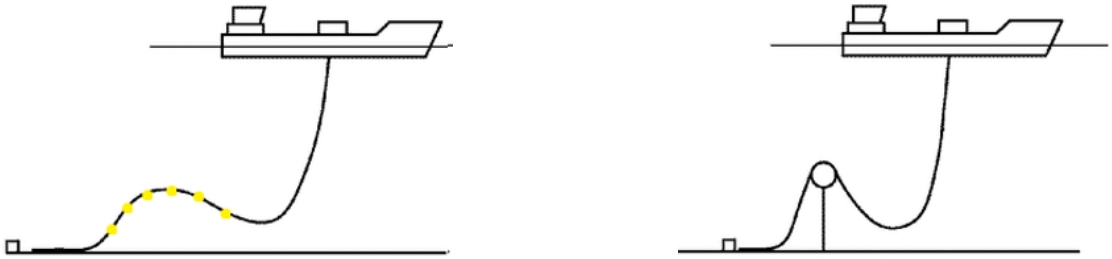

(a) Buoys support (b) Floating mid-water arch

Figure 3.11: Dynamic power cable set-ups [10]

Current loads on the cable configuration result in sideways movement of the configuration. Sideways movements are counteracted by a subsea tether arrangement attached near the TDP of the cable. This changes the configuration name form 'lazy wave' to 'pliant wave'. A pliant wave configuration supported by buoys is used in this thesis, since for a single dynamic cable it is the most suitable configuration.

The design of the dynamic cable configuration is influenced by many parameters, which are presented in Figure 3.12. Cable supplier JDR [9] provided the corresponding parameters of a representative configuration for this research. These parameters are presented in Table 3.2.

Symbols	Properties	Values	Units
A	Vertical distance between MSL and I-tube exit	2.6	m
B	Upper catenary section	165	m
C	Buoyancy section	60	m
D	Between byoyant section and touchdown point	17	m
E	Between buoyant section and tether	4.5	m
F	Tether radius	147	m
G	Touchdown point radius	153.5	m
H	Waterdepth	100	m
J	Tether length	8.3	m
K	Minimum seabed clearance	10	m
L	Buoyant section above seabed	25 ± 5	m

Table 3.2: Cable configuration parameters [9]

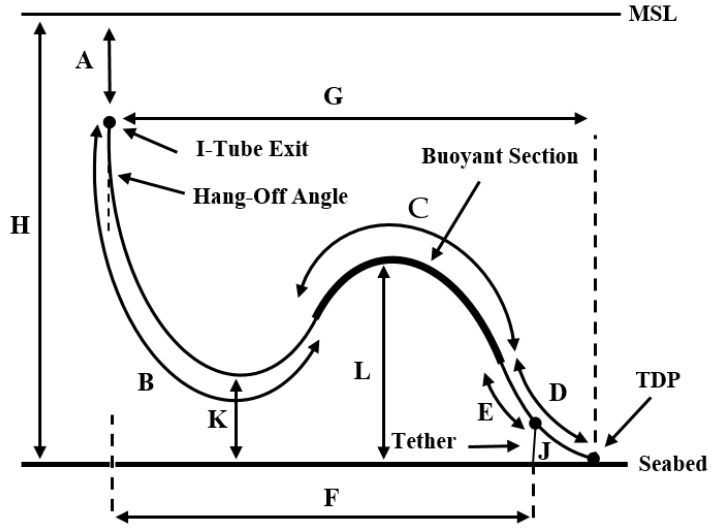

Figure 3.12: Cable configuration lay-out

3.2.4 Validation cable configuration

The cable configuration is designed using multiple parameters which are all influencing the behaviour of the cable during installation and operation period. Two checks of the configuration are performed based on rules and regulations supplied by the cable supplier JDR [9]. A maximum offset of 10 m of the FOWT during operation is assumed and used in these checks.

Firstly the configuration is checked to remain 10 m above the seabed in the ahead condition. The ahead condition is the condition where the FOWT moves towards the TDP of the cable. This check is assessed for the end of life conditions because the system is the slackest then. At the end of life the buoys have lost buoyancy capacity and marine growth is fully developed, resulting in the FOWT having a larger draught.

The configuration is secondly checked if it is not deformed in the behind condition, leading to excessive axial loads. In the behind condition the FOWT moves away from the TDP of the cable. This check should be assessed for the start of life conditions because then the system is as tight as possible. Both checks are successfully performed, thus the configuration is assumed to be valid.

3.3 Subsea tether arrangement

A subsea tether arrangement is required to prevent downstream migration of the cable when transverse environmental loading is applied to the cable configuration and protects the TDP of the cable against fatigue. Figure 3.13 presents a typical tether system design, which consists a bellmout clamp, a braided rope tether and a gravity base.

Bellmouts are attached on both ends of the cable clamp to avoid exceeding of the maximum cable curvature at the entrance and exit of the clamp. Installation of the clamp is performed prior to the attaching of the buoys on the dynamic cable. Table 3.3 presents the tether arrangement properties used in this research, supplied by Trelleborg Offshore [18].

The maximum tether capacity depends on the angle the tether makes perpendicular with the seabed, combined with the weight of the gravity base structure. Figure 3.14 presents the result of the maximum tether force according to its angle. For this calculation some simplifications are

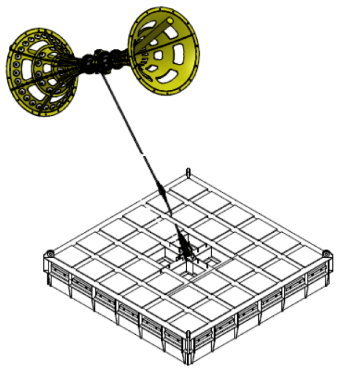

Figure 3.13: Typical tether arrangement [9]

Objects	Values	Units
Clamp length	1	m
Clamp inner diameter	175	mm
Bellmouth length	1.1	m
Bellmouth radius	4	m
Maximum axial load at clamp	150	kN
Total weight clamp	2	mT
Total weight gravity base	36.5	mT

Table 3.3: Tether arrangement properties [18]

made:

- Geometry of the shape of the gravity base is not taken into account, so tilt moments are not used.
- A friction coefficient of 0.6 is used for sand-steel friction.

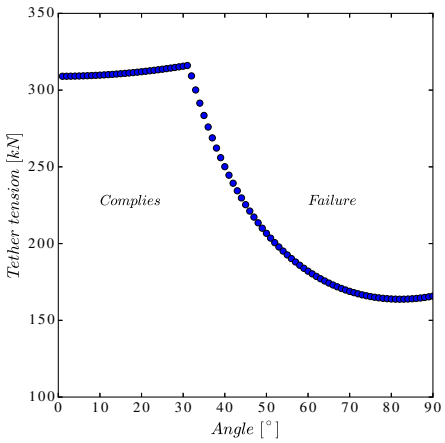

Figure 3.14: Maximum tether tension regarding the angle

The maximum axial load capacity of the cable clamp is 150 kN. The cable clamp fails on exceeding of the maximum axial load capacity prior to the gravity base starts moving, based on the results presented in Figure 3.14.

3.4 Buoys

Creation of a floating mid-water arch for a pliant wave configuration, is done by attaching Distributed Buoyancy Modules (DBMs) to the cable. These DBMs are designed to ensure the capacity over the design life of the product. Clamps inside the DBMs are used to connect the DBMs to the cable. These clamps have to be installed with great accuracy, because failure of one of them results in failure of the system, since the clamps have the capacity to hold only one DBM.

The dynamic cable configuration used in this research requires 5 mT buoyancy. This amount of buoyancy is provided by 20 DBMs attached on the cable with 3 m spacing in between. The properties of the DBMs are presented in Table 3.4.

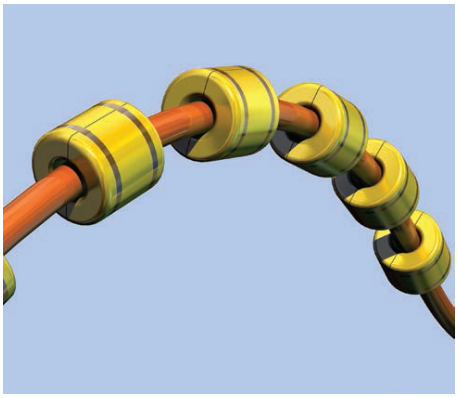

Figure 3.15: Impression DBMs [11]

Properties	Values	Units
Buoyancy per buoy	250	kg
Diameter	761	mm
Length	870	mm
Amount of DBMs	20	–
Centre-to-centre spacing	3	m

Table 3.4: DBMs properties [11]

3.5 Dynamic Bend Stiffener

Where a cable is connected to a structure, normal movement during operation or forces incurred during installation and retrieval may cause failure of the cable at the termination point. This results in a decrease of the cable capacity as a result of excessive loads during installation or through fatigue damage over time. Protection of the cable against these failure mechanism is possible using a dynamic bend stiffener as Cable Protection System (CPS). It maintains the recommended MBR and reduces point loading at the termination to an acceptable level. For simplicity reasons is the dynamic bend stiffener called CPS in this research.

Figure 3.16 presents the profile of the CPS used in this research. The corresponding properties are presented in Table 3.5.

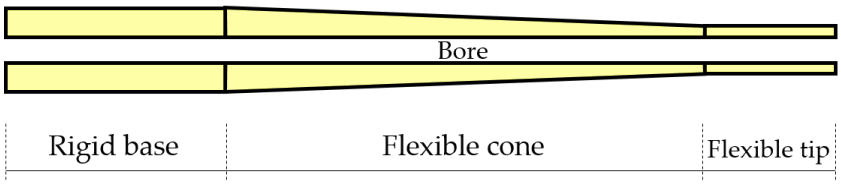

Figure 3.16: CPS profile

A stress-strain relation of this CPS is presented in Figure 3.17. The Young's modulus of the CPS is calculated in OrcaFlex using the derivative of this stress-strain relation. The CPS is provided by Trelleborg [26], based on the boundary conditions of this research.

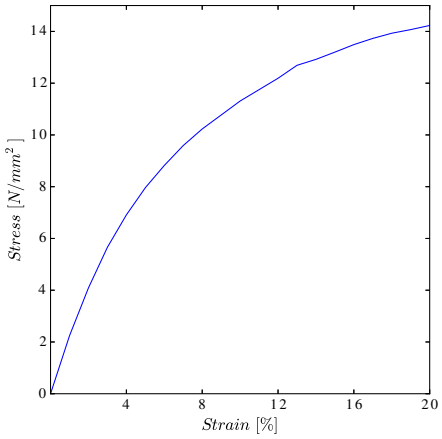

Figure 3.17: Stress-strain bend stiffener [9]

CPS	Values	Units
Rigid base outer diameter	410	mm
Flexible tip outer diameter	194	mm
Bore diameter	154	mm
Overall length	4817	mm
Weight in Air	2143	kg
Material	$PU\ 60D$	–
Maximum bend moment	150	kNm

Table 3.5: CPS properties [9]

3.6 Floating Offshore Wind Turbine

Collu, Kolios, Chahardehi and Brennan [2] showed that in deeper water, FOWTS become more economically viable than fixed support foundations. A FOWT is equipped with a turbine and a substructure. There are multiple designs possible choosing these two components, however the designs of the components are chosen based on available literature and described in this Section.

3.6.1 Turbine

The FOWT is equipped with a turbine is the component of the FOWT which generates energy from the wind. There are two types of turbines used in the wind energy industry:

- Horizontal axis wind turbines (HAWTs) (Figure 3.18a)
- Vertical axis wind turbines (VAWTs) (Figure 3.18b)

(a) HAWT (b) VAWT

Figure 3.18: Turbine methods [12]

Borg en Collu [27] investigated the static and dynamic behaviour of HAWTs and VAWTs. They found that VAWTs have some benefits related to HAWTs:

- HAWTs need to turn the hub in the direction of the wind in order to rotate the blades, which is not needed for VAWTs, resulting in larger operational time for the latter.

- HAWTs have their turbine behind the nozzle, high above the waterline and VAWTs have their turbine near the waterline. Lower COG results in better stability performance of the structure.

The wind energy market is reluctant using new turbine concepts such as VAWTs, however a VAWT is used in this research, based on the availabilty of a VAWT design within the company [13]. Figure 3.19 presents the a 3D impression of the turbine used in this research. Corresponding properties of the VAWT are presented in Table 3.6. A technical drawing of the turbine is attached in Appendix A.

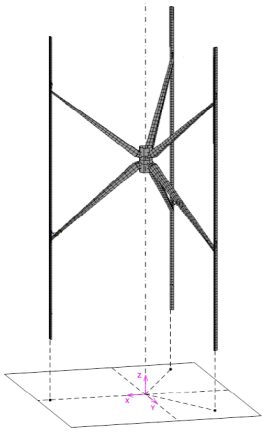

Figure 3.19: Turbine 3D impression [13]

Objects	**Values**	**Units**
Blade height	100.0	m
Blade diameter	0.5	m
Number of blades	3	-
Pylon height	73.5	m
Pylon diameter	6.0	m
Total turbine diameter	60.0	m
Airgap	20	m
COG_x	0	m
COG_y	0	m
COG_z	66.6	m
Total weight turbine	333135	kg

Table 3.6: Turbine properties [13]

3.6.2 Sub-structure

The sub-structure is the foundation of a FOWT, which ensures the FOWT to stay afloat. There are multiple designs of sub-structures possible. Figure 3.20 presents a tri-floater sub-structure design which is used in this research based on the available literature. The corresponding properties of the sub-structure are presented in Table 3.7.

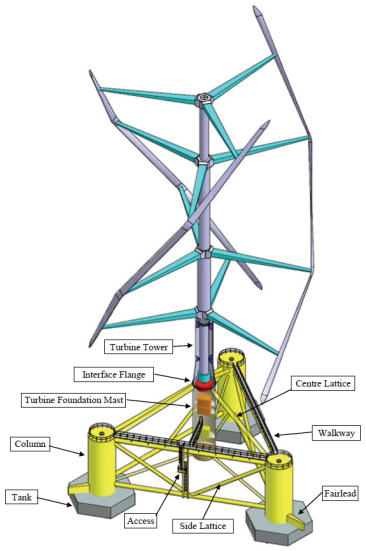

Figure 3.20: Sub-structure 3D impression [14]

Objects	Values	Units
Column height	15.2	m
Column diameter	6.3	m
Hexagon tank height	3.0	m
Hexagon tank diameter	15.7	m
Spacing between columns	42.0	m
Displacement	1950	mT

Table 3.7: Sub-structure properties [14]

Cahay, Luquiau, Smadja and Silvert [14] investigated the behaviour of this sub-structure. They performed wave frequency analyses to investigate the RAOs of the FOWT. The results of the RAOs in heave and pitch direction for a wave direction of 90 degrees are presented in Figure 3.21a and 3.21b, respectively. These RAOs are used for validation purposes in this research,

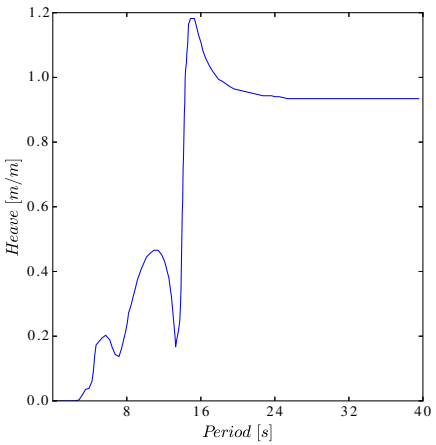

(a) Heave RAO

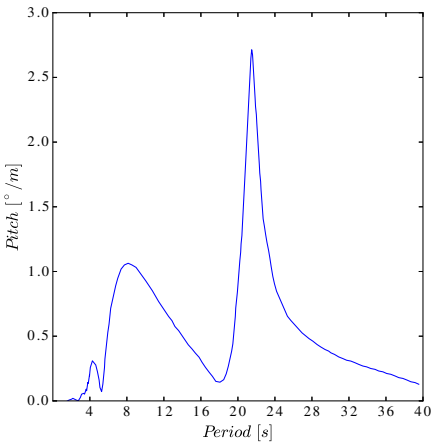

(b) Pitch RAO

Figure 3.21: RAOs of the FOWT for a 90° heading at the COG [14]

3.7 I-tube

The FOWT is equipped with an I-tube. An I-tube is a cable path to enter the FOWT. At the end of the I-tube the CPS as described in Section 3.5 is connected. The I-tube has a inner diameter of 324 mm and a total length of 15.15 m from entrance point towards the hang-off point.

3.8 Pull-in winch

The FOWT is equipped with a pull-in winch, which is necessary to perform the cable pull-in. This pull-in winch could be temporary and used in other FOWTs, depending on the accessibility. Figure 3.22 present a friction winch designed by Couperus. This which is suitable for this pull-in operation. The Couperus winch used by VBMS has a maximum capacity of 12 mT.

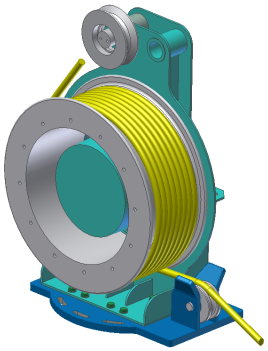

Figure 3.22: Couperus winch [15]

3.9 Cable Lay Vessel

A CLV is used to perform the installation of the dynamic cable. In this research VBMS´ CLV Ndurance is used as reference CLV. Figure 3.23 presents an impression of the CLV.

An important aspect of the cable installation into a FOWT is the interaction between two floating structures. Collision between the FOWT and CLV needs to be avoided. For this reason a minimum clearance between the structures is required. The CLV is equipped with a DP system to perform station keeping. The FOWT is equipped with a mooring system, which is less controllable against motions. The International Marine Contractors Association (IMCA) [28] regulates that a vessel needs to have a minimum clearance of 10 m with respect to a moored floating structure.

The main properties of the CLV Ndurance are presented in Table 3.8. The cable path location with respect to the COG of the CLV determines the accelerations of the cable in the environmental conditions. The location of the cable path is marked in the technical drawings of the CLV attached in Appedix B

3.9.1 Tension equipment

The Ndurance is equipped with a Linear Cable Engine (LCE), which is a two-track cable tensioner, presented in Figure 3.24a. This LCE is positioned on the starboard side of the CLV in line with the cable path as presented in Appendix B. The maximum capacity of the LCE on the Ndurance is 15 mT.

Figure 3.23: Impression CLV Ndurance [16]

Objects	Values	Units
Length overall	99	m
Breadth	30	m
Moulded depth	7.0	m
Draught	4.2	m
Displacement	12285	mT
Turntable capacity	5000	mT
Product cable size	50 - 300	mm
MBR cable highway	4.5	m
Accommodation	60	POB
Sailing speed	11.5	$knots$
Crane capacity	25 mT at 25 m	–
DP system	DP-2	–
Cable path height	11.7	m
Cable path offset	5.3	m

Table 3.8: Properties CLV Ndurance [16]

The Ndurance is also equipped with a pay-out winch, presented in Figure 3.24b. This winch is used to overboard the last part of the cable, after the cable end leaves the LCE. The minimum requirements for the pay-out winch depends on expected loads during an operation.

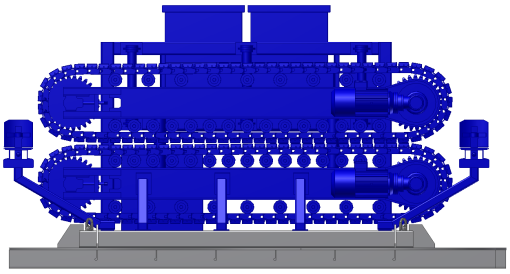

(a) LCE

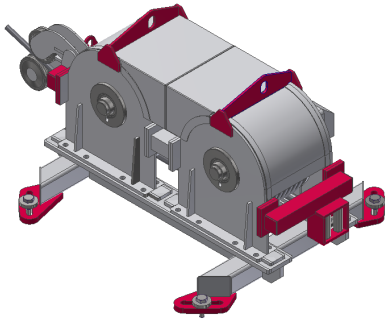

(b) Pay-out winch

Figure 3.24: Tension equipment [15]

3.9.2 Chute

A chute is installed on the stern of the CLV to support the cable when it leaves the CLV. The radius of the chute is important to ensure the cable integrity during the pull-in operation. The radius needs to be larger than the MBR of the cable. Figure 3.25 presents the chute which is currently available on the CLV. The bottom plate of the chute has a top radius of 7.2 m and a bottom radius of 5 m. A similar construction is used for the sides of the chute, the horizontal radii there are 9.5 m and 4.1 m, respectively. The radius of the inner sides of the chute is 7.2 m.

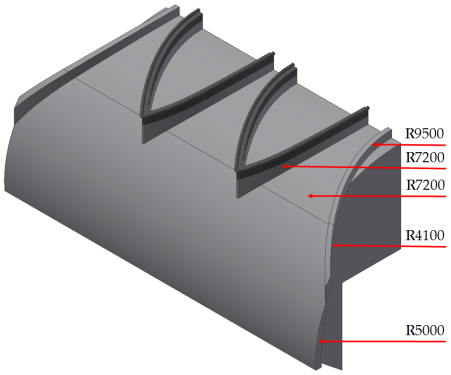

Figure 3.25: Chute of the CLV Ndurance [15]

CHAPTER 4

System modelling

This Chapter describes how the operations together with the different equipment are modelled. Firstly, a system controlling the winches is designed, investigated and outlined. The modelling of the different objects is presented afterwards starting with the dynamic power cable together with the equipment which is connected to the cable rising from the seabed towards the FOWT. Furthermore, the modelling of the FOWT and the CLV are described. The Section finishes with a description of the free-lay model and the three pull-in method models.

4.1 Control system winches

Ensuring cable integrity during installation is the main priority of a cable contractor. Avoiding of interaction of the cable with the seabed and controlling of the tension on the configuration is important to ensure integrity. This section describes a system which has been developed to control the pull-in and pay-out winches during the pull-in operation.

4.1.1 Design of the system

Designing of a system to control the winches during the pull-in operation starts with an investigation of the possible parameters which can be influenced by the system. A schematising of the possible parameters to control the winches is presented in Figure 4.1.

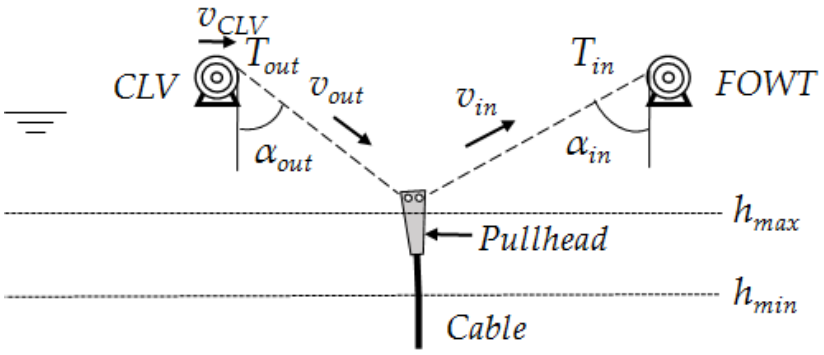

Figure 4.1: Schematisation control system of the winches

- T is the tension in the pull-in and pay-out winch.
- v is the rate of the pull-in and pay-out winch.
- α is the angle of the pull-in an pay-out wire.
- h_{min} and h_{max} are the minimum and maximum heights in which the pullhead of the cable needs to be during pull-in of the cable.

4.1.2 Operational possibilities

An investigation is performed to indicate parameters which are available on the CLV and can be used to design the system. The results are listed below:

- The tension at both winches is known real time during pull-in with a measurement system.
- The pull-in and pay-out velocity of the winches are known real time during pull-in with a measurement system.
- Angles of the messenger wires cannot be measured accurately, with the current equipment.
- Distance between the CLV and the FOWT is known real time via a GPS and a survey system.
- An altimeter can be placed on the pullhead to have a real time measurement of the position above the seabed.
- A beacon can be connected to the pullhead and it can measures the distance between the CLV and the pullhead.

The position of the pullhead is known real time during the pull-in operation with respect to the CLV, the FOWT and the height above the seabed. Equipment to perform the measurement of the pullhead position are relatively simple. For this reason controlling of the position of the pullhead during the pull-in operation is used to design the system for the winches in this research.

4.1.3 Limitations

Figure 4.2 presents an approach of the area in which the pullhead of the cable needs to be during the pull-in operation to ensure cable integrity.

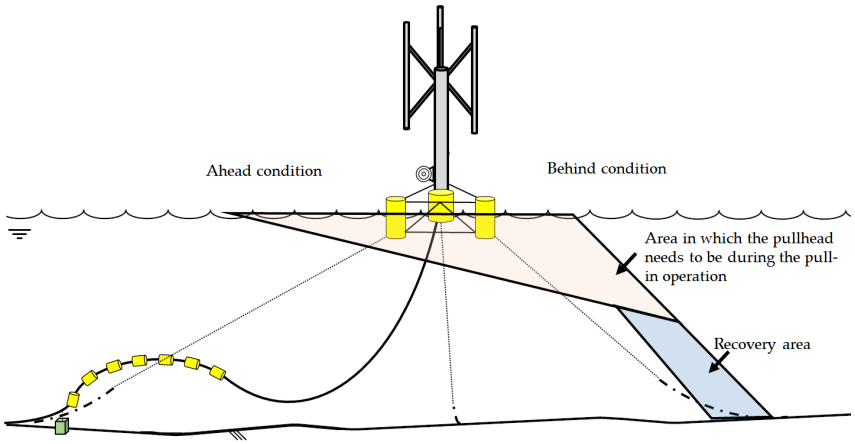

Figure 4.2: Safe area for the pullhead to guarantee cable integrity

The ahead and behind conditions as presented in Figure 4.2 are investigated in this Section, based on the guidelines of the cable supplier JDR [9].

4.1.4 Ahead condition

The ahead condition determines the minimum horizontal distance between the pullhead and the cable TDP, where the sag bend has a minimum clearance with the seabed, presented in Figure 4.3.

Investigation on the sag bend movement of the cable in environmental conditions resulted in maximum vertical movement amplitude of 0.25 m. For this reason the dynamic cable behaviour does not contribute to the minimum seabed clearance.

The seabed clearance needs to be inspected with an ROV during the pull-in operation. Inspecting and controlling of the sag bend above the seabed is difficult due to the delay between observation and action. A minimum seabed clearance of 10 m is assumed to be sufficient, based on operational experience of the installation contractor. This minimum seabed clearance is used as an important limitation to design and control the system for the winches.

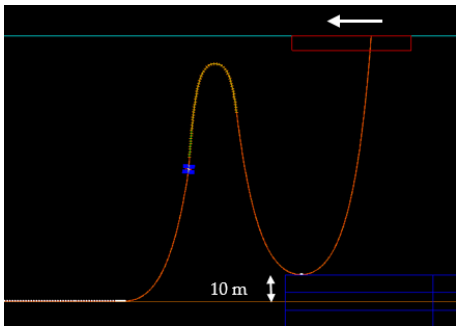

Figure 4.3: Ahead condition

4.1.5 Behind condition

The behind condition determines the maximum distance between the pullhead and the TDP of the cable, presented in Figure 4.4. The cable supplier requires that the cable configuration is not deformed, leading to excessive axial loads. In this condition the tether should not act like an anchor, instead the cable configuration should be able to withstand the movement of the pullhead away from the TDP. A maximum effective tension in the TDP of the cable is used as limitation for the behind condition. A maximum tension of 20 kN is assumed, since burial of the cable afterwards is still possible with this tension in the TDP.

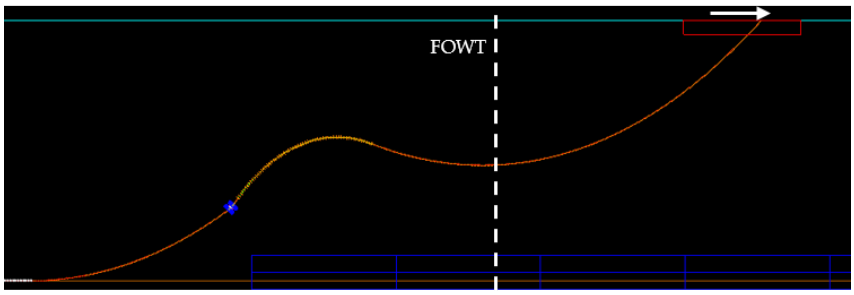

Figure 4.4: Behind condition

4.1.6 Investigated cases

Four different cases are investigated to create insight in the limitations controlling the winches:

1. A cable configuration with an tether installed and ensuring only 0 m seabed clearance in the ahead condition. The behind condition is tested for a maximum tension of 20 kN in the behind condition.

2. Similar cable configuration with tether is investigated, but now ensuring 10 m seabed clearance in the ahead condition. The behind conditions is investigated similar to the first investigation.

3. Similar cable configuration without tether and ensuring 10 m seabed clearance in the ahead condition. Similar approach is used for the behind condition.

4. Same cable configuration with a tether installed is also investigation for the behind condition for a different direction to be used in pull-in method 2.

The first three investigations are performed in the same manner. First the pullhead travels in positive $y - direction$, according to the coordinate system described in Section 2.4.1, to find the ahead condition. Afterwards the pullhead travels in negative $y - direction$ to find the behind condition. The cable does not transfer in $x - direction$ during this investigation. 100 simulations are performed to investigate the ahead and behind conditions over the water depth in steps of 1 m.

The fourth investigation is only performed in the behind condition for the direction the CLV recovers the cable from the seabed before pull-in starts for pull-in method 2. Also 100 simulations are performed every 1 m over the water depth, but now with an angle of 100 degrees according to the $y - axis$, presented in Figure 4.5.

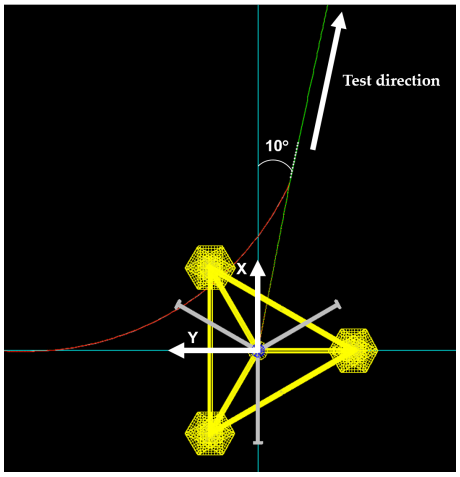

Figure 4.5: Top view of testing number four

4.1.7 Outline of the control system winches

Figure 4.6 presents the results of the first three investigated cases, in which the bullets represent the ahead condition and the triangles the behind conditions. The dotted lines through the bullets and triangles represent a function fitting the curves, which will be to control the winches.

The cable becomes somewhere over its length lower than the seabed clearances if the pullhead is lower than the ahead condition lines. So the system needs to control the winches such that the pullhead remains above these ahead condition lines. In addition, the system control the winches to avoid that the pulllhead passes the behind condition lines.

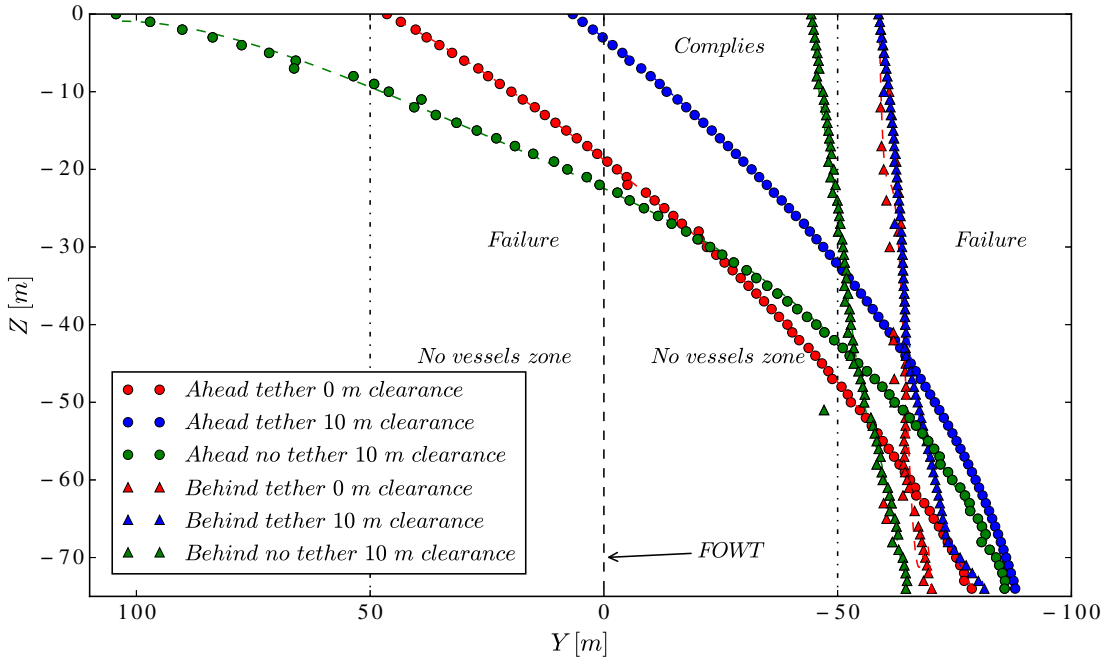

Figure 4.6: Results limitations investigation

For the behind condition lines it is visible that after crossing the ahead condition lines the gradient changes. Passing the ahead condition results in touchdown of the cable on the seabed or 10 m clearance, respectively. The behind conditions are calculated by exceeding 20 kN effective tension in the TDP, so if the cable touches the seabed the effective tension over the cable decreases. For this reason the gradient of the behind condition lines changes after crossing the ahead condition lines.

The control system for the winches is designed for every pull-in method based on the information gained from Figure 4.6, which makes this figure one of the most important figures in this research.

4.2 Dynamic power cable

Modelling of the dynamic power cable is described in this Section. Modelling of a subsea tether arrangement and a CPS is described afterwards.

4.2.1 Cable properties

The dynamic cable is built up from two different line types:

- Dynamic
- Dynamic BM

The dynamic line type is modelled according to Table 3.1 of Section 3.2.1.

A line type called Dynamic BM is modelled to attach DBMs to the cable. This linetype has the same properties as the dynamic line type, however, DBMs are attached based on the configuration presented in Figure 4.7.

Table 4.1 presents the used properties to model the Dynamic BM line type. With these two line

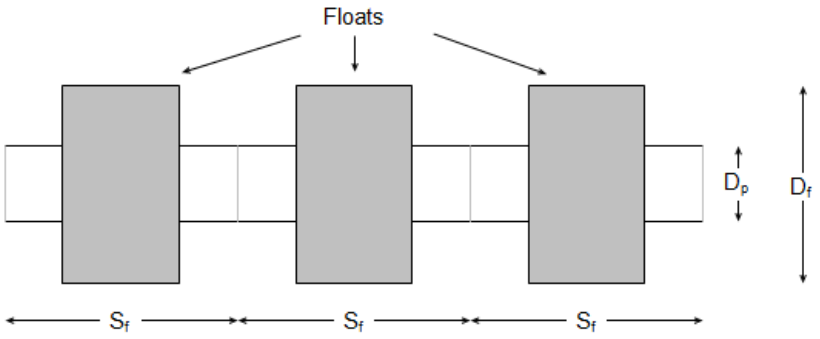

Figure 4.7: Geometry of Line and Buoys [6]

types a combined line is modelled with different sections as presented in Table 4.2.

Symbols	Properties	Values	Units
D_p	Cable diameter	150	mm
D_f	Buoy diameter	761	mm
L_f	Buoy length	870	mm
S_f	Centre-to-centre spacing	3	m

Table 4.1: Dynamic BM line type properties [11]

Increasing of accuracy is possible by decreasing the segment length, but more segments results in longer simulation time. The line sections which have interaction with the CLV, FOWT and the TDP are modelled with the smaller segment length with respect to the cable which lies on the seabed.

No.	Line type	Section length $[m]$	Segment length $[m]$	Number of segments $[-]$	Cumulative	
					length $[m]$	segments $[-]$
1.	Dynamic	165	0.5	330	165	330
2.	Dynamic BM	60	0.5	120	225	450
3.	Dynamic	67	0.5	134	292	584
4.	Dynamic	196	1.0	196	488	780

Table 4.2: Cable sections

4.2.2 Subsea tether arrangement

The cable clamp of the subsea tether arrangement as described in Section 3.3 is modelled with an inner radius profile as presented in Figure 4.8. The clamp properties are used in a separate line type and is connected with the dynamic power cable with the line contact data module. The dynamic power cable is penetrating the clamp line.

The gravity base of the tether arrangement is modelled infinitely heavy. The clamp is fixed on the seabed using a tether line, which has the properties of a steel wire. A pre-tension of 30 kN in the tether is used.

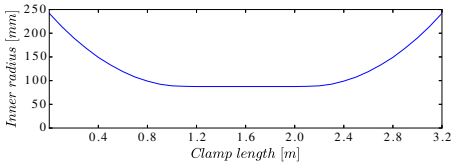

Figure 4.8: Clamp inner radius profile

4.2.3 CPS

The CPS is modelled according to the properties described in Section 3.5. Figure 4.9 presents the variable radius as function of the CPS length and is based on Table 3.5. This graph combined

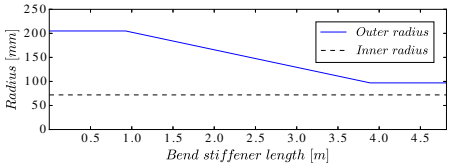

Figure 4.9: Variable radius CPS

with the stress-strain relation of the material, presented in Figure 3.17, are used to model the CPS. The CPS is pre-installed at the FOWT. The dynamic cable penetrates the CPS.

4.2.4 Overview cable configuration

Figure 4.10 presents an overview of the cable configuration modelled in OrcaFlex.

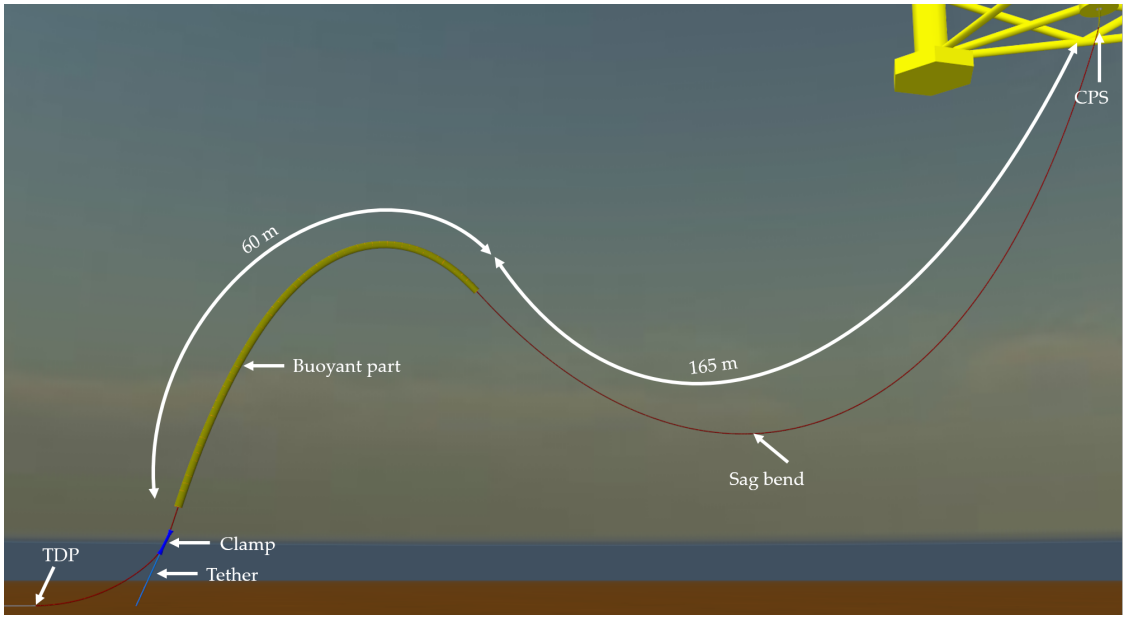

Figure 4.10: Cable configuration in final position

4.3 Floating Offshore Wind Turbine

Modelling of the FOWT is described in this Section.

4.3.1 Input FOWT model

The dimensions presented in Section 3.6 are used as input for modelling the FOWT in Ansys AQWA. Modelling of the FOWT is performed based on Figure 2.13 of Section 2.6.1. The geometry of the FOWT is built in the workbench of Ansys AQWA. The important input parameters are presented in Table 4.3. The COG is defined according to the coordinate system presented in Figure 2.8.

Objects	**Values**	**Units**
Water depth	100	m
Water density	1025	kg/m^2
Total structural mass	1787	mT
COG_x	0	m
COG_y	0	m
COG_z	5.27	m
K_{xx}	24.79	m
K_{yy}	24.79	m
K_{zz}	25.49	m

Table 4.3: Model input parameters Ansys AQWA

The model is meshed program controlled by Ansys AQWA and the used meshing parameters are presented in Table 4.4. Generating a suitable mesh is done experimentally, since decreasing the mesh size results in more accuracy. A mean mesh size of 0.3 m is found as the smallest mesh size the model could calculate without failure. A meshed impression of the geometry below the water surface is presented in Figure 4.11.

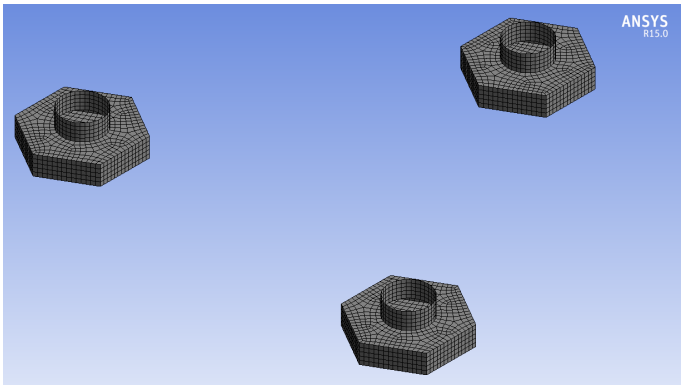

Figure 4.11: Meshed geometry FOWT

Calculation of the response of the FOWT model is performed using waves acting on the model. There are 50 wave periods used in a range from 3.5 to 35 seconds. This range is used to find the natural frequency of the model. The wave periods are combined with a omnidirectional range of wave directions with a interval of 15 degrees. Only one side of wave directions is investigated, since the FOWT is symmetric. The results of the RAO investigation are presented in Section 4.3.2.

Objects	Values	Units
Defeaturing tolerance	0.5	m
Max element size	1	m
Maximum allowed frequency	0.529	Hz
Number of diffracting nodes	4524	–
Number of diffracting elements	4450	–

Table 4.4: Model meshing parameters

4.3.2 Results FOWT model

The hydrostatic results calculated with Ansys AQWA are presented in Table 4.5. The metacentric height of the FOWT is 14.3 m, which implies that the FOWT is very stable.

Objects	Values	Units
COG to centre of buoyancy (COB)	8.8	m
Metacentric height	14.3	m
COB to metacentric point	23.1	m
Restoring moment	76423	$Nm/^\circ$

Table 4.5: Hydrostatic results

The inertia of the reference model, as described in Section 3.6.2, together with the draught are unknown. These input parameters are presented in Table 4.3 and are varied until the RAOs of the model and reference model reach similarity. A draught of 5.6 m resulted in RAOs corresponding to the reference RAOs. The RAOs for all the motions regarding different wave directions are presented in Figure 4.12.

The RAOs of the FOWT show values which are reasonable for such a floater type. A spike, however, around 20 s is noticed after analysing the RAOs. This spike could be driven by a natural period. Another 50 periods from 18 s to 23 s are released on the structure resulting in the graphs presented in Figure 4.13. A natural period for both roll and pitch is found at 20.2 s. This natural period is a typical value for floater types with a semi-submerged structure [4].

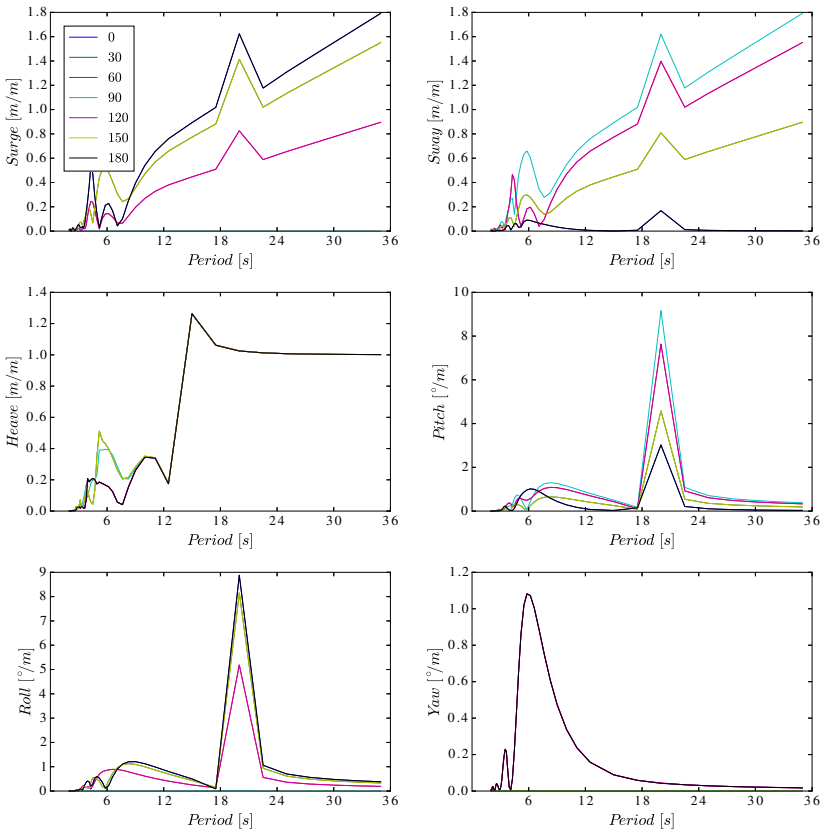

Figure 4.12: RAOs FOWT

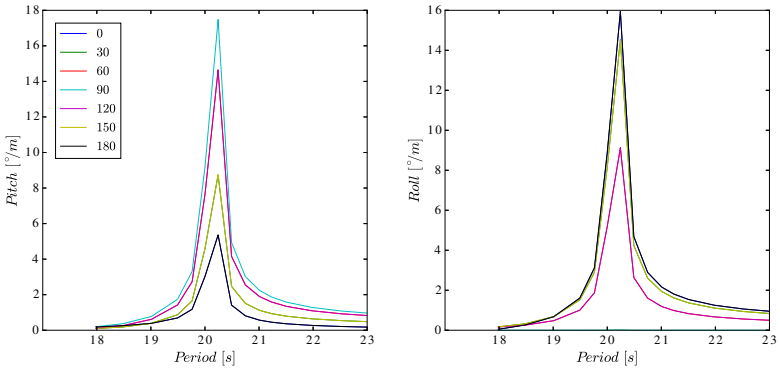

Figure 4.13: Natural period FOWT

4.3.3 Model validation

The RAOs of the model are compared with the RAOs of the reference model, which is described in Section 3.6.2. The reference model only includes heave and roll RAOs for one direction. The compared RAOs for heave and pitch are presented in Figure 4.14.
The compared RAOs show similarity, but a large spike around 20 s is noticed in the FOWT model. The reference model describes a natural period in both roll and pitch direction at approximately 21 s. So the natural periods of both models are almost the same. The spike of the FOWT model is only higher with respect to the reference model. The reference model may include some tricks

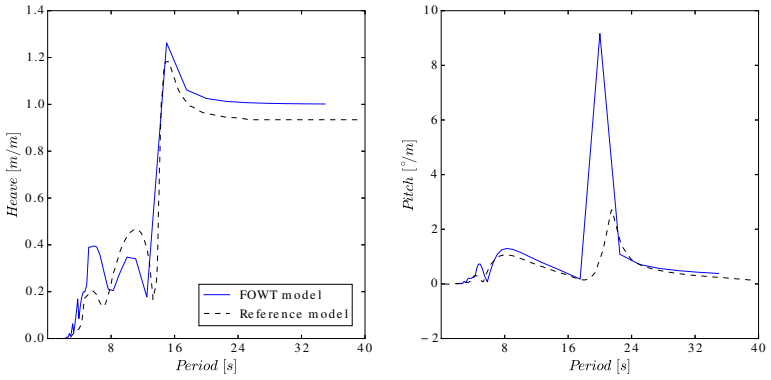

Figure 4.14: Comparison RAOs reference model with FOWT model

to reduce the resonance at the natural period.

However, the large peak in the RAOs of the FOWT model does not influence the results of this research, since the range of wave periods the cable installation takes place is between 4 and 12 s.

4.3.4 Import in OrcaFlex

The RAOs of the FOWT model can be imported in OrcaFlex as load RAOs or as displacement RAOs, both described in Section 2.4.4. The use of displacement RAOs during numerical analysis of the FOWT are preferred based on the following benefits:

- The model is faster with displacement RAOs because it determines at every time step excursions and rotations of the FOWT, based on the harmonic motion behaviour, with a fixed equilibrium position. Load RAOs calculate at every time step the equilibrium of the hydrodynamic loads and all other forces and loads acting on the FOWT, which is time consuming.
- The use of load RAOs requisite a real design of a mooring system to maintain the position of the FOWT. The introduction of mooring lines in the model increases the risk of line clashes and increases complexity of the simulations.

A design of a mooring system consist of several parameters of influence. The design of a suitable mooring system for this FOWT is not available. The creation of a mooring system is time consuming and out of the scope of this research. An investigation is performed to find the influence of second order wave drift forces on the FOWT. This investigation is added in Appendix C. Most important conclusions from this analysis are:

- The design of the mooring system influences only the low frequency motion behaviour of the FOWT.
- Increasing the stiffness of the mooring system reduces second order motions.

Low frequency motions are only existing in irregular sea states, as explaneed in Section 2.3. The cable installation in this research is performed using a regular wave approach. For this reason it is allowed to use displacement RAOs for this research.

4.3.5 Clearance area

The FOWT is imported in OrcaFlex with displacement RAOs as described in Section 4.3.4. The use of the RAOs requires an investigation on the footprint of the FOWT in environmental conditions.

The weakest mooring system, used in the mooring investigation described in Appendix C, is used to determine the footprint of the FOWT. An irregular wave approach with a H_s of 1.5 m and a T_s of 7.85 s is used, combined with the current conditions as described in Section 4.10.5.

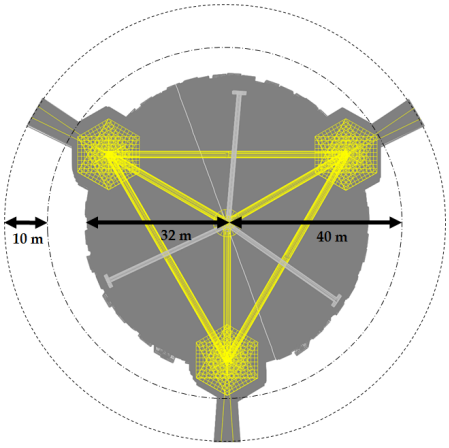

Figure 4.15: Clearance area around the FOWT

The turbine rotated during the footprint test, which resulted in movement area presented in Figure 4.15. The grey area in Figure 4.15 represents the movement of the FOWT, its turbine and the mooring lines. Combining this movement area together with the 10 m minimum vessel clearance regarding the IMCA [28] results in a clearance circle with a radius of 50 m from the centre of the FOWT.

4.4 Cable Lay Vessel Ndurance

Modelling of the CLV is described in this Section.

4.4.1 Input CLV model

The CLV Ndurance is modelled according to the radiation diffraction theory. The Ndurance model is created by VBMS and is used for this research, but confidentially applies. The model is meshed based on the line plan of the CLV. The loading conditions based on the stability book determined the draught of the CLV. A draught of 4.2 m is used in the model.

The hull of the CLV is meshed with an maximum element size of one meter, resulting 5583 elements. An impression of the meshed CLV in Ansys AQWA is presented in Figure 4.16, based on contractors experience to have 6 elements vertical over the draught.
Calculation of the response of the CLV model is performed using waves acting on the model. There are 50 wave periods used in a range from 3 to 30 seconds. Successive spacing is used around the pitch and roll natural frequencies to increase the accuracy of the RAOs. The wave periods are combined with a omnidirectional range of wave directions with a interval of 15 degrees. Only one side of wave directions is investigated, since the CLV is symmetric.

4.4.2 Results CLV model

The results of the RAOs of the CLV are presented in Figure **??** (Confidential).

The CLV is imported in OrcaFlex by the displacement RAOs as calculated in Ansys AQWA.

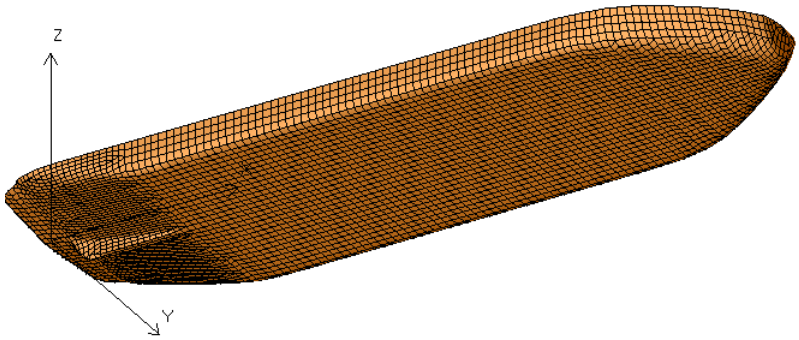

Figure 4.16: Impression Ndurance in Ansys AQWA

The geometry described in Section 3.9 is used to model the CLV in OrcaFlex. Figure 4.17a presents a top view of the stern of the CLV in OrcaFlex and Figure 4.17b a side view of the CLV. The deck of the CLV is modelled longer than the CLV actually is, due to the amount of cable length laying on this deck. The cable is normally stored in a carousel, but this is not modelled in OrcaFlex, since this results in numerical errors. Only the blue part of the deck has deck friction, which represents the cable interacting with the rollerbars.

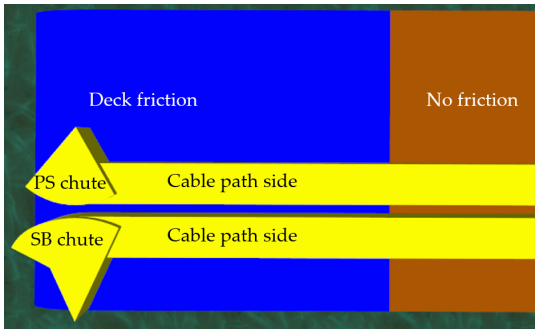

(a) Top view

(b) Side view

Figure 4.17: Impression CLV modelled in OrcaFlex

4.5 Free lay model

The free lay model is created to investigate the cable behaviour during CLV positioning prior to the pull-in operation. The three pull-in methods as described in Section 3.1.3 all have different CLV positioning. The CLV positioning of pull-in method 1 is modelled in the free lay model.

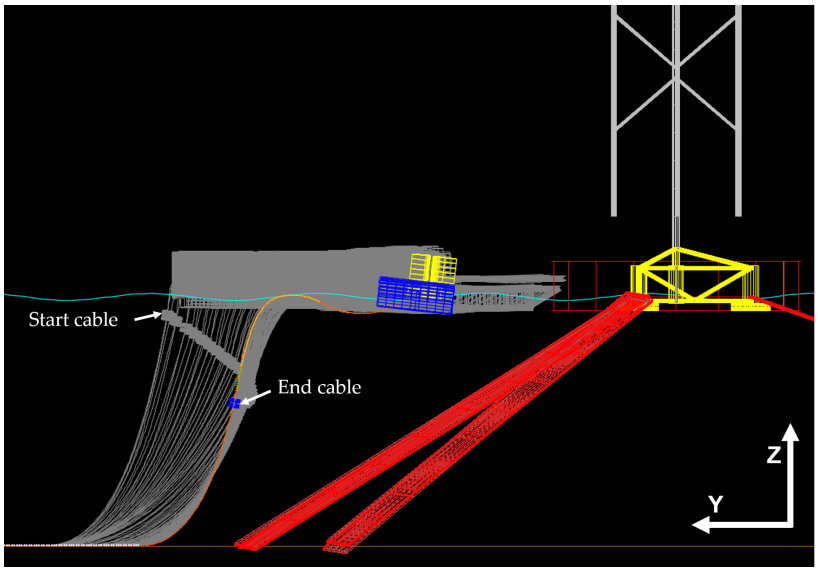

Figure 4.18: Side view of the free lay model

At the start of the model the dynamic cable, with the buoys attached to it, lies on the deck of the CLV. The cable clamp just entering the splash zone behind the CLV. Figure 4.18 presents a side view of the free lay model. The grey cable path visualises the position of the cable during the simulation.

The CLV sails towards the FOWT, until the bow of the vessel is close to the clearance zone of the FOWT. At this moment the CLV makes a turn of 90 degrees, visualised in Figure 4.19. This turn is necessary to get the CLV at the starting position for pull-in method 1. For the other methods the CLV follows the determined cable route while laying down cable on the seabed. There is 128 m cable removed in this model, since this lies on deck of the CLV the entire simulation. This decreases the simulation time without impacting the model. Compression of the cable occurs if the cable interacts with the chute at the stern of the vessel, presented in Figure 5.8. This interaction is avoided by changing the turning rate of the CLV.

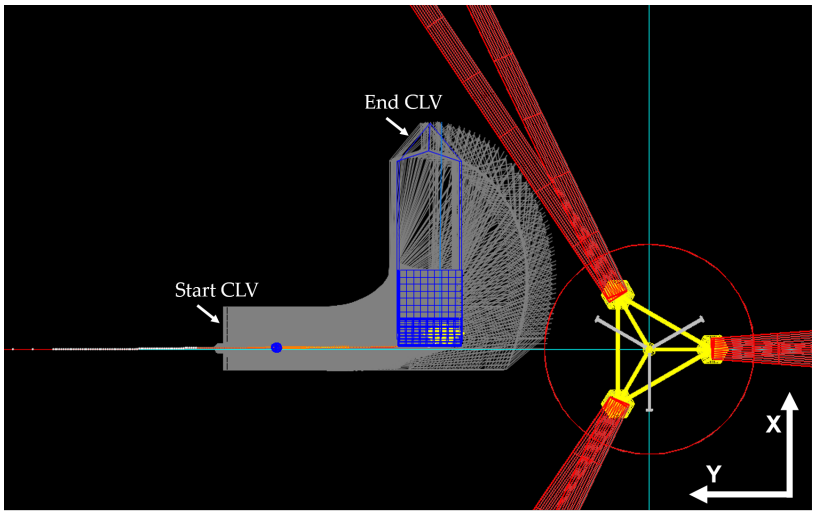

Figure 4.19: Top view of the free lay model

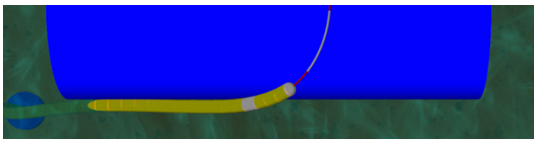

(a) Before changing of turn CLV

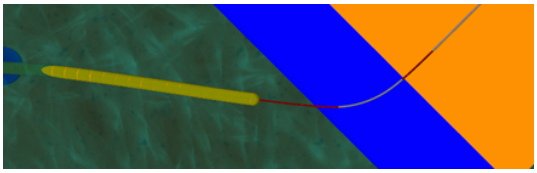

(b) After changing turn CLV

Figure 4.20: Cable chute interaction

4.5.1 Stages Description

The freelay model is created using the stages presented in Table 4.6, in which the *Dir* column of the CLV explains the sail direction.

Stage	**Start**	**End**	**Pay-out**	**CLV**		
$[-]$	$[s]$	$[s]$	$[m]$	**Sails** $[m]$	**Dir** $[°]$	**Turns** $[°]$
0	-25	0	-	-	-	-
1	0	300	13	30	-90	-
2	300	900	5	-	-	90
3	900	1549	78	64.9	-90	-
4	1549	1559	-	0.5	0	-
5	1559	1659	1.1	-	-	-

Table 4.6: Stage description freelay

4.6 Method 1: Pull-in in pre-installed FOWT model

The model created to simulate pull-in method 1 is described in this Section.

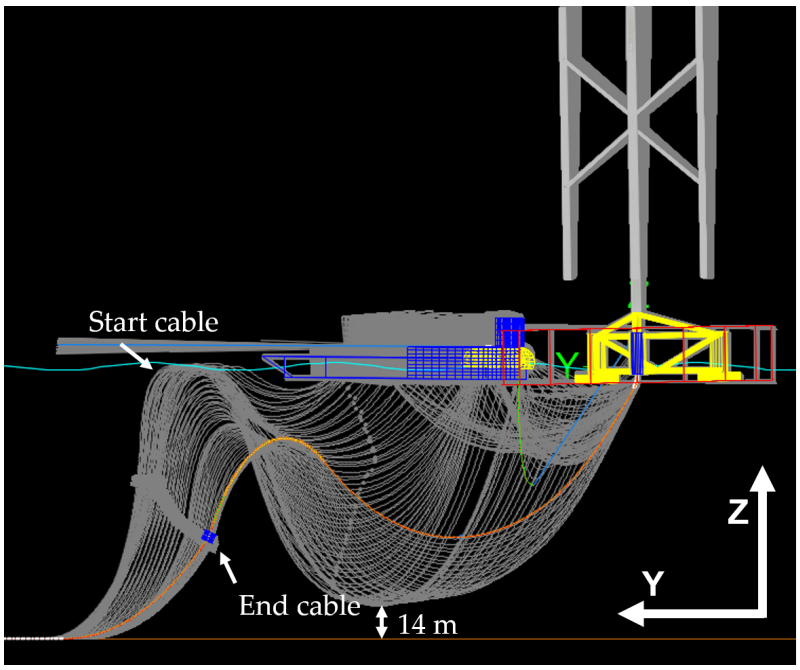

Figure 4.21: Side view of the pull-in in pre-installed FOWT model

The starting position of the cable is the end position of the free lay model as described in Section 4.5. Figure 4.21 presents the cable path over the simulation of the model. The lowest part of the cable remains approximately 14 meters above the seabed.

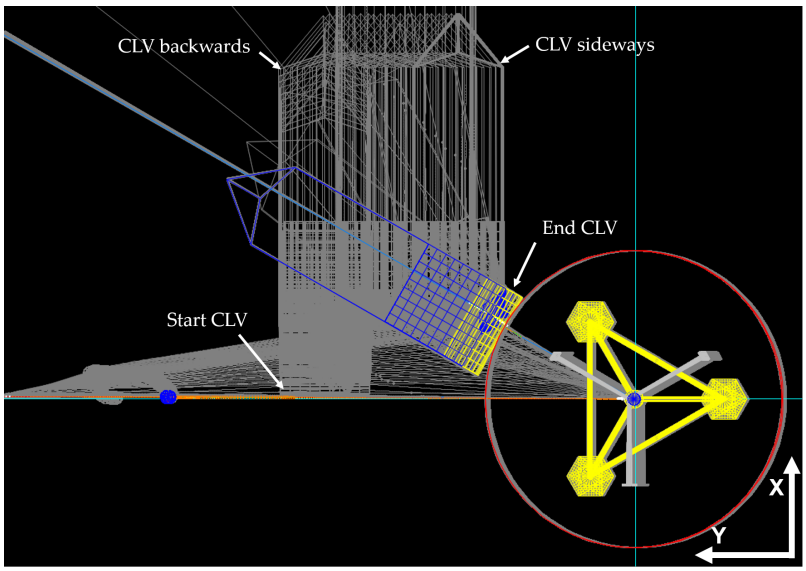

Figure 4.22: Top view of the pull-in in pre-installed FOWT model

Figure 4.22 presents the top view of method 1. The CLV sails backwards and sideways to come as close by as possible to the FOWT. This movement is necessary to ensure enough seabed clearance.

After the pullhead is in the water the CLV makes another turn in order to get the cable closer to the FOWT. The pull-in is controlled by a system for the winches, described in Section 4.6.1.

4.6.1 Winches control system

Controlling of the winches for this pull-in method is based on the results presented in Figure 4.6 of Section 4.1.7. The Figure shows that pull-in from the left side of the FOWT and ensuring 10 m seabed clearance is only possible if the pull-in is performed without a tether. This means that the tether will be installed after the pull-in is completed. The control system is only influenced by the ahead conditions.

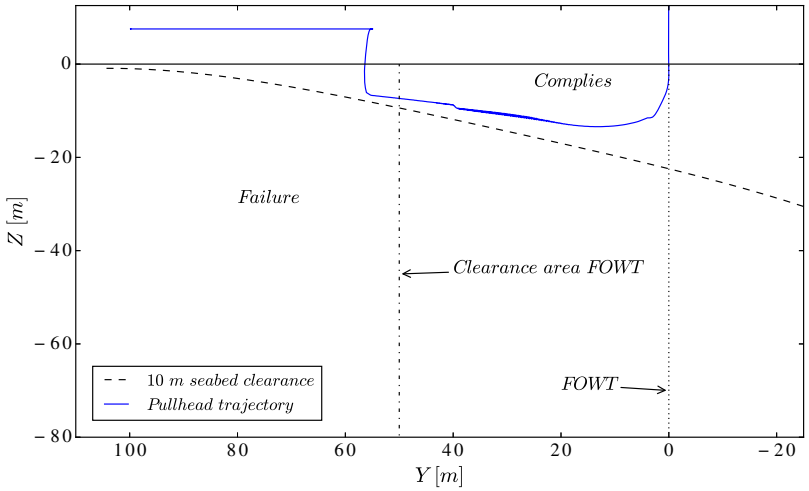

Figure 4.23: Control system winches method 1

Figure 4.23 presents the 10 m seabed clearance from the ahead condition and the trajectory of the pullhead during installation, without environmental conditions. It is visible that the pullhead does not cross the limit. The limit is calculated with a script, added in Appendix **??**. The system is controlled via an external script, added in Appendix **??**. The regulation of the system is presented in Table 4.7. The rate of the winches is chosen based on contractors experience.

Object	Rate above limit $[m/s]$	Rate below limit $[m/s]$
Pull-in winch	-0.09	-0.09
Pay-out winch	0.1	0

Table 4.7: System regulation Method 1

4.6.2 Stages Description

Similar to the freelay model in Section 4.5.1 is pull-in method 1 modelled using the stages presented in Table 4.8.

Stage	**Start**	**End**	**Pull-in**	**Pay-out**	**CLV**		
$[-]$	$[s]$	$[s]$	$[m]$	$[m]$	**Sails** $[m]$	**Dir** $[°]$	**Turns** $[°]$
0	-25	0	-	-	-	-	-
1	0	220	-33	24.5	22	0	-
2	220	670	-61	45	45	-90	-
3	670	1150	-65	48	-	-	-
4	1150	1300	-20	5	-	-	-
5	1300	1400	-9.5	1	12	250	60
6	1400	2300	-73	39	-	-	-

Table 4.8: Stage description pull-in method 1

4.7 Method 2: Post-lay pull-in via CLV model

The model created to simulate pull-in method 2 is described in this Section.

Storage of the cable in a favourable direction is used in pull-in method 2, presented in Figure 3.7c. This method is chosen based on the accessibility regarding the direction of the cable configuration in combination with the restrictions due to the mooring system of the FOWT.

The starting position of the cable is marked in Figure 4.24. The CLV recovers the cable from the seabed and sails towards the FOWT in a straight line which is similar to the angle the cable end makes with the coordinate system, presented in Figure 4.24.

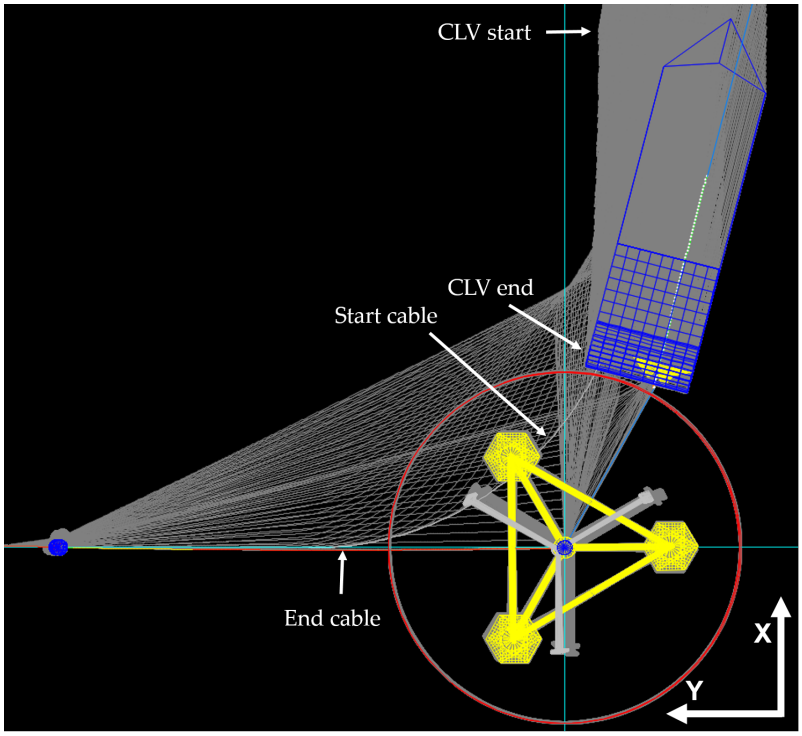

Figure 4.24: Top view of the post-lay pull-in via CLV model

Figure 4.25 presents a side view in the $ZY-plane$ of the model. At the start of the simulation the CLV starts recovering the cable.

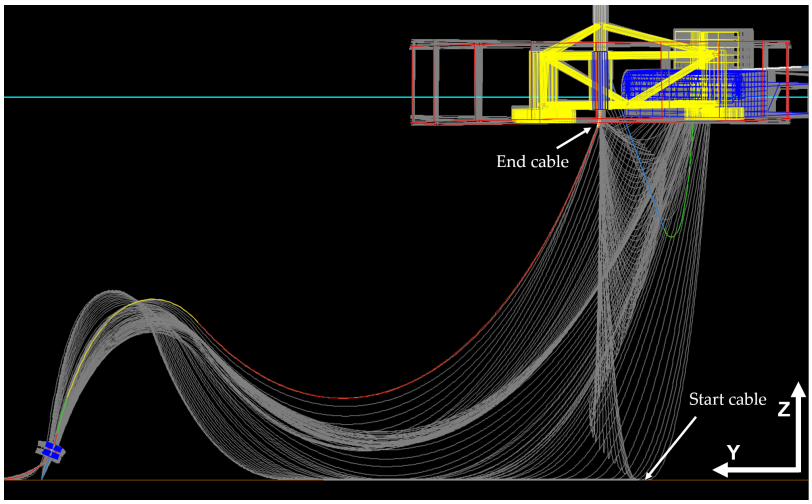

Figure 4.25: Side view $ZY - plane$ of the post-lay pull-in via CLV model

Figure 4.26 presents another side view in the $ZX - plane$ of the model. Recovery of the cable and sailing backwards of the CLV is visible in this Figure. The interaction between the cable, pull-in and pay-out winch is marked in this Figure.

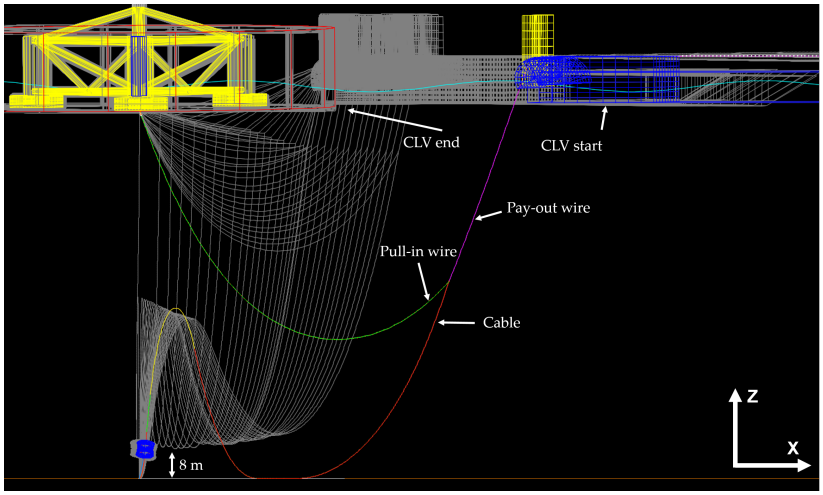

Figure 4.26: Side view $ZX - plane$ of the post-lay pull-in via CLV model

The cable is recovered from the seabed prior to the pull-in. Figure 4.25 presents the seabed clearance during transferring of the cable from the CLV towards the FOWT. The seabed clearance of 10 m is not possible in this pull-in method. The reason for this is described in Section 4.7.1.

4.7.1 Control system of the winches

Controlling of the winches for this pull-in method is based on the results presented in Figure 4.6 of Section 4.1.7. The cable tether is installed prior to the pull-in with aid of the CLV, since the tether ensures integrity of the cable configuration during the storage period.

The dotted lines in Figure 4.27 represent the 0 m and 10 m seabed clearance, respectively, taken

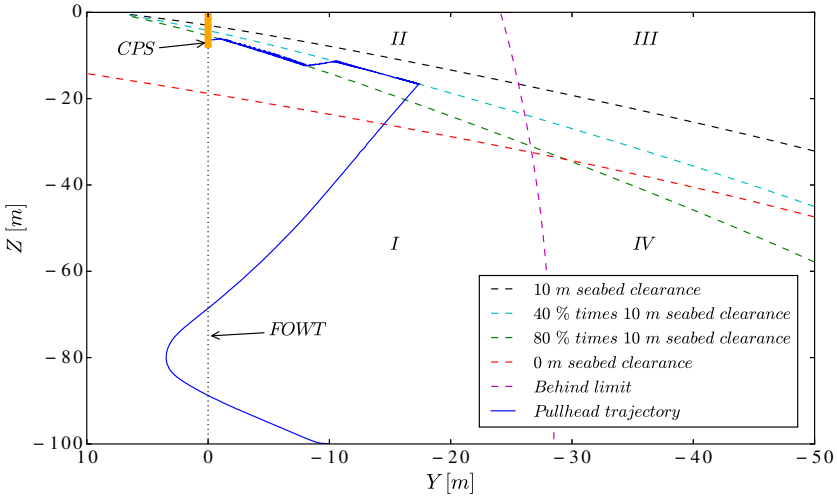

Figure 4.27: Control system winches pull-in method 2

from the ahead condition of Section 4.1.7. Ensuring 10 m seabed clearance is not possible for this pull-in method since the clearance line is above the entrance of the CPS. For this reaseon the pullhead is transferred lower than the 10 m seabed clearance line. The system is allowed to be 40 percent lower than the 10 m seabed clearance line from the position after recovery until a Y value of -10.5 m has been reaced. The pullhead is allowed to be 80 percent lower than the 10 m seabed clearance line afterwards, presented in Figure 4.27. This is necessary to successfully perform the pull-in. This makes it possible that the system transfers the cable towards with the largest seabed clearance possible.

Figure 4.27 also presents the behind limit. This limit is not exceeded in the base case of the model. The trajectory of the cable pullhead is marked blue in Figure 4.27. The trajectory moves in 3D but only a side view is presented here.

Area	Ahead condition	Behind condition	Cable failure	Pull-in rate $[m/s]$	Pay-out rate $[m/s]$
I	Unstatisfied	Statisfied	No	0	-0.1
II	Statisfied	Statisfied	No	-0.1	0.1
III	Unsatisfied	Unsatisfied	Yes	0	0.1
IV	Unsatisfied	Unsatisfied	Yes	0	0.1

Table 4.9: System regulation pull-in method 2

Table 4.9 presents the winch rates of the control system for the winches. Theses rates are chosen based on contractors experience. Calculations of the limits in performed by a script added in Appendix **??**. The winches in OrcaFlex are controlled via an external script added in Appendix **??**.

4.7.2 Stages Description

Pull-in method 2 is also modelled using the stages presented in Table 4.10.

Stage [−]	Start [s]	End [s]	Pull-in [m]	Pay-out [m]	CLV		
					Sails [m]	Dir [°]	Turns [°]
0	-25	0	-	-	-	-	-
1	0	1920	-65	-128.9	-96	10	-4.8
2	1920	3420	-69	29	-	-	-

Table 4.10: Stage description pull-in method 2

4.8 Method 3: Post-lay pull-in via FOWT model

The model created to simulate pull-in method 3 is described in this Section.

The s-lay storage method is chosen for this pull-in method. This storage method, presented in Figure 4.28, is used to keep the pullhead of the cable before the point at the seabed perpendicular under the entrance point of the CPS.

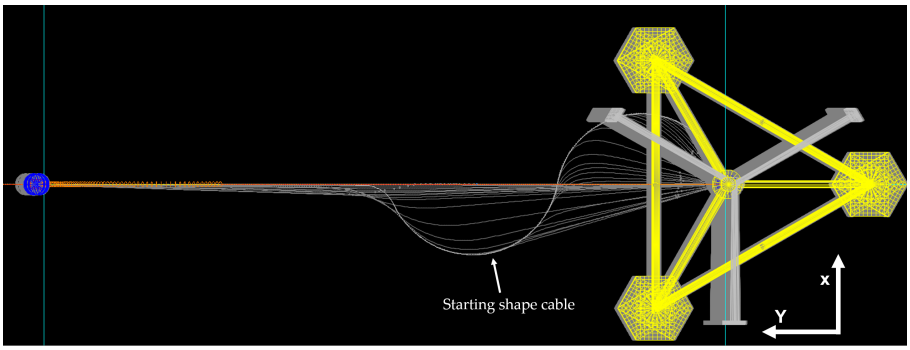

Figure 4.28: Top view of the post-lay pull-in via FOWT model

Recovery of the cable is performed by a pull-in winch which is installed on the FOWT. No advanced system is necessary to perform the pull-in. The pull-in winch has a constant pull-in velocity of 0.1 [m/s]. The pull-in of the cable is presented in Figure 4.29.

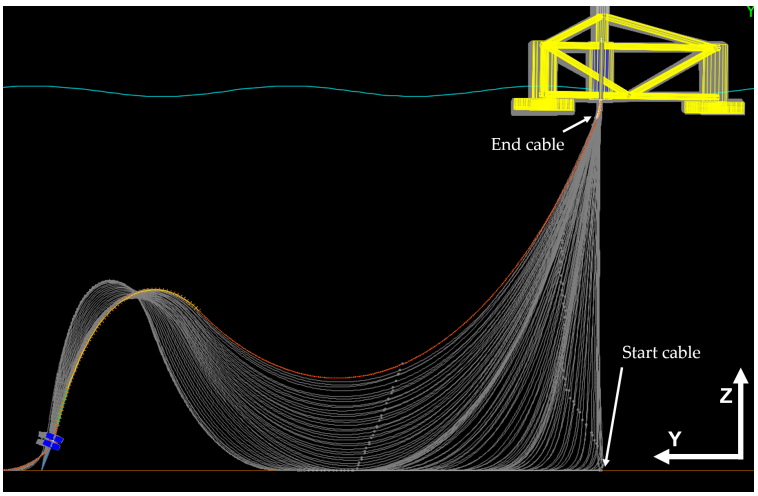

Figure 4.29: Side view of the post-lay pull-in via FOWT model

4.8.1 Stages Description

Pull-in method 3 is also modelled using the stages presented in Table 4.11.

Stage $[-]$	**Start** $[s]$	**End** $[s]$	**Pull-in** $[m]$
0	-25	0	-
1	0	2000	-113.5

Table 4.11: Stage description pull-in method 3

4.9 Boundary conditions

The boundary conditions at which the models are run are described in this Section. Included are the environmental conditions, the limitations and a description of the workability calculation.

4.10 Environmental conditions

4.10.1 Weather restricted operation

The installation of power cables is generally defined as a weather restricted operation according to DNV [17]. This means that each operational step in an installation procedure may be executed safely within the time frame of a 72 hour weather forecast. The characteristic environmental conditions under which the operation may be carried out, are determined by the installation contractor.

4.10.2 Project location

The location of the wind farm is off the coast of Southern France, close to Marseille, near the entry of the Golf of Fos, visualised in Figure 4.30. The wind farm is located in nautical zone number 26, which determines the long term wave distribution parameters, presented in Appendix E.

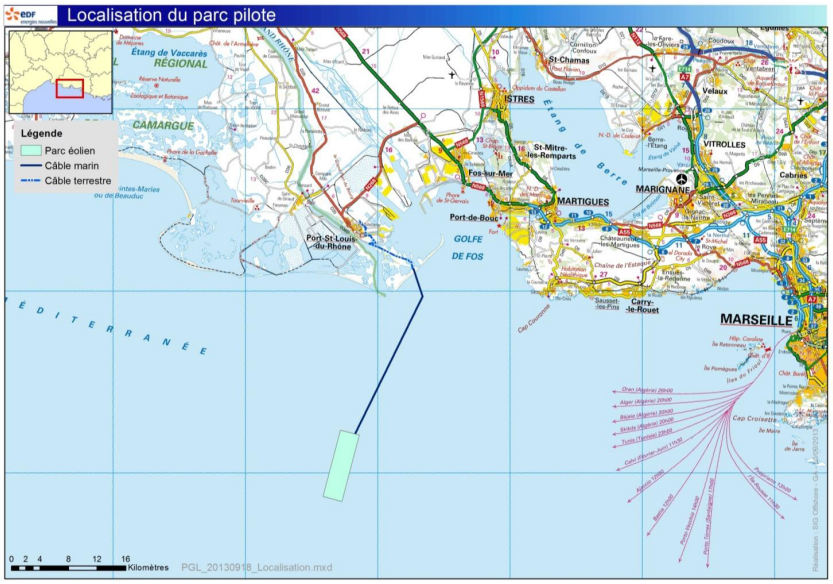

Figure 4.30: Location of the floating wind farm [13]

The western basin of the Mediterranean Sea is characterised by long periods of calm conditions alternating with sudden strong gales. This location is exposed to the frequent occurrence of the Mistral. The wind generated by this Mistral can be very strong and unstable. The waves generated by the wind, coming from the sea, may be very severe due to the long fetches. Sea states with a significant wave height above four meters are not exceptional at this location. Data from the locations showed a peak enhancement factor, γ of 1.4 for the return period of one year. This peak enhancement factor indicates a wide banded spectrum. The mean water depth on this location is 100 m.

4.10.3 Wave height

A wave scatter of the location is created to get insight in the sea-states on location and is presented in Appendix E. A summary of the wave scatter is presented in Table 4.12 with the chosen sea-states boxed.

	T_z $[s]$						
H_s $[m]$	**3.0**	**3.5**	**4.0**	**4.5**	**5.0**	**5.5**	**6.0**
0.25	**2362**	**2804**	**2466**	**1777**	**1119**	**641**	**344**
0.5	**1674**	**2557**	**2783**	**2412**	**1785**	**1181**	**721**
0.75	**1109**	**2022**	**2552**	**2510**	**2074**	**1512**	**1006**
1.0	**717**	**1510**	**2148**	**2338**	**2109**	**1660**	**1182**
1.25	**457**	**1091**	**1721**	**2044**	**1986**	**1668**	**1258**
1.5	288	**771**	**1334**	**1713**	**1779**	**1583**	**1254**

Table 4.12: Wave scatter area 26

Three significant wave heights are used in the dynamic analysis, to check a range in workability. When using regular waves, the design wave approach is implemented. The wave height of the regular waves is defined by the maximum wave height as explained in Section 2.2.2. The relation between H_{max} and H_s is defined in Equation 2.16 and repeated here:

$$H_{max} \approx 1.86 \cdot H_s \tag{4.1}$$

4.10.4 Wave period

For each H_s three T_z, are chosen as marked in Table 4.12. Since the wave scatter is generated with a T_z is the T_p curve-fitted based on the peak enhancement factor, γ, described by DNV [22]:

$$\begin{aligned} \frac{T_z}{T_p} &= 0.6673 + 0.05037\gamma - 0.006230\gamma^2 + 0.0003341\gamma^3 \\ \frac{T_{m1}}{T_p} &= 0.7303 + 0.04936\gamma - 0.006556\gamma^2 + 0.0003610\gamma^3 \end{aligned} \tag{4.2}$$

For a peak enhancement factor of $\gamma = 1.4$ the T_p is:

$$T_p = 1.376417007 \cdot T_z \tag{4.3}$$

The equivalent peak periods are calculated using Equation 4.3.

$$T_s \approx 0.95 \cdot T_p \quad \text{(for wind dominated seas)} \tag{4.4}$$

The T_s belonging to the T_p is calculated according to Equation 4.4, since the location used in this research is dominated by a wind-sea spectrum.

Total overview of used maximum wave heights with corresponding significant wave periods are given in Table 4.13.

H_s $[m]$	H_{max} $[m]$	T_z $[s]$	T_p $[s]$	T_s $[s]$
0.5	0.93	3.0	4.13	3.92
		4.0	5.51	5.23
		5.0	6.88	6.54
1.0	1.86	3.5	4.82	4.58
		4.5	6.19	5.88
		5.5	7.57	7.19
1.5	2.79	4.0	5.51	5.23
		5.0	6.88	6.54
		6.0	8.26	7.85

Table 4.13: Wave properties

The wave conditions apply for every wave direction (dir), θ_{wave}. The wave directions are distributed uniformly in 30 degree bins. To total amount of simulations performed for every model is calculated by:

$$n_{H_{max}} \cdot n_{T_s} \cdot n_{\theta_{wave}} = 3 \cdot 3 \cdot 12 = 108 \quad \text{simulations} \tag{4.5}$$

4.10.5 Current

The tidal stream at the location is very weak and negligible with respect to the wind driven current. Metocean data of the location showed surface current velocities with different return periods presented in Table 4.14.

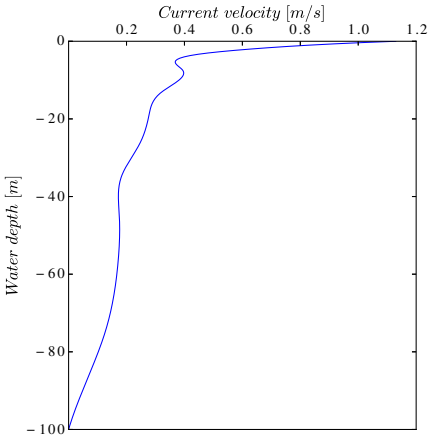

Figure 4.31: Current profile [13]

Return period [years]	Surface current [m/s]
1	1.12
50	1.58

Table 4.14: Current values [13]

Since the installation is a weather restricted operation with a short forecast window, the surface current value for 1 year is used in this research. The current has a profile presented in Figure 4.31 with decreasing velocity with increasing depth. The current direction is taken omni-directional and collinear with the wave direction.

4.10.6 Drag and added mass

The drag coefficients used in the models are Reynolds number dependent. This gives a more realistic description with respect to a constant drag coefficient based on DNV [29]. A combined

drag coefficient dependent on Reynolds number and Keulegen-Carpenter number is the most realistic solution, however this is not possible in OrcaFlex. The used graph for the drag coefficients in OrcaFlex is presented in Figure 4.32. OrcaFlex extrapolates the Reynolds drag coefficients to both sides of the graph if the Reynolds number in the calculation is outside the range of the Reynolds numbers given in Figure 4.32.

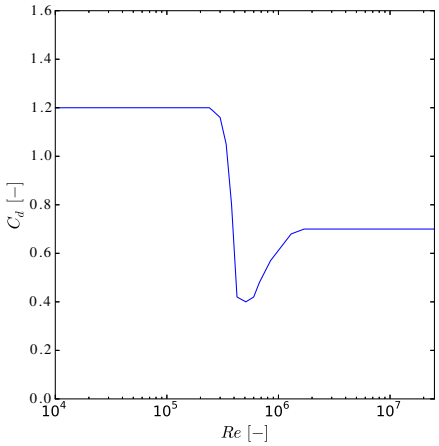

Figure 4.32: Reynolds dependent drag coefficient

A added mass coefficient of 1.0 is chosen for the cable, according to DNV [29]. The define this added mass coefficient for a cylinder with a infinite length over radius ratio. This is valid for cable in cable installation calculations.

4.10.7 Wind load

Wind load should only be considered particularly during operations close to platforms. Wind loads have limited influence on the cable behaviour, since the cable is mainly below the water surface. Although wind load is not considered directly in the dynamic installation analyses, it affects vessel heading and station keeping. Since station keeping is not part of this research, it is assumed that the contractor includes the wind loads in the station keeping assessment.

4.10.8 Friction coefficients

The pull-in method models include interaction between the cable and several equipment. Forces on the cable due to this interaction are included by using friction coefficients. The friction coefficients are based on the interaction between materials.

Modelling of the cable clamp is performed by line-in-line contact. To ensure that the cable stays in the clamp a friction coefficient of 1000 is used. Pulling of the cable trough the CPS has a friction coefficient of 0.3, since the CPS bends during the cable pull-in and abutment of the cable in curves contributes to this friction factor. Pulling of the cable over the chute has a friction coefficient of 0.1, because both will be made wet during installation. Friction of the cable on the deck is prevented by using rollers. These rollers have a friction coefficient with the cable of 0.05. Pulling of the cable through the a steel I-tube has a friction coefficient of 0.3, because of the narrow diameter combined with cable interacting with steel.

The seabed on location is influencing the installation of the cable. The soil on location is assumed as sand, based on documentation of the project. The axial friction factor is assumed 0.5 based on contractors experience. The relief of the seabed is unknown. Two pull-in methods make use of a storage period, so for this reason an additional factor is included for the bulldozing effect.

Bulldozing effect is a result of sideways movement of the cable creating small hills of sand which give an additional resisting force on the cable. A normal friction coefficient of 1.0 is added to include this effect. A summary of the friction coefficients is presented in Table 4.15.

	Friction coefficient	
Objects	Axial [−]	Normal [−]
Inside cable clamp	1000	1000
Inside CPS	0.3	0.3
Chute CLV	0.1	0.1
Deck CLV	0.05	0.05
Inside I-tube	0.3	0.3
Seabed	0.5	1.0

Table 4.15: Friction coefficients

4.11 Limitations

This Section presents a summary of the limitations used to create the models, presented in Table 4.16, and the limitations on which the models are tested, presented in Table 4.17. These limitations are used to check if a certain sea state is suitable for the cable installation. If the limits are exceeded, cable integrity can not be ensured.

Limitations	**Values**	**Units**
Clearance between the CLV and the centre of the FOWT	50	m
Seabed clearance	10	m
Cable clearance with the braces of the FOWT	5	m

Table 4.16: Limitations influencing building of the models

Limitations	**Values**	**Units**
Minimum cable tension	0	kN
Maximum cable tension	300	kN
Maximum cable curvature	0.33	$-$
Maximum pull-in tension	120	kN
Maximum pay-out tension	150	kN
Maximum bottom tension	20	kN
Maximum bending moment in CPS	150	kNm
Maximum tension in tether	150	kN
Maximum cable offset from centre line	± 5	m
Structure interaction	0	m
Seabed clearance	10	m

Table 4.17: Limitations tested for all models

4.12 Indication workability

The wave scatter used in this research does not include the wave scatter for every direction. The distribution of wave scatter over the wave directions is assumed equal, so the amount of waves

is divided by 12 directions. Normally the distribution is based on a dominant wave direction. A dominant wave direction could be based on the project location, but the orientation of the wind farm regarding this dominant wave direction is unknown. For this reason an equal distribution over the wave directions is chosen as presented in Figure 4.33.

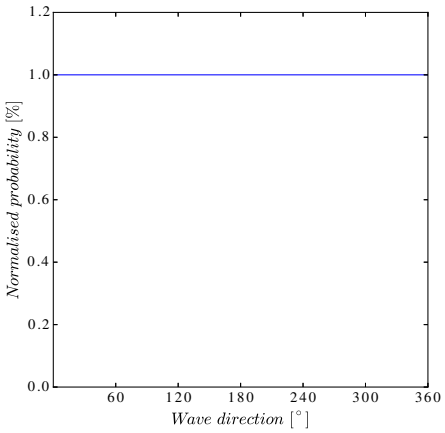

Figure 4.33: Wave scatter distribution

In this research only the percentage based on the investigated sea states is taken. So if the workability of a method is all positive in the investigated sea states, it gets 100 percent. This approach is not valid for the total workability, but it gives a indication of the differences in workability for the methods investigated in this research.

CHAPTER 5

Results & Discussion

In this Chapter the results of the models as described in Chapter 4 are presented and discussed. The results are given for the base cases of the different models. The base case is the total simulation without environmental conditions. First, the results of the free lay model are described extensive, in order to show how the results are post-processed, since the free lay model is applicable for all pull-in methods. Model specific results per pull-in method are described afterwards. This Section contains multiple range graphs of different output parameters. A range graph shows the minimum, mean and maximum values of an output parameter for each node along the length of the cable during a specified time interval. For all range graphs shown in this Chapter the pullhead is located at a cable length of 0 m. The anchor point is located at 360 m cable length for the free lay model and 488 m cable length for the pull-in methods.

5.1 Free lay results

In this Section the results of the free lay model are described. Table 5.1 represents the failure modes for which all cases are tested in the free lay model. Firstly, the workability is given to have an indication which failure modes are occurring. Furthermore the minimum and maximum effective tensions in the cable for the base case are described. The failure mode cable compression is described afterwards. Next is the curvature of the cable in the base case followed by a description of exceeding of the maximum curvature. The last part contains the tension in the winches, the bottom tension, offset of the cable and structure interaction in the free lay model, to explain the results of these objects found in the dynamic analyses. The results of the limitations which are presented in Table 5.1 and not covered in this Section are added to Appendix F.1.

Number	Limitation
1	Successive sea state
2	Cable compression
3	Exceeding maximum cable tension
4	Exceeding maximum cable curvature
5	Maximum pay-out tension
6	Exceeding maximum bottom tension
7	Exceeding maximum cable offset
8	Structure interaction

Table 5.1: Failure modes on which the free lay model is tested

5.1.1 Workability

The workability of an installation operation determines the possibility to successfully perform the installation in a certain sea state. The workability of the free lay model is presented in Table 5.2. The workability of this method is 40 percent related to the used environmental conditions, calculated according to Section 4.12. The numbers in Table 5.2 represent the failure modes on which the cases are failed, corresponding to the explanation as already presented in Table 5.1. The workability indicates that exceeding of the minimum effective cable tension and maximum curvature are the only failure modes found in the free lay model.

	$H_{max} = 0.93[m]$			$H_{max} = 1.86[m]$			$H_{max} = 2.79[m]$		
Dir/T_s	$3.92[s]$	$5.23[s]$	$6.54[s]$	$4.58[s]$	$5.88[s]$	$7.19[s]$	$5.23[s]$	$6.54[s]$	$7.85[s]$
0°	1	1	1	2	2	2	2 & 4	4	2
30°	2	1	1	2 & 4	2	2 & 4	2 & 4	2 & 4	2 & 4
60°	1	1	1	2	2	1	2 & 4	2 & 4	2
90°	1	1	1	2	1	2	2	2	4
120°	1	1	1	2	1	1	2	2	2
150°	1	1	1	2	1	1	2	2	2
180°	1	1	1	1	2	2	2	2	2
210°	1	1	1	2	2	2	2	2	2
240°	1	1	1	2	2	1	2	2	2
270°	1	1	1	2	2	2	2	2	2
300°	2	1	1	2 & 4	2	1	2 & 4	2	2
330°	2	1	1	2	1	2	2 & 4	2	2

Table 5.2: Workability free lay [−]

5.1.2 Cable tension in the base case

The minimum and maximum effective tension over the cable length for the base case are presented in Figure 5.1. The minimum effective tension is higher than the minimum required effective tension of 0 kN, so cable compression is not observed in the base case. The maximum effective tension is below the maximum tension of 300 kN. The upward spike in Figure 5.1 is a result of the weight of the cable clamp which is attached to the cable, resulting in larger local tension. There is a difference between the amplitudes of the spike for the minimum, mean and maximum, since the cable tether is not installed. The cable moves free in the water since this cable tether is not installed in the free lay model.

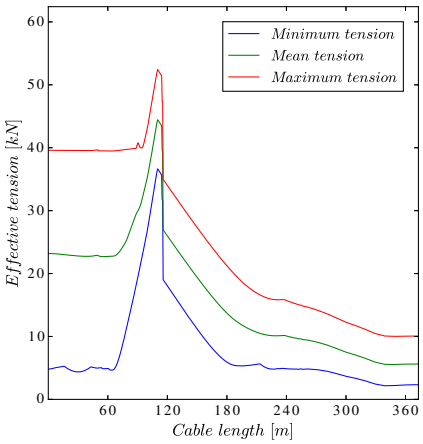

Figure 5.1: Effective tension of the cable

The maximum effective cable tension is not exceeded for the cases with environmental conditions. For this reason the Table with the maximum effective cable tension is added to Appendix F.1.

5.1.3 Cable compression

Cable compression is a failure mode which is a common issue in subsea power cables. The results of the workability in Table 5.2 indicates that cable compression has a significant contribution limiting the workability of the free lay model. An explanation for the cable compression in the free lay model is presented in this Section.

The result of the minimum cable tension for the cases with environmental conditions are presented in Table 5.3. This Table indicates cable compression in multiple cases. The boxed case in Table 5.3, which has the lowest minimum effective tension of $-31.4\ kN$, is analysed in more detail to investigate the cause of this compression, presented in Figure 5.2.

	$H_{max} = 0.93[m]$			$H_{max} = 1.86[m]$			$H_{max} = 2.79[m]$		
Dir/T_s	$3.92[s]$	$5.23[s]$	$6.54[s]$	$4.58[s]$	$5.88[s]$	$7.19[s]$	$5.23[s]$	$6.54[s]$	$7.85[s]$
0°	3.8	4.6	4.4	-0.1	-0.8	-4.7	-10.6	0.2	-4.0
30°	-0.2	1.9	4.9	-1.6	-4.1	-10.4	-3.2	-11.9	-11.2
60°	0.5	3.2	4.1	-4.2	-1.5	1.3	-2.1	-1.8	-0.2
90°	0.7	3.8	2.0	-2.1	1.2	-1.2	-3.7	-5.7	1.2
120°	0.9	3.3	4.1	-2.8	2.4	1.6	-6.8	-4.3	-1.8
150°	1.3	1.0	2.9	-1.4	2.8	1.8	-3.0	-4.0	-5.6
180°	3.5	5.1	5.1	1.0	-0.8	-3.4	-1.4	-1.8	-3.4
210°	1.5	4.0	4.6	-3.4	-1.0	-5.5	-10.6	-10.3	-7.7
240°	0.3	1.6	3.2	-7.5	-1.9	1.6	-12.3	-13.1	-2.3
270°	1.4	2.8	2.0	-17.9	-6.6	-1.8	$\boxed{-31.4}$	-17.8	-7.3
300°	-1.8	2.5	2.8	-13.2	-6.7	0.8	-15.5	-6.7	-2.6
330°	-2.1	3.0	4.2	-9.0	1.3	-1.4	-21.9	-17.3	-1.8

Table 5.3: Minimum cable tension free lay model $[kN]$

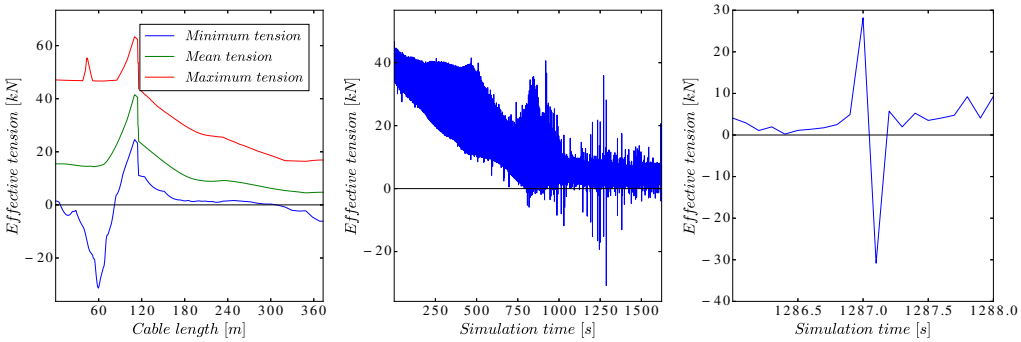

(a) Tension over cable length (b) Tension over time (c) Close-up of the maximum spike

Figure 5.2: Compression results free lay model

A range graph of the effective tension over the cable length corresponding to the boxed case is presented in Figure 5.2a. The downward spike around cable length at 58 m is located in the cable section where the DBMs are located. A time series of the effective tension in the corresponding node is presented in Figure 5.2b. This graph indicates that compression occurs multiple times during the simulation. A close up of the maximum downward spike in the time series between 1286 s and 1288 s is presented in Figure 5.2c. This spike goes in one time-step of 0.1 s from 29 kN to -31 kN and immediately back to positive tension. This spike indicates that large oscillations in very short time periods may cause numerical inaccuracies in OrcaFlex's implicit solving scheme.

A maximum time-step of 0.1 s is used for the implicit solving scheme in OrcaFlex for the free lay model. The implicit solving scheme is used instead of the explicit solving scheme, since the implicit solving scheme is unconditionally stable and thus larger time-steps can be used. The required maximum time-step using the explicit solving scheme is related to $1/10^{th}$ of the shortest natural nodal period of the cable which is 41E−6 s for this cable configuration. In general, larger time steps result in shorter simulation times. The implicit method is therefore the default setting for OrcaFlex's solving scheme. The influence of the used maximum time-step on the cable compression results is compared to the results for a smaller maximum time-step of 0.05 and 0.01 using the implicit solving scheme. The results using a maximum time-step of 0.05 s does not show improvement and are not showed in this research. The results of the boxed case with a maximum time-step of 0.01 s are presented in Figure 5.3.

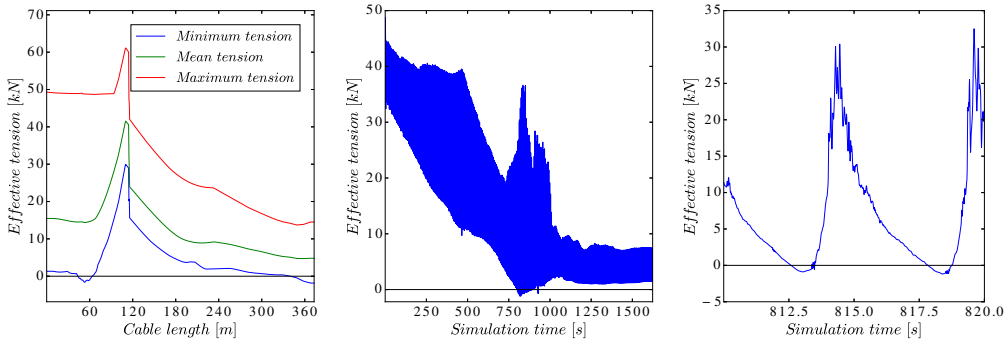

(a) Tension over cable length (b) Tension over time (c) Close-up of compression period

Figure 5.3: Compression results with a maximum time-step of 0.01 s

Figure 5.3a presents a range graph of the effective tension over the cable length. Especially the results of the minimum effective tension in Figure 5.3a are different compared to the results in Figure 5.2a, since cable compression is less noticed. A time series of the effective tension of the node corresponding to a cable length of 58 m is presented in Figure 5.3b. The maximum spike as observed in Figure 5.2c has disappeared, which proves that this spike is caused by numerical errors. However, cable compression is still found in Figure 5.3b. A close-up of a interval in which cable compression occurs is presented in Figure 5.3c. The cable compression oscillations observed in Figure 5.3c have a longer period, which looks more realistic compared to the compression oscillations presented in Figure 5.2c. An explanation for the longer compression oscillations by decreasing the maximum time-step is investigated in Figure 5.4.

Figure 5.4a presents the interaction scheme during the simulation time for the boxed case using a maximum time-step of 0.1 s, which has been used for the cases with environmental conditions. The maximum number of iterations per time-step is 20 and Figure 5.4a shows that this maximum number is reached often. OrcaFlex reduces the maximum time-step with a factor two if the maximum number of iterations is reached. The chance of a numerical error is higher if OrcaFlex has to reduce the time-step by itself, which is a result of the variable time-step algorithm in OrcaFlex. The implicit solver iteration count when using a maximum time-step of 0.1 s is presented in Figure 5.4b. The average of the number of iterations in Figure 5.4b is significantly lower compared to the number of iterations observed in Figure 5.4a. This indicates that there is a correlation between the number of iterations and the number of oscillations.

The comparison between the maximum time-steps indicates that the results of the minimum cable tension presented in Table 5.3 could be better when a maximum time-step of 0.01 s instead of 0.1 s is used. The cases with environmental conditions are simulated again to investigated if this change in maximum time-step decreases the compression for all cases. The results of the

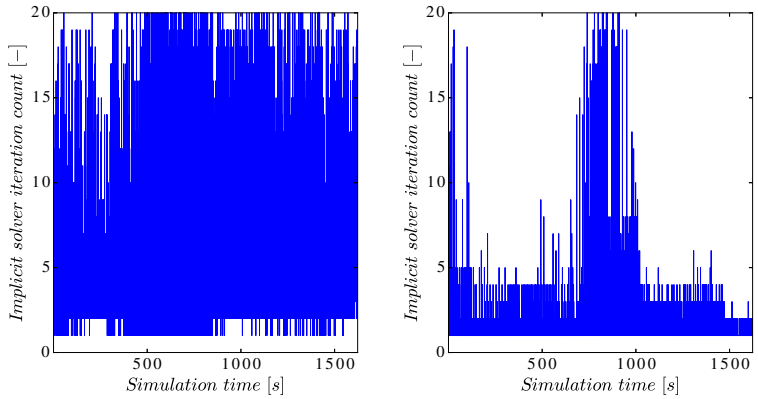

(a) Maximum time-step of 0.1 s (b) Maximum time-step of 0.01 s

Figure 5.4: Implicit solver iteration count

minimum cable tension for the cases with environmental conditions using a maximum time-step of 0.01 s are presented in Table 5.4.

	$H_{max} = 0.93[m]$			$H_{max} = 1.86[m]$			$H_{max} = 2.79[m]$		
Dir/T_s	**3.92**$[s]$	**5.23**$[s]$	**6.54**$[s]$	**4.58**$[s]$	**5.88**$[s]$	**7.19**$[s]$	**5.23**$[s]$	**6.54**$[s]$	**7.85**$[s]$
0°	3.8	4.5	4.2	2.6	-0.7	-2.6	0.4	-4.2	-11.0
30°	1.4	3.9	4.4	0.1	-2.1	-9.2	-10.0	-6.7	-19.0
60°	1.4	3.2	4.0	-1.6	1.7	-0.1	-4.3	-2.2	-3.7
90°	1.8	3.9	-4.7	0.3	-0.7	1.9	-0.3	-0.4	-0.2
120°	1.6	3.6	3.8	0.4	-1.0	1.6	-4.1	-1.5	-5.2
150°	1.5	3.4	2.4	0.7	3.1	2.3	-1.5	-3.7	-7.5
180°	3.5	5.1	5.0	2.0	0.2	-2.9	-0.2	-7.6	-0.7
210°	2.2	4.0	4.3	1.6	-0.6	-8.3	-1.4	-4.0	1.3
240°	2.5	2.1	3.3	-0.6	0.3	-4.4	-3.1	-4.7	-3.3
270°	2.5	2.8	2.0	0.2	-0.1	0.6	-1.3	-1.2	-1.5
300°	2.2	2.5	2.8	0.8	-3.3	1.6	-7.6	0.2	1.0
330°	2.4	-0.2	4.0	-0.3	2.1	3.5	-20.8	-7.4	-0.8

Table 5.4: Minimum cable tension using a maximum time-step of 0.01 s $[kN]$

Table 5.4 indicates that the workability in general is improved from 40 percent to 55 percent. Especially the results for the lowest wave periods per wave height are significant better. Table 5.4 proves that decreasing of the maximum time-step solves the compression problem for some cases, but not for all cases. Although the values of the cable compression of some cases are decreased significantly, cable compression is still a problem in this model. The physical cable compression becomes visible in Figure 5.3c due to the decrease of the amount of tension oscillations in a short time interval. In addition, the influence of the wave period with corresponding wave height and direction is investigated for the grey marked cases in Table 5.4.

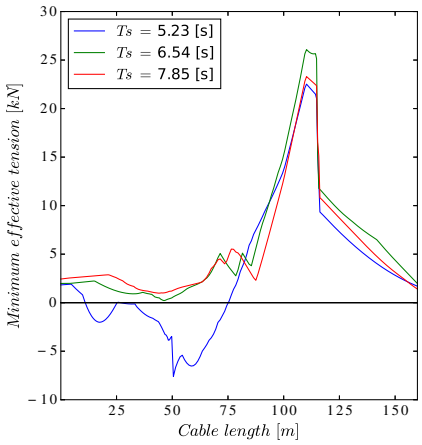

Figure 5.5: Minimum effective tension of the cases with $H_{max} = 2.79$ $[m]$ and $Dir = 300$ °

Range graphs of the minimum effective tension for the cases with a $H_{max} = 2.79$ $[m]$ and $Dir = 300$ ° are presented in Figure 5.5. The downward spike in effective tension at a cable length of 50 m becomes lower for increasing wave periods. Figure 5.6 presents times series of the corresponding node.

Time series of the effective tension are presented in Figure 5.6a. The cable compression observed in this Figure 5.6a shows correlation with larger global X (GX) and global Z (GZ) accelerations of this node, presented in Figure 5.6b and 5.6c. Large accelerations are observed at the same intervals when the cable compression occurs. With increasing accelerations the forces also increase, which may cause compressive waves.

The accelerations in the cable are also related to the motions of the CLV. The accelerations in the first 700 s of simulation time are dominated by the CLV motions, because the DBMs are on deck of the CLV. The RAOs of the CLV show that the motions of the CLV are most severe in wave periods between 6 and 9 s. This is shown already in Figure 5.6b and 5.6c, the accelerations increase with increasing T_s.

After 700 s the buoyant cable section is in the water. Therefore, cable motions are influenced less by the CLV. However, it is free floating in the splash zone. In general, here the orbital velocities and accelerations are largest. The linear wave theory describes a relation between particle velocity v and accelerations a regarding wave period T, is found and presented in Equation 5.1.

$$v \propto \frac{1}{T} \quad ; \qquad a \propto (\frac{1}{T})^2 \tag{5.1}$$

The relation presented in Equation 5.1 shows that an increase of the wave period results in a decrease of the particle velocity and accelerations. A higher particle velocity results in larger drag forces on the cable using the Morison Equation 2.43. The DBMs have a large drag area, so combining this with higher particle velocities results in a increase of the forces that act on the cable and DBMs in the splash zone compared to higher wave periods. Figure 5.6 shows that the GX and GZ accelerations are decreasing for increasing wave periods, supporting the statement above.

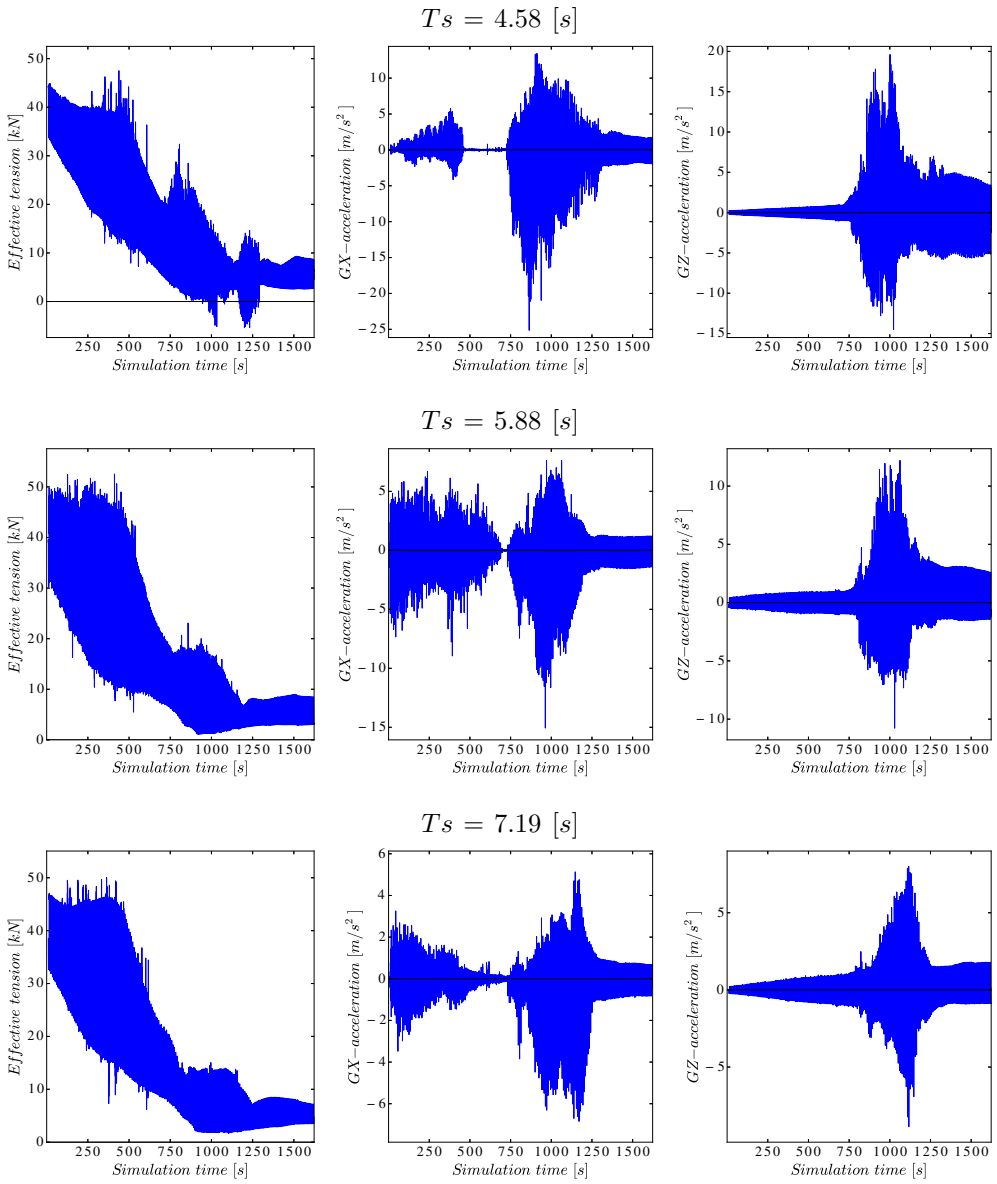

(a) Tension over time (b) GX accelerations over time (c) GZ accelerations over time

Figure 5.6: Results of the cases with $H_{max} = 2.79$ [m] and $Dir = 300$ °

5.1.4 Cable curvature in the base case

A range graph of the maximum curvature over the cable length for the base case is presented in Figure 5.7a. An upward spike is observed at 50 m cable length.

A time series of the maximum curvature of the corresponding node is presented in Figure 5.7b. High curvature of the node is observed in Figure 5.7b between 750 s and 850 s. In this interval the last node of the buoyant part leaves the side of the chute while the CLV is still turning. The cable itself has a smaller diameter than the buoyant section. For this reason the first cable node after this diameter transition is not supported, as presented in Figure 5.8. This absence of cable contact with the chute enables the cable to move freely, resulting is a high curvature.

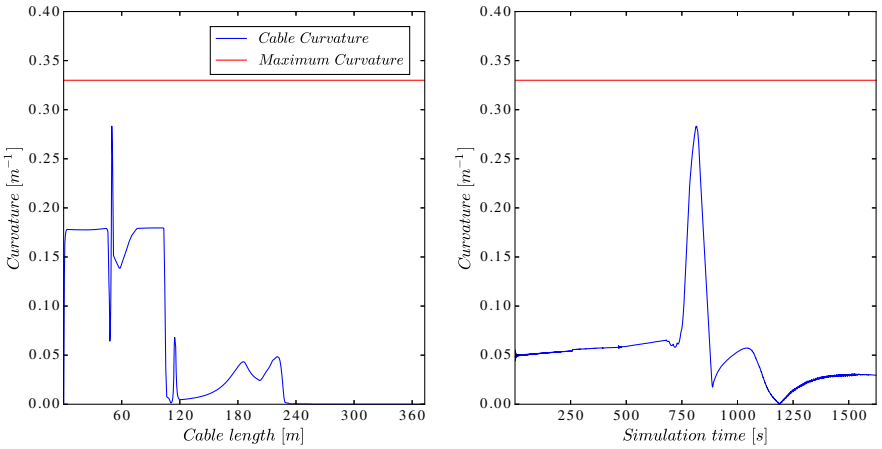

(a) Curvature of the cable (b) Curvature over time

Figure 5.7: Maximum curvature results free lay model

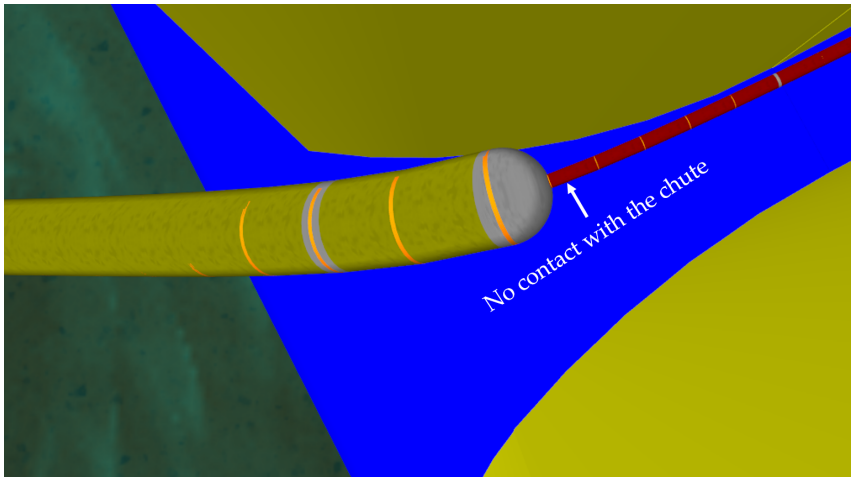

Figure 5.8: Cable support on the chute

5.1.5 Exceeding of the maximum Cable curvature

The results of the workability in Table 5.2 indicates that the maximum curvature is exceeded for some cases with environmental conditions. An explanation for the exceeding of the maximum curvature is presented in this Section.

The results of the maximum curvature for the cases with environmental conditions are presented in Table 5.5. This table indicates that exceeding of the maximum curvature occurs for multiple wave heights for certain wave directions.

The results presented in Table 5.5 show a curvature of approximately 0.30 m^{-1} for all cases with environmental conditions. This high value is caused by the upward spike as observed in Figure 5.7. For some cases the maximum curvatures are lower than the highest upward spike in the base case. In these cases, the wave direction is such that the waves are pushing the cable away from the side of the chute of the CLV. The cases which are exceeding the maximum curvature are those in which the wave direction is pushing the cable towards the CLV. Pushing of the cable towards the CLV combined with the absence of cable contact with the side of the chute results in exceeding of

	$H_{max} = 0.93[m]$			$H_{max} = 1.86[m]$			$H_{max} = 2.79[m]$		
Dir/T_s	$3.92[s]$	$5.23[s]$	$6.54[s]$	$4.58[s]$	$5.88[s]$	$7.19[s]$	$5.23[s]$	$6.54[s]$	$7.85[s]$
0°	0.30	0.30	0.29	0.33	0.31	0.31	0.36	0.34	0.32
30°	0.31	0.30	0.30	0.36	0.31	0.34	0.40	0.34	0.34
60°	0.31	0.30	0.30	0.32	0.32	0.30	0.35	0.38	0.31
90°	0.31	0.30	0.30	0.31	0.31	0.31	0.32	0.32	0.34
120°	0.30	0.29	0.29	0.30	0.30	0.30	0.30	0.31	0.33
150°	0.30	0.28	0.28	0.30	0.30	0.29	0.29	0.29	0.29
180°	0.29	0.28	0.28	0.29	0.29	0.28	0.28	0.30	0.29
210°	0.29	0.28	0.29	0.30	0.29	0.32	0.31	0.31	0.29
240°	0.29	0.29	0.29	0.28	0.29	0.29	0.30	0.28	0.28
270°	0.30	0.30	0.29	0.32	0.31	0.30	0.32	0.32	0.30
300°	0.31	0.31	0.30	0.34	0.33	0.31	0.38	0.33	0.32
330°	0.31	0.31	0.30	0.33	0.32	0.32	0.39	0.32	0.32

Table 5.5: Maximum curvature free lay $[m^{-1}]$

the maximum curvature. This could be solved in practice using a tapered bend restrictor at the end of the DBMs. In addition, avoiding of exceeding of this maximum curvature is possible by introducing a structure which supports the DBMs at the stern of the vessel. An example of this structure, for cable installation over the side, is presented in Figure 5.9.

Figure 5.9: Support structure launching DBMs [11]

5.1.6 Tension equipment

Besides the failure modes as described earlier is the tension in the LCE during free lay processed to have an indication of the minimum capacity of this LCE. A time series of the tension in the LCE during the base case of the free lay model is presented in Figure 5.10. This Figure shows a decrease in pay-out tension in time, since more DBMs are entering the water. These DBMs are creating buoyancy which supports the cable and decreases the tension action on the LCE. The events presented in Figure 5.10 are explained in Table 5.6.

The results of the dynamic analyses for the maximum LCE tensions are presented in Table 5.7. The values in Table 5.7 represent the maximum LCE tension observed in the time series, as presented in Figure 5.10. The maximum tension in the LCE is observed at the start of the simulation as already mentioned. For this reason the maximum tension in the LCE is mainly influenced by the motion behaviour of the CLV. In addition, the tensions are increasing for increasing a increasing wave period, since these wave period are more interfering with the natural period found in the RAOs of the CLV as presented in Section 4.3.2.

A maximum LCE tension of 60.5 kN is found in the results and boxed in Table 5.7. The capacity of the LCE on the CLV is 120 kN, so this LCE is sufficient to perform the free lay installation.

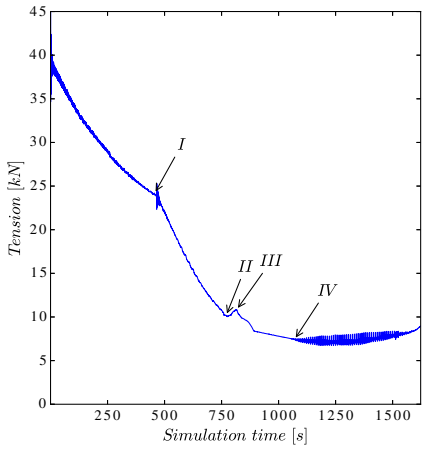

Figure 5.10: LCE tension during simulation

Number	Event
I	The CLV starts turning.
II	Equilibrium between weight and buoyancy is reached.
III	Last DBM leaves the side of the chute.
IV	Last DBM enters the splash zone, cable catenary between chute and DBMs arises.

Table 5.6: Events explanation

	$H_{max} = 0.93[m]$			$H_{max} = 1.86[m]$			$H_{max} = 2.79[m]$		
Dir/T_s	$3.92[s]$	$5.23[s]$	$6.54[s]$	$4.58[s]$	$5.88[s]$	$7.19[s]$	$5.23[s]$	$6.54[s]$	$7.85[s]$
0°	41.4	41.2	46.8	42.2	50.6	60.0	53.4	57.4	55.4
30°	39.9	41.0	42.6	40.7	47.3	51.6	47.3	59.0	53.4
60°	39.1	40.2	40.0	39.8	40.6	43.0	44.5	45.8	46.2
90°	39.5	40.0	39.6	40.9	42.5	40.8	42.5	41.4	44.2
120°	39.2	40.6	40.4	39.9	40.7	43.2	44.8	49.2	46.7
150°	39.5	41.0	42.5	40.1	48.6	51.5	49.6	56.8	56.4
180°	42.0	42.0	44.5	44.0	48.7	60.5	50.4	55.5	59.3
210°	39.5	41.0	42.3	40.6	47.3	45.9	46.2	53.5	47.2
240°	39.9	40.9	40.7	41.5	42.5	44.4	45.2	45.9	46.8
270°	40.4	40.9	40.9	42.2	43.6	42.0	45.1	44.7	44.9
300°	39.9	40.8	41.0	41.6	43.2	45.7	45.2	51.9	47.7
330°	39.5	41.4	43.8	41.3	47.9	51.7	49.1	56.1	52.6

Table 5.7: Maximum tension in LCE free lay $[kN]$

5.1.7 Bottom tension

The bottom tension in the part of the dynamic cable which lies on the seabed determines if burying of the cable is possible. A burial assessment is difficult when the mean tension of the cable which needs to be buried is higher than 20 kN. A range graph of the effective tension in this cable section is presented in Figure 5.11.

The results of the cases with environmental conditions are presented in Table 5.8. The results are processed as the maximum value of the mean bottom tension of the cable section which lies on the seabed. At the start of the simulation the front of this cable section is free hanging in the water. The tensions in the cable during this free hanging period prior to the period on the seabed count for the mean cable tension. For this reason the bottom tension are decreasing for increasing wave periods, since the cable moves more in the lowest wave periods. An explanation for this is already explained in Section 5.1.3. However, the maximum bottom tension is for all the cases below the maximum bottom tension of 20 kN.

5.1.8 Cable offset

Offset of the cable from the cable route can create problems during the burial assessment. For this reason the maximum offset is proceed and the results for the freelay model are presented in

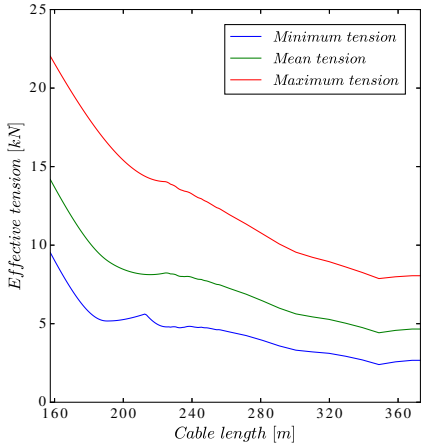

Figure 5.11: Effective tension cable part on the seabed

	$H_{max} = 0.93[m]$			$H_{max} = 1.86[m]$			$H_{max} = 2.79[m]$		
Dir/T_s	$3.92[s]$	$5.23[s]$	$6.54[s]$	$4.58[s]$	$5.88[s]$	$7.19[s]$	$5.23[s]$	$6.54[s]$	$7.85[s]$
0°	14.4	14.3	14.3	14.6	14.4	14.3	14.8	14.6	14.4
30°	14.3	14.1	14.0	14.4	14.1	13.9	14.5	14.0	14.0
60°	14.0	13.9	13.9	13.9	13.9	13.7	13.8	13.8	13.6
90°	13.9	13.9	13.9	13.7	13.7	13.8	13.6	13.7	13.6
120°	14.0	13.9	13.9	13.9	13.9	13.8	13.9	13.8	13.7
150°	14.3	14.2	14.1	14.5	14.1	14.1	14.5	14.2	14.1
180°	14.4	14.4	14.3	14.7	14.5	14.4	14.9	14.7	14.6
210°	14.6	14.5	14.4	14.8	14.6	14.5	15.0	14.8	14.7
240°	14.5	14.5	14.5	14.8	14.7	14.6	15.1	14.9	14.9
270°	14.4	14.5	14.5	14.6	14.7	14.7	14.9	14.9	15.0
300°	14.5	14.5	14.5	14.7	14.7	14.7	15.1	15.0	15.0
330°	14.5	14.4	14.4	14.8	14.6	14.6	15.0	14.9	14.8

Table 5.8: Maximum bottom tension free lay $[kN]$

Table 5.9. These maximum offset values represent the maximum offset of the cable section which lies on the seabed at the end of the simulation. Table 5.9 shows that the presence of cable offset is related to the wave direction. There is cable offset in the cases where the wave directions are acting perpendicular on the cable configuration. The maximum offset of 5 m is not exceeded in any case.

	$H_{max} = 0.93[m]$			$H_{max} = 1.86[m]$			$H_{max} = 2.79[m]$		
Dir/T_s	$3.92[s]$	$5.23[s]$	$6.54[s]$	$4.58[s]$	$5.88[s]$	$7.19[s]$	$5.23[s]$	$6.54[s]$	$7.85[s]$
0°	1.6	1.2	1.4	2.3	1.7	2.2	2.5	2.6	3.0
30°	2.0	1.5	1.3	3.1	2.0	2.0	3.5	2.8	2.6
60°	1.4	0.8	1.1	1.9	1.2	1.3	1.8	1.6	1.9
90°	0.4	0.4	0.4	0.4	0.4	0.5	0.4	0.5	0.5
120°	0.0	0.0	0.0	0.0	0.0	0.0	0.0	0.0	0.0
150°	0.0	0.0	0.0	0.0	0.0	0.0	0.0	0.0	0.0
180°	0.0	0.0	0.0	0.0	0.0	0.0	0.0	0.0	0.0
210°	0.0	0.0	0.0	0.0	0.0	0.0	0.0	0.0	0.0
240°	0.0	0.0	0.0	0.0	0.0	0.0	0.0	0.0	0.0
270°	0.3	0.3	0.3	0.3	0.3	0.4	0.3	0.3	0.4
300°	0.8	1.0	0.8	1.2	1.5	1.1	2.2	1.9	1.5
330°	1.4	1.6	1.6	2.1	2.5	2.1	3.2	3.2	2.6

Table 5.9: Maximum offset free lay $[m]$

5.1.9 Structure interaction

The last limitation on which the free lay model is checked is if the dynamic cable or the messenger wires interacts with the FOWT during the simulation. In the free lay model the cable cannot have interaction with the FOWT. For the pull-in methods this interaction is possible, but is avoided during the creation of the models. No interaction is found in any of the models and the results for all models are for this reason added to Appendix F.

5.2 Method 1: Pull-in in pre-installed FOWT

In this Section the results of the pull-in method 1 are described. Table 5.10 represents the failure modes for which all cases are tested in pull-in method 1. Firstly, the workability is presented to have an indication which failure modes are occurring. Furthermore the minimum, maximum effective tensions and the maximum curvature in the cable for the base case are described in the cable behaviour section. The failure mode cable compression is described afterwards. Thereupon, the tension in the winches and the controlling of them using the system is described. This Section finishes with the behaviour of the CPS in the base case followed by the results of the dynamic analyses. The results of the limitations which are presented in Table 5.10 and not covered in this Section are added to Appendix F.2.

Number	Limitation
1	Successive sea state
2	Cable compression
3	Exceeding maximum cable tension
4	Exceeding maximum cable curvature
5	Maximum pull-in tension
6	Maximum pay-out tension
7	Exceeding maximum bottom tension
8	Maximum bend moment of the CPS
9	Exceeding maximum cable offset
10	Structure interaction
11	Not ensuring 10 m seabed clearance

Table 5.10: Failure modes on which pull-in method 1 is tested

5.2.1 Workability

Similar to Section 5.1 are the results of the workability presented in Table 5.11 to show the possibility to perform the cable installation using method 1. The workability of method 1 is 75 percent, calculated similar to Section 5.1. The workability indicates that exceeding of the minimum effective cable tension is the only failure mode found in pull-in method 1. In addition, cable compression is mainly found around the wave directions form 60 to 150 degrees.

5.2.2 Cable tension and curvature in the base case

A range graph of the effective tension over the cable length in the base case is presented in Figure 5.12a. The upward spike in Figure 5.12a is again a result of the cable clamp attached on the cable. The difference between the amplitudes of the upward spike for the minimum, mean and maximum are closer to each other in comparison with the results presented in Figure 5.1 of the free lay model. The tether is not installed in this pull-in method, however the cable configuration

	$H_{max} = 0.93[m]$			$H_{max} = 1.86[m]$			$H_{max} = 2.79[m]$		
Dir/T_s	$3.92[s]$	$5.23[s]$	$6.54[s]$	$4.58[s]$	$5.88[s]$	$7.19[s]$	$5.23[s]$	$6.54[s]$	$7.85[s]$
0°	1	1	1	1	1	1	2	1	1
30°	1	1	1	1	1	1	1	1	1
60°	1	1	1	1	2	1	2	2	2
90°	1	1	2	2	2	2	2	2	2
120°	1	1	2	2	2	2	2	2	2
150°	1	1	1	1	1	2	2	1	2
180°	1	1	1	1	1	1	1	1	1
210°	1	1	1	1	1	1	2	1	1
240°	1	1	1	1	1	1	1	1	1
270°	1	1	1	1	1	2	2	2	2
300°	1	1	1	1	1	1	1	1	1
330°	1	1	1	1	1	1	2	1	1

Table 5.11: Workability pull-in method 1 [−]

is more submerged in comparison to the cable configuration in the free lay model. For this reason the difference between the minimum, mean and maximum effective tension is smaller and the maximum spike is lower compared to the free lay model.

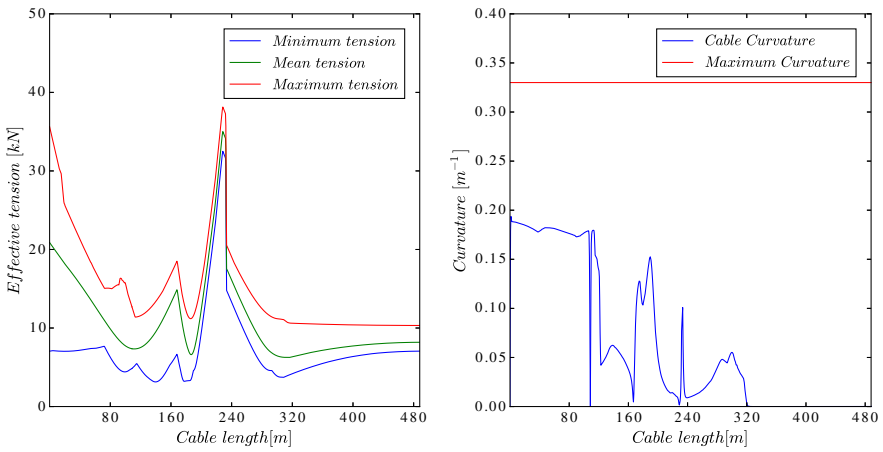

(a) Effective tension of the cable

(b) Curvature of the cable

Figure 5.12: Cable behaviour pull-in method 1

The maximum curvature of the cable over its length is presented in Figure 5.12b. The curvature of the cable over its length is below the maximum curvature. The graph of the curvature is similar to the curvature in the free lay model, but the spike observed in the free lay model is not found. This is explained by the fact that the absence of contact with the side of the chute as described in Section 5.1.5 is not an issue in this pull-in method, since the DMBs are overboarded at the start of the simulation.

The maximum effective tension and maximum curvature are not exceeded in the cases with environmental conditions. For this reason both Tables are added to Appendix F.2.

5.2.3 Cable compression

The results of the minimum effective tension for the cases with environmental conditions are presented in Table 5.12. The cable compression is mainly observed in Table 5.12 between the wave directions form 60 to 150 degrees. The case with the highest compression value is boxed in Table

5.12 and investigated in more detail.

	$H_{max} = 0.93[m]$			$H_{max} = 1.86[m]$			$H_{max} = 2.79[m]$		
Dir/T_s	$3.92[s]$	$5.23[s]$	$6.54[s]$	$4.58[s]$	$5.88[s]$	$7.19[s]$	$5.23[s]$	$6.54[s]$	$7.85[s]$
0°	2.9	3.3	3.1	1.6	3.1	2.9	-1.9	2.4	2.7
30°	2.9	3.3	2.2	1.4	1.9	2.4	0.3	2.3	1.3
60°	2.7	2.9	2.9	0.8	-0.6	1.0	-7.2	-2.1	-2.9
90°	2.4	3.0	-2.2	-9.6	-3.1	-3.8	−14.0	-6.7	-6.3
120°	2.6	3.1	-1.5	-6.8	-2.0	-3.3	-12.4	-3.2	-4.2
150°	2.8	3.2	3.5	0.3	1.5	-0.1	-0.8	0.7	-2.0
180°	3.1	3.3	3.3	2.2	0.2	3.3	0.2	1.0	3.1
210°	3.1	3.2	3.3	2.0	3.2	2.7	-0.7	1.8	2.9
240°	2.5	3.0	2.9	0.2	2.3	0.2	0.8	0.6	2.1
270°	2.5	2.5	2.4	0.5	1.3	-3.5	-0.6	-0.4	-2.7
300°	2.3	2.9	2.1	0.6	0.7	1.9	0.4	0.6	1.3
330°	2.4	2.8	2.8	0.9	2.5	1.4	-0.1	2.1	1.9

Table 5.12: Minimum cable tension pull-in method 1 $[kN]$

A range graph of the effective tension over the cable length corresponding to the boxed case is presented in Figure 5.15.

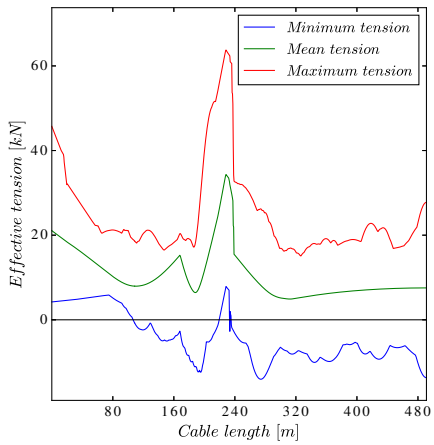

Figure 5.13: Effective tension over cable length of the boxed case

As can be seen in Figure 5.15 , nearly the entire cable experiences compression at some point during the operation. Two downward spikes are observed at a cable length of 193 m and 273 m. Time series of the corresponding nodes are presented in the top and bottom part of Figure 5.14, respectively.

Time series of the effective tension are presented in Figure 5.14a. The effective tension in both nodes show a similar result. Also, the amplitude of the oscillations in Figure 5.14a are decreasing after a simulation time of approximately 900 s. From this point in time, the cable configuration is fully submerged. The orbital velocities and accelerations become less quickly, resulting in a significantly smaller amplitude of the oscillations.

Similar to the compression issues in Section 5.1, the cable shows compression which correlates with larger GZ-accelerations of these nodes, presented in Figure 5.14b. A close-up of the largest compression observed in Figure 5.14a, is presented in Figure 5.14c. For both nodes a downward

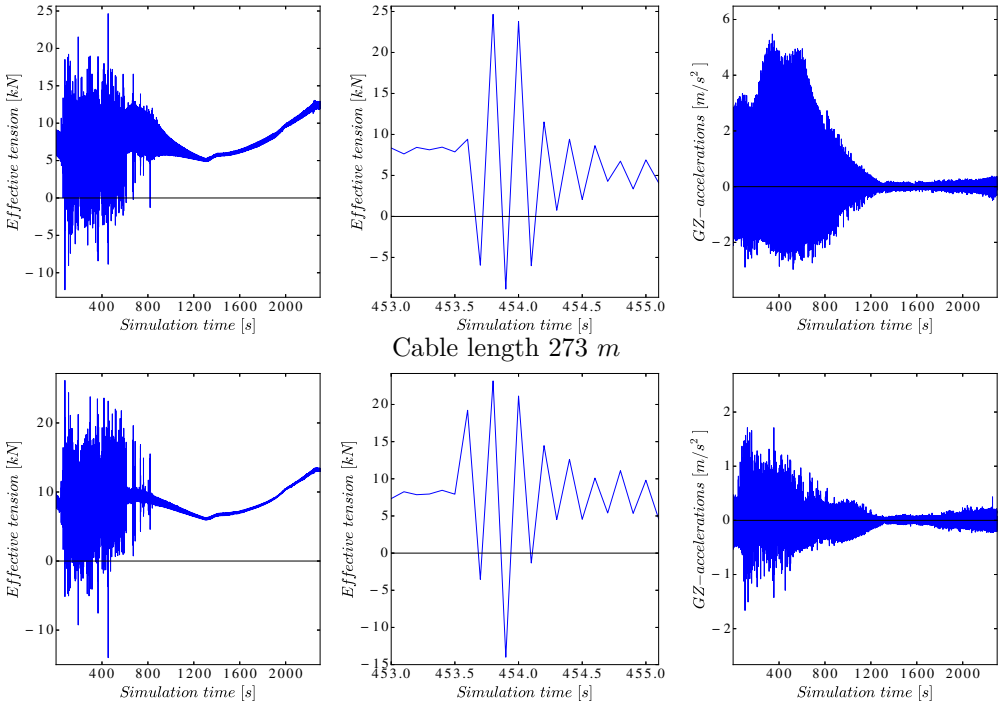

(a) Tension over time (b) Vertical accelerations over time (c) Close-up of spike

Figure 5.14: Compression results pull-in method 1 of the boxed case

compression spike is observed at exactly the same point in time. A delay should be observed if the compression wave travels through the cable. This delay is not notice between the compression spikes of the nodes as presented in Figure 5.14c. This indicates that the compression spikes may be caused by numerical inaccuracies. For this reason the influence of the maximum time-step of OrcaFlex's implicit solving scheme is investigated for the boxed case.

Initially, A maximum time-step of 0.05 s is used for the implicit solving scheme in OrcaFlex for method 1. The influence of this time-step on the cable compression is compared to the compression results for the boxed case using a maximum time-step of 0.01 and 0.005 s. The results of the corresponding range graphs are presented in Figure 5.15.
The results in Figure 5.15 indicates that the cable compression in general becomes better for a maximum time-step of 0.01 s and becomes worse for 0.005 s. Time series of the node corresponding to a cable length 193 m for a maximum time-step of 0.01 and 0.005 s are presented in the top and bottom part of Figure 5.16, respectively. The simulation time increased for both time-steps from approximately 4 hours to approximately 2 days. For this reason further investigation of the influence of the maximum time-step for every single case is not performed in this research.

The results presented in Figure 5.16a indicate that decreasing of the maximum time-step changes the results, but cable compression is still found for the boxed case. The correlation between the large compression oscillations and vertical accelerations is still found in Figure 5.16b. Close-ups of the spike for a similar interval are presented in Figure 5.16c and indicates that the tension oscillations are changed using a different maximum time-step. However, the oscillations are still present and cable compression is found. The origin of cable compression for the other exceeding cases in Table 5.12 is the same as investigated for the boxed case. Large GZ-acceleration are present when the wave direction is parallel to the cable configuration direction. For this reason this method has lots of failed cases around the wave directions parallel to the cable configuration. This indicates that cable compression occurs when the cable follows the wave.

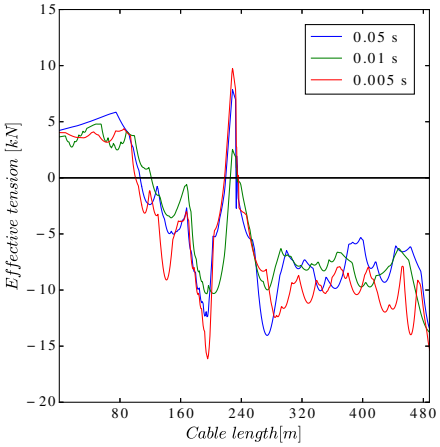

Figure 5.15: Comparison of the effective tension over cable length for different maximum time-steps for the boxed case

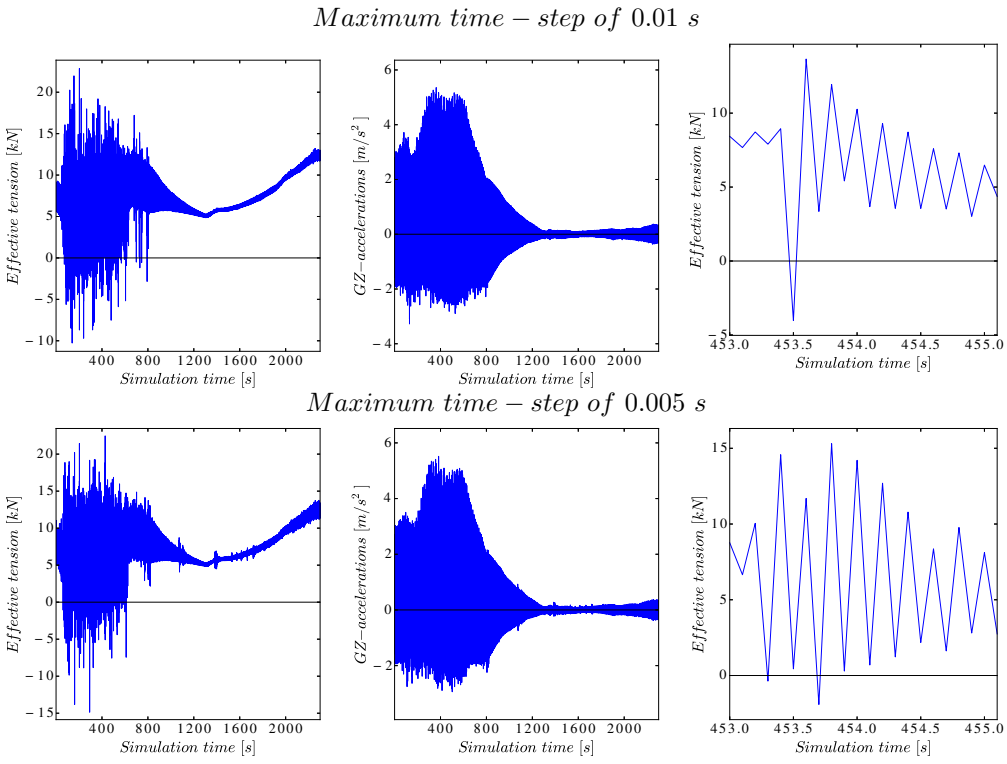

(a) Tension over time (b) Vertical accelerations over time (c) Close-up of spike

Figure 5.16: Comparison results for a different maximum time-step

5.2.4 Tension equipment

The tension equipment is very important for this pull-in method. An advanced system is designed to control the winches via an external script as described in Section 4.6.1. For clarity purposes, the important events that occur during the operation are numbered. These events are listed in Table 5.13.

The tensions over time of the pull-in and pay-out winches are presented in Figure 5.17a and 5.17b,

Number	Event
I	The CLV sails towards the FOWT, the pull-in winch starts pulling and the pay-out winch starts releasing.
II	The CLV stops sailing, both winches continue.
III	The CLV turns towards the FOWT, the pull-in winch decreases its velocity, the pay-out winch holds the pullhead on the same position.
IV	The CLV stops turning, the pay-out winch still holds the cable on the same position, the pull-in winch continues.
V	The pull-in wire becomes tight, pay-out winch starts releasing of the cable. Interaction between both winches starts.
VI	Pay-out winches passed the critical point in the trajectory and the interaction between both winches decreases.
VII	Pay-out winch is disconnected by an ROV link.
$VIII$	Cable reaches the hang-off point.

Table 5.13: Events explanation

respectively. The high tensions found in both winches were not found in the cable. This indicates that the winches are interacting which each other and the resultant force is acting on the cable. The corresponding winch velocities are presented in the Figure 5.18a and 5.18b. The pull-in velocity as presented in Figure 5.18a indicates that the system controls the transfer by applying a constant pull-in velocity. The oscillations in pay-out velocity as presented in Figure 5.18b shows that the dynamics in the system are counteracted by the pay-out winch on the CLV. The winches on the CLV are mostly more advanced compared to the pull-in winch in the FOWT. The results of the maximum tensions found for the pull-in and pay-out winch for the cases with environmental conditions are presented in Appendix F.2. The minimum required tension of the pull-in winch is marked as 118 kN and the minimum tension of the pay-out tension is 54.3 kN.

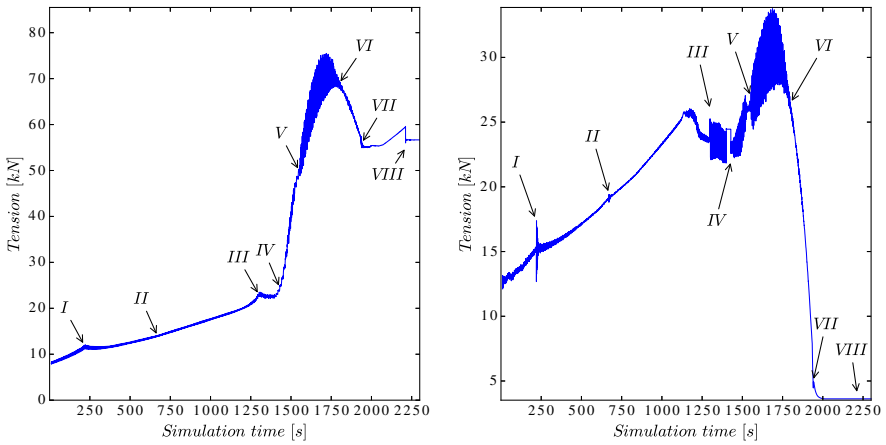

(a) Pull-in tension

(b) Pay-out tension

Figure 5.17: Tension on the winches during the simulation

The winches are controlled by a system, as described in Section 4.6.1, which ensures a minimum seabed clearance of 10 m. The sagbend of the cable is the cable section which is the closest to the seabed, but the nodes corresponding to the sagbend are changing during the pull-in operation. For this reason, the system is designed to control the winches based on the elevation of the pullhead above the seabed. The trajectory of this pullhead in the $Y-$ and $Z-direction$ for a random case with environmental conditions is presented in Figure 5.19a and 5.19b, respectively.

The limitations on which the system controls the winches are the same as described in Section

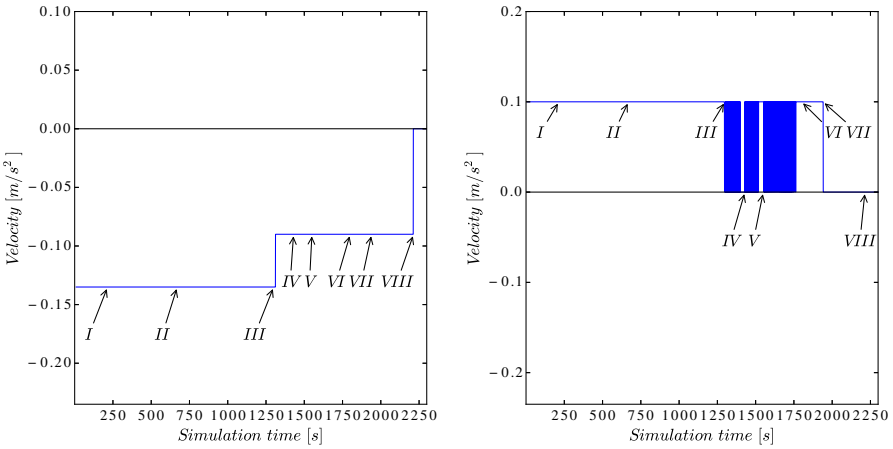

(a) Pull-in velocity (b) Pay-out velocity

Figure 5.18: Velocity of the Winches during the simulation

4.6.1, but they are translated to time dependent limitations. The maximum Z position on every time step in Figure 5.19b is calculated based on the Y position at the same time step.

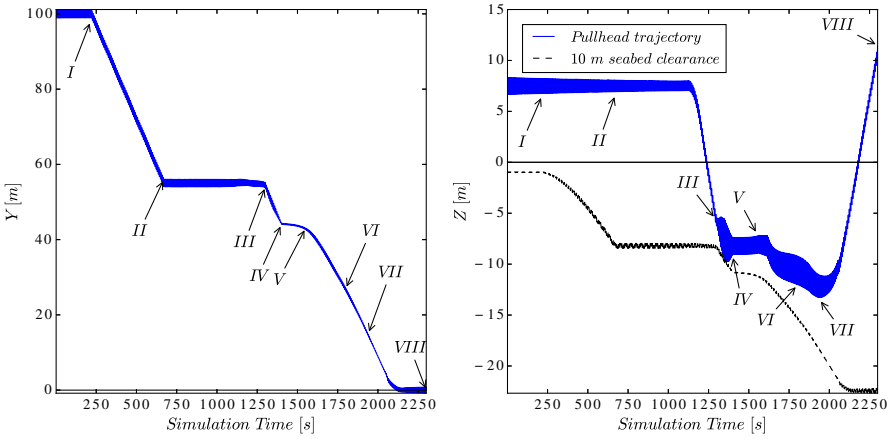

(a) $Y - direction$ (b) $Z - direction$

Figure 5.19: Pullhead trajectory during the simulation of the boxed case

The elevation of the sagbend above the seabed corresponding to the events is presented in Figure 5.20. The sagbend start high above the seabed and goes down in the water slowly. The pullhead becomes lower in the water between III and VII, but the sagbend remains on the same elevation above the seabed in this interval, which indicates that the minimum seabed clearance is ensured during the total pull-in operation.

The results of the seabed clearance for the cases with environmental conditions is added to Appendix F.2. All cases are ensuring 10 m seabed clearance.

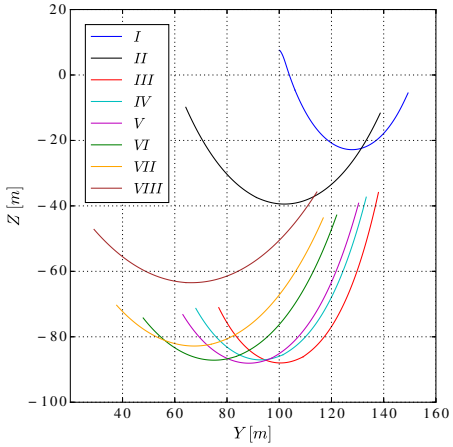

Figure 5.20: Elevation of the sag bend corresponding to the events

5.2.5 CPS behaviour

The CPS is loaded during method 1, since the CPS ensures an entrance point for the cable into the FOWT. The CPS generates more reaction forces when the angle in which it is pulled increases. For this reason are the highest bending moments in the CPS observed during transfer of the pullhead from the CLV towards the FOWT. The interaction between the winches during this period results in oscillations of the CPS. The reaction forces generated by the CPS influence the tension in the winches, since the CPS tends to return to its equilibrium position. The CPS is fixed in the I-tube of the FOWT at a CPS-length 0 m. The other end is hanging freely below the FOWT.

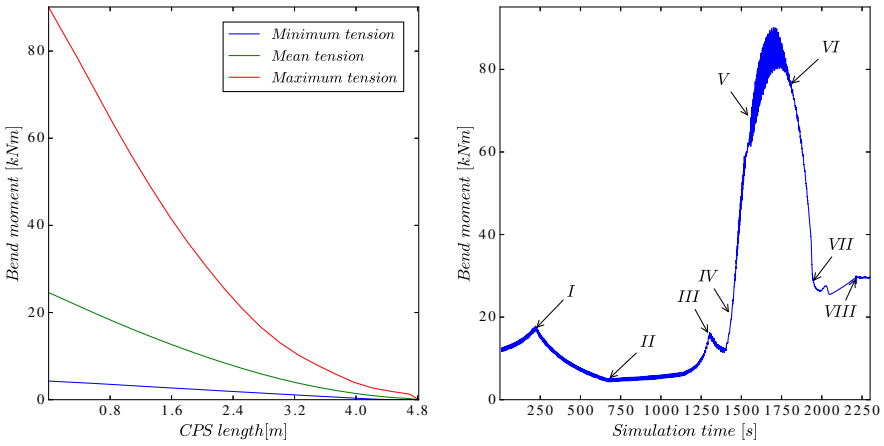

(a) Bend moment over the length

(b) Bend moment during simulation

Figure 5.21: Bend moment on the CPS

A range graph of the bending moments over the CPS length is presented in Figure 5.21a. A time series of the bending moments of the fixed end is presented in Figure 5.21b. The interaction of the winch system is observed between V and VI. The CPS has to encounter the highest bending moments during this interval. The shape of the CPS corresponding to the events is presented in Figure 5.31. The highest bending moments observed in Figure 5.21b are correlated with the shape of the CPS. The stress-strain relation of this CPS is presented in Section 3.5 and explains that for increasing curvature the bending moment also increases.

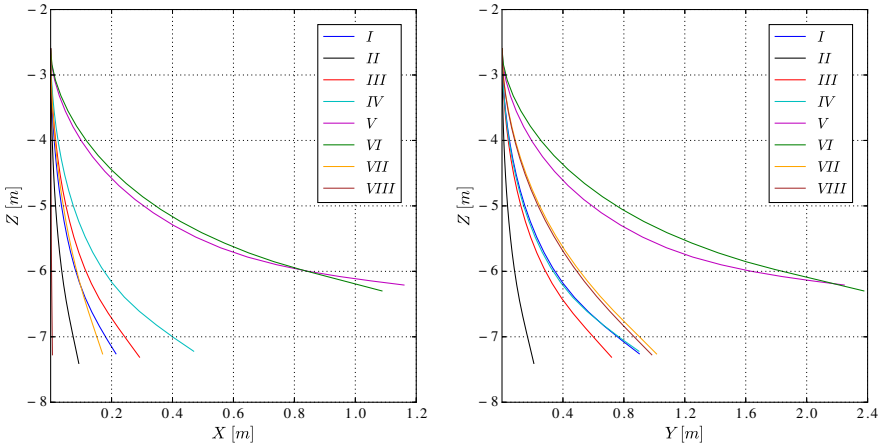

(a) $X-directions$ (b) $Y-directions$

Figure 5.22: CPS shape corresponding to the events

The maximum values of the maximum bending moments in Figure 5.21b are presented in Table 5.14 for the cases with environmental conditions. A maximum bend moment of 117 kNm is found during the dynamic analyses. This value indicates the required capacity of the CPS.

	$H_{max} = 0.93[m]$			$H_{max} = 1.86[m]$			$H_{max} = 2.79[m]$		
Dir/T_s	**3.92**$[s]$	**5.23**$[s]$	**6.54**$[s]$	**4.58**$[s]$	**5.88**$[s]$	**7.19**$[s]$	**5.23**$[s]$	**6.54**$[s]$	**7.85**$[s]$
0°	94.1	89.8	92.2	94.7	97.6	93.3	98.2	104.3	94.7
30°	97.5	96.4	89.5	99.2	93.0	96.3	117.1	94.7	98.2
60°	99.2	90.2	90.5	102.8	101.8	94.6	100.4	99.0	101.2
90°	96.6	93.3	93.4	95.3	107.3	95.4	109.9	108.0	98.6
120°	94.1	89.4	92.8	94.6	96.5	97.3	96.4	104.7	97.4
150°	88.4	88.7	89.2	88.3	89.5	98.0	87.9	96.4	100.3
180°	89.9	88.7	91.7	90.2	95.1	97.7	94.2	105.1	95.3
210°	92.0	89.8	89.7	91.6	95.2	91.8	97.9	90.5	97.4
240°	94.8	88.4	88.9	97.8	91.9	89.1	89.6	92.8	93.9
270°	94.8	94.2	91.3	96.4	92.1	93.9	113.2	102.7	95.1
300°	93.1	88.7	91.6	92.7	97.1	95.1	96.8	103.9	96.0
330°	90.7	89.6	89.1	89.2	88.6	92.1	88.7	90.4	94.3

Table 5.14: Maximum bend moment CPS pull-in method 1 $[kNm]$

5.3 Method 2: Post-lay pull-in via CLV

In this Section the results of pull-in method 2 are described. Table tab:PreferredLimitations represents the failure modes for which all cases are tested in the pull-in method 2. Firstly, the workability is presented to have an indication which failure modes are occurring. Subsequently the minimum, maximum effective tensions and the maximum curvature in the cable for the base case are described in the cable behaviour Section. The failure mode cable compression is described afterwards. Thereupon the tension in the winches, controlling of them using the system and the ensured minimum seabed clearance is described. This Section ends with the behaviour of the CPS in the base case followed by the results of the dynamic analyses. The results of the limitations which are presented in Table 5.15 and not covered in this Section are added to Appendix F.3.

Number	Limitation
1	Successive sea state
2	Cable compression
3	Exceeding maximum cable tension
4	Exceeding maximum cable curvature
5	Maximum pull-in tension
6	Maximum pay-out tension
7	Exceeding maximum bottom tension
8	Maximum bend moment of the CPS
9	Maximum tension in the tether
10	Exceeding maximum cable offset
11	Structure interaction

Table 5.15: Failure modes on which pull-in method 2 is tested

5.3.1 Workability

Similar to Section 5.1 are the results of the workability presented in Table 5.16 to show the possibility to perform the cable installation using pull-in method 2. The workability of pull-in method 2 is 75 percent, which is similar to pull-in method 1. The workability indicates that exceeding of the minimum effective cable tension is the only failure mode found in pull-in method 2. In addition, cable compression is mainly found for the cases with the highest wave height.

	$H_{max} = 0.93[m]$			$H_{max} = 1.86[m]$			$H_{max} = 2.79[m]$		
Dir/T_s	$3.92[s]$	$5.23[s]$	$6.54[s]$	$4.58[s]$	$5.88[s]$	$7.19[s]$	$5.23[s]$	$6.54[s]$	$7.85[s]$
0°	1	1	1	1	1	1	2	2	2
30°	1	1	1	1	1	1	2	2	2
60°	1	1	1	1	1	2	2	2	2
90°	1	1	1	1	1	2	1	2	2
120°	1	1	1	1	1	2	1	2	2
150°	1	1	1	1	1	1	1	1	1
180°	1	1	1	1	1	1	1	2	1
210°	1	1	1	1	1	1	1	2	2
240°	1	1	1	1	1	1	2	2	2
270°	1	1	1	1	1	2	2	2	2
300°	1	1	1	1	1	1	1	2	2
330°	1	1	1	1	1	2	1	2	2

Table 5.16: Workability pull-in method 2

5.3.2 Cable tension and curvature in the base case

A range graph of the effective tension over the cable length for the base case is presented in Figure 5.23a. The tensions are similar to the tension observed in pull-in method 1 for the base case. The upward spike in Figure 5.23a is due to the weight of the cable clamp attached to the dynamic cable. The tether connecting the cable clamp with the anchor on the seabed is installed for this method prior to the pull-in operation. The differences between the amplitudes of the upward spikes for the minimum, mean and maximum are closer to each other, since the tether restricts the cable clamp to move freely.

The maximum curvature of the cable over its length is presented in Figure 5.23b. The curvature is lower compared to pull-in method 1. The dynamic cable in pull-in method 2 is wet stored on the seabed. For this reason the curvature of the cable is mainly determined by the entrance point of the FOWT. The CPS is the entrance point for the cable and the CPS is bended during the simulation. The interaction between the winches is finished at the moment the cable enters

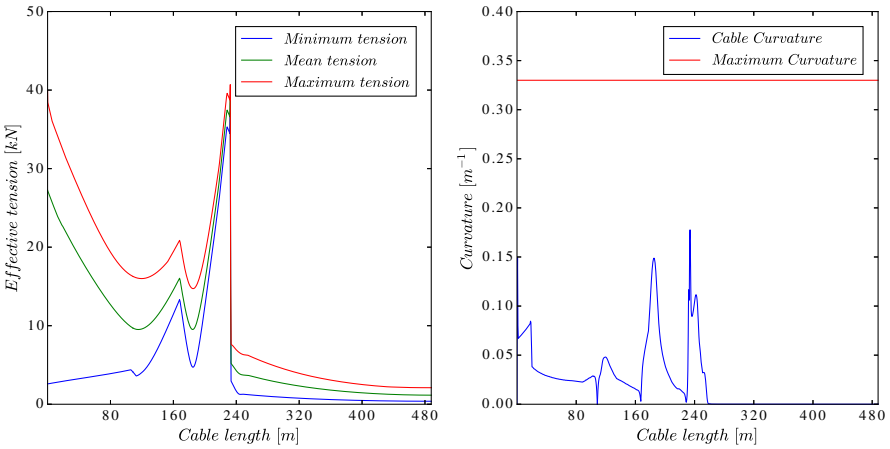

(a) Effective tension of the cable (b) Curvature of the cable

Figure 5.23: Cable behaviour of the pull-in method 2

the CPS. For this reason the cable is hardly bended during the simulation, resulting in a small maximum curvature.

The maximum effective tension and maximum curvature are not exceeded in the cases with environmental conditions. For this reason both Tables with the results are added to Appendix F.3.

5.3.3 Cable compression

The results of the workability in Table 5.16 showed that cable compression is the only failure mode in pull-in method 2.

The results of the minimum effective tension for the cases with environmental conditions are presented in Table 5.17. Cable compression is mainly observed for the cases with the highest wave height. The case with the highest compression value is boxed in Table 5.17 and investigated in more detail. Figure 5.24 presents a range graph of the effective tension over the cable length

	$H_{max} = 0.93[m]$			$H_{max} = 1.86[m]$			$H_{max} = 2.79[m]$		
Dir/T_s	$3.92[s]$	$5.23[s]$	$6.54[s]$	$4.58[s]$	$5.88[s]$	$7.19[s]$	$5.23[s]$	$6.54[s]$	$7.85[s]$
0°	0.4	0.4	0.4	0.4	0.4	0.4	-0.2	-0.1	-0.9
30°	0.4	0.4	0.4	0.4	0.4	0.1	-0.0	-3.0	-2.7
60°	0.4	0.4	0.4	0.3	0.2	-0.5	-0.1	-3.7	-3.0
90°	0.4	0.4	0.2	0.4	0.4	-1.9	0.3	$\boxed{-4.0}$	-2.5
120°	0.4	0.4	0.3	0.4	0.4	-0.3	0.4	-2.2	-1.8
150°	0.4	0.4	0.4	0.4	0.4	0.4	0.4	0.3	-0.0
180°	0.4	0.4	0.4	0.2	0.1	0.4	0.4	-0.9	0.4
210°	0.4	0.4	0.4	0.4	0.2	0.2	0.1	-0.8	-1.2
240°	0.4	0.4	0.4	0.3	0.4	0.2	-0.2	-1.3	-3.6
270°	0.4	0.4	0.4	0.1	0.4	-0.4	-0.6	-0.3	-0.0
300°	0.4	0.4	0.4	0.4	0.2	0.4	0.4	-3.6	-0.0
330°	0.4	0.4	0.4	0.4	0.4	-0.0	0.4	-0.4	-0.9

Table 5.17: Minimum cable tension pull-in method 2 $[kN]$

corresponding to the boxed case. Cable compression in the front part of the cable is observed in Figure 5.24. This part of the cable lies on the seabed at the start of the simulation.

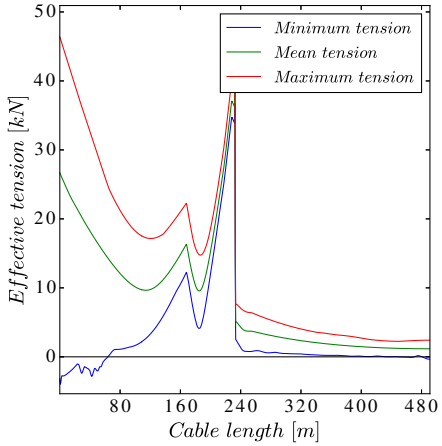

Figure 5.24: Tension over cable length

A time series of a node corresponding to the front of the cables, is presented in the top part of Figure 5.25a. Cable compression is observed in Figure 5.24 at the start of the simulation. At this point in time, the CLV starts picking up the cable. The first ten seconds of the simulation is presented in the top part of Figure 5.25b. The period of the tension oscillations in Figure 5.25b is approximately 6 s, which is almost the same as the wave period. This indicates that the motions due to the wave oscillations are travelling as tension oscillations through the cable.

Analysing of the boxed case showed interaction of the cable with the seabed at the start of the simulation. The corresponding GZ-accelerations are presented in the top part of Figure 5.25c. The highest GZ-accelerations are observed at the start of the simulation, which indicates again a correlation of the cable compression and the GZ-accelerations. The difference with the GZ-accelerations found for pull-in method 1 is that the GZ-accelerations found in method 2 are interacting with the seabed instead of the splash zone.

The workability of the cases corresponding to a wave direction of 150 degrees is very high. Similar for the boxed case with a wave direction of 90 degrees are the results of the grey marked case of Table 5.17 presented in the bottom part of Figure 5.25. There is no cable compression observed in the bottom part of Figure 5.25a. The lower GZ-accelerations presented in 5.25c prove that the cable compression is a result of the GZ-accelerations of the cable.

An explanation of the difference between the wave directions of 90 and 150 degrees is found is found after analysing the accelerations of the CLV. The waves for the case with a wave direction of 150 degrees are acting almost on the bow of the CLV. This results in a pitch acceleration of the CLV which are ten times lower for 150 degrees compared to the 90 degrees waves direction. The possibility to weather vane the CLV during the pick up of the cable could increase the workability.

The results of the maximum curvature and tension for the cases with environmental conditions are not exceeded and added to Appendix F.3.

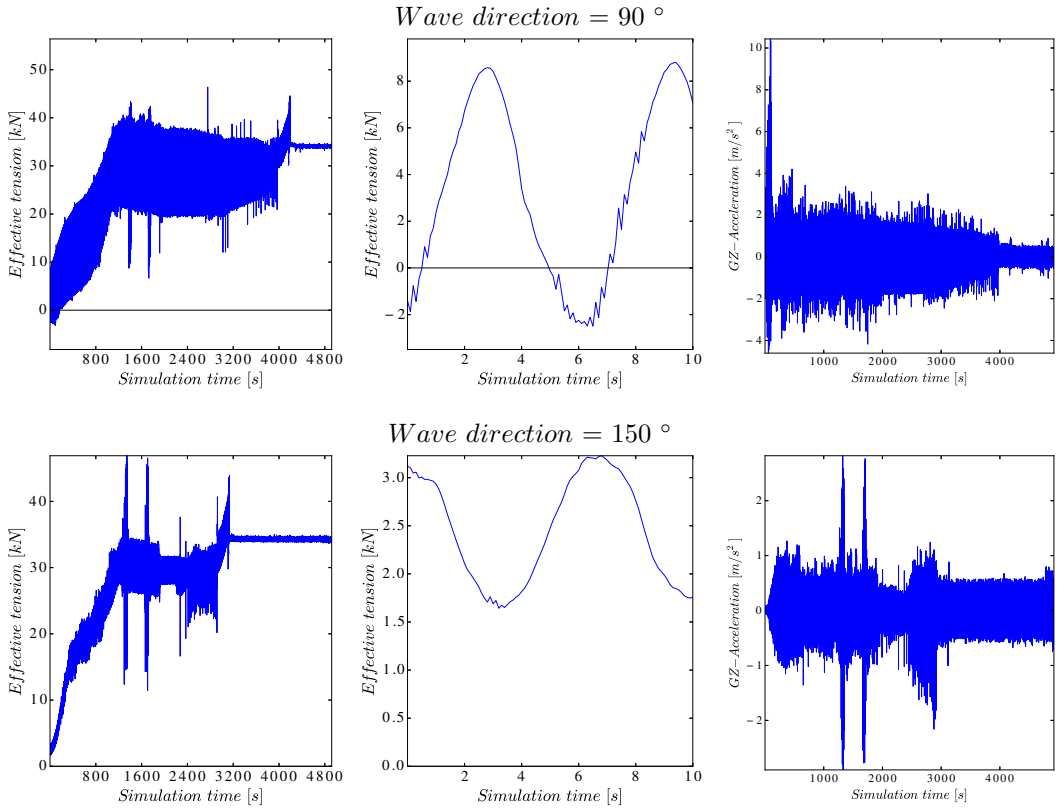

(a) effective tension in time (b) Close-up of spike (c) GZ-accelerations in time

Figure 5.25: Results of cases with $H_{max} = 2.79$ $[m]$ and $Ts = 6.54$ s

5.3.4 Tension equipment

The same advanced system controlling the winches is used for this pull-in method. The difference of the system for method 2 compared to the system for method 1 are the limitations on which the system regulates the pull-in. Firstly, the system controls on the behind condition which ensures that the CLV does not recovers the cable from the seabed too fast. The system starts controlling the winches on a minimum seabed clearance afterwards. From this moment in time the system behaves similar to the system for method 1, but from another direction towards the FOWT. For clarity purposes, the important events that occur during the operation are again numbered and listed in Table 5.18.

Number	Event
I	The pay-out wire becomes tight, pick up of the cable starts. CLV sails towards the FOWT.
II	The cable has no contact with the seabed anymore.
III	The pullhead reaches the position where 8 m seabed clearance is ensured. The pay-out winch holds the cable on this position. The pull-in winch starts.
IV	The CLV reaches his final position. The pull-in winch becomes tight and transfer of the cable towards the FOWT starts.
V	The pullhead reaches the position where the system of the winches controls on a seabed clearance of 7 m instead of 8 m.
VI	The pay-out winch is disconneted via an ROV link
VII	The hang-off point is reached, so pull-in is finished.

Table 5.18: Events explanation

The tensions over time of the pull-in and pay-out winches for the base case are presented in Figure 5.26a and 5.26b, respectively.

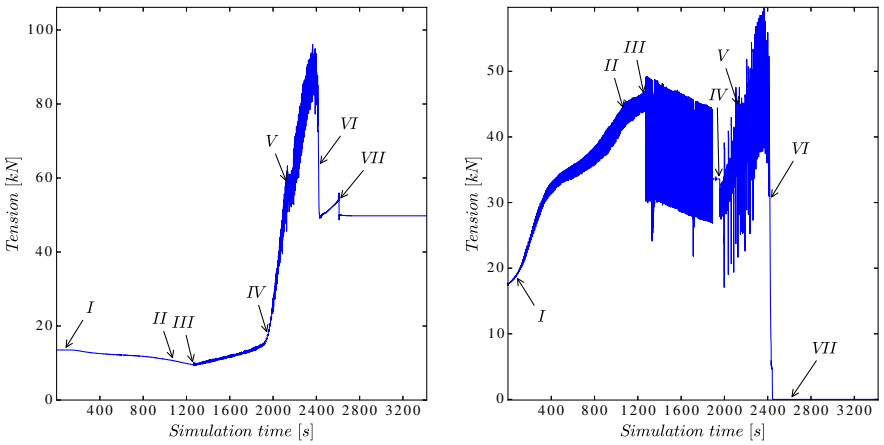

(a) Pull-in tension (b) Pay-out tension

Figure 5.26: Tension on the winches during the simulation

The control system of the winches regulates that after the cable recovery the pay-out winch continues until the cable has sufficient seabed clearance. The oscillations after point III in Figure 5.26b are a result of forward sailing of the CLV combined with the fact that the pay-out winch holds the cable at the same position above the seabed. The interaction between both winches starts after point V and is noticed by the increasing tension in both winches presented in Figure 5.26a and 5.26b.

The results of the maximum tensions found for the pull-in and pay-out winch for the cases with environmental conditions are presented in Appendix F.3. The minimum required tension of the pull-in winch is marked as 104.2 kN and the minimum tension of the pay-out tension is 61.9 kN.

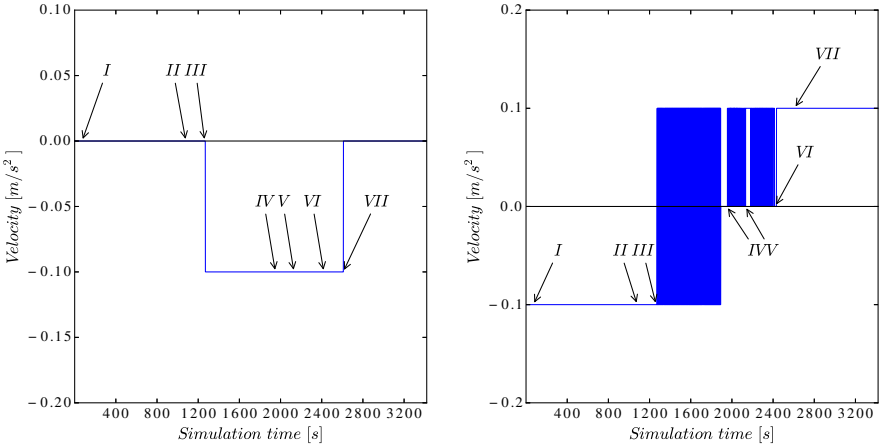

(a) Pull-in velocity (b) Pay-out velocity

Figure 5.27: Velocity of the winches during the simulation

The corresponding velocities of the winches during the simulation of the base case are presented

in 5.27. The pull-in winch, presented in Figure 5.27a, is not used between I and III, since this is the interval in which the dynamic cable is recovered up from the seabed using the pay-out winch only. For this reason the velocity of the pay-out winch, presented in Figure 5.27b, is negative in this interval. The pay-out winch holds the pullhead on the same position between III and IV, which is indicated in Figure 5.27b by the fact that the pay-out velocity is oscillation between -0.1 and 0.1 m/s resulting in a mean velocity of 0 m/s. The pull-in winch starts the pull-in from III and the pull-in wire is tight from IV. Transfer of the cable towards the FOWT starts from IV, since the pull-in velocity is still continuous and the pay-out velocity oscillates between 0.1 and 0 m/s, which has a mean velocity of 0.05 m/s.

The winches are controlled by a system as described in Section 4.7.1. The system is designed to control the winches such that the cable has a seabed clearance of 10 m during the transfer of it towards the FOWT. However, the base case model failed using this seabed clearance, since the pullhead had to be above the entrance point of the FOWT to ensure 10 m seabed clearance, which is impossible. For this reason the system is controlled such that it ensures the largest seabed clearance as possible.

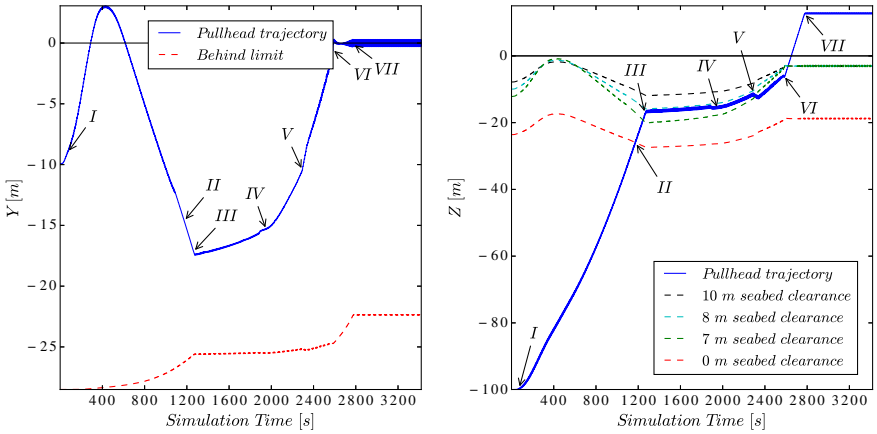

(a) $Y - direction$ (b) $Z - direction$

Figure 5.28: Pullhead trajectory during the simulation

The trajectory of the pullhead for a random case with environmental conditions is presented in Figure 5.28. The pullhead trajectory in $Y - direction$ is presented in Figure 5.28a and shows that the behind limit is not exceeded during the simulation. The pullhead trajectory in $Z - direction$ is presented in Figure 5.28b. The corresponding elevation of the cable sagbend above the seabed is presented in Figure 5.29. After recovery of the cable remains the sagbend on a elevation of 12 m above the seabed corresponding to point III. As already explained starts the transfer of the cable towards the FOWT from IV and the system controls on a seabed clearance which can be 40 percent lower with respect to the 10 m seabed clearance limitation. This results in a seabed clearance of the sagbend at V of approximately 9 m. The system needs more space from VI to perform the pull-in, so for this reason the system is allowed to be which results in a seabed clearance of approximately 8 m. The final elevation of the sagbend is located at point VII.

The results of the minimum seabed clearance for the cases with environmental conditions are presented in Table 5.19. An important note regarding the results of Table 5.19 has to be made that the minimum seabed clearance is tested in steps of 0.5 m.

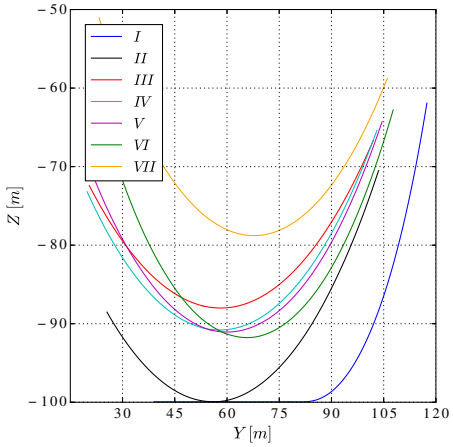

Figure 5.29: Elevation of the cable sag bend above the seabed corresponding to the events

	$H_{max} = 0.93[m]$			$H_{max} = 1.86[m]$			$H_{max} = 2.79[m]$		
Dir/T_s	$3.92[s]$	$5.23[s]$	$6.54[s]$	$4.58[s]$	$5.88[s]$	$7.19[s]$	$5.23[s]$	$6.54[s]$	$7.85[s]$
0°	7.0	7.0	7.0	7.0	6.5	6.0	7.0	7.5	7.0
30°	7.0	7.0	7.0	7.0	8.0	7.5	7.0	7.0	6.5
60°	7.0	7.0	7.0	7.0	8.0	7.5	7.0	7.5	7.0
90°	7.0	7.0	7.0	7.0	6.0	7.5	6.5	5.5	7.0
120°	7.0	7.0	7.0	7.0	7.0	7.5	7.0	6.0	5.5
150°	7.0	7.0	7.0	7.0	6.0	6.0	5.5	7.0	5.5
180°	7.0	7.0	7.0	7.0	7.0	6.5	7.0	7.0	7.5
210°	7.0	7.0	7.0	7.0	7.0	7.5	6.5	7.0	7.0
240°	7.0	7.0	7.0	7.0	7.5	7.0	7.5	7.0	6.5
270°	7.0	7.0	7.0	7.0	7.5	7.0	7.5	5.5	7.5
300°	7.0	7.0	7.0	7.0	7.0	7.5	6.5	7.0	5.5
330°	7.0	7.0	7.0	7.0	6.5	7.5	7.0	5.5	7.0

Table 5.19: Seabed clearance pull-in method 2 $[m]$

5.3.5 CPS behaviour

Similar to pull-in method 1 is the CPS used to protect against exceeding of the maximum cable curvature. A range graph of the bending moments over the CPS length is presented in Figure 5.30a. A time series of the bending moments of the fixed end is presented in Figure 5.30b. The bending moments in the CPS in this pull-in method are higher compared to method 1. An explanation for these higher values is found in the shape of the CPS during the pull-in operation, presented in Figure 5.31.

The CPS is bended in both X and $Y-direction$, presented in Figure 5.31a and 5.31b, respectively. The CPS bends more compared to method 1 resulting in higher forces on the pull-in and pay-out wire, during transfer of the cable towards the FOWT. The change in shape between V and VI in Figure 5.31 corrolates to the high bending moments in this interval as presented in Figure 5.30. The shape of the CPS is also the reason that the system controlling the winches cannot ensure 10 m seabed clearance, since excessive bend moments due to a too small angle result is failure of the CPS.

The maximum bending moments of the cases with environmental conditions are presented in Table 5.20. In general, the bending moment are higher in this pull-in method compared to method 1. The maximum value of the bending moment of 119 kNm is found during the dynamic analyses.

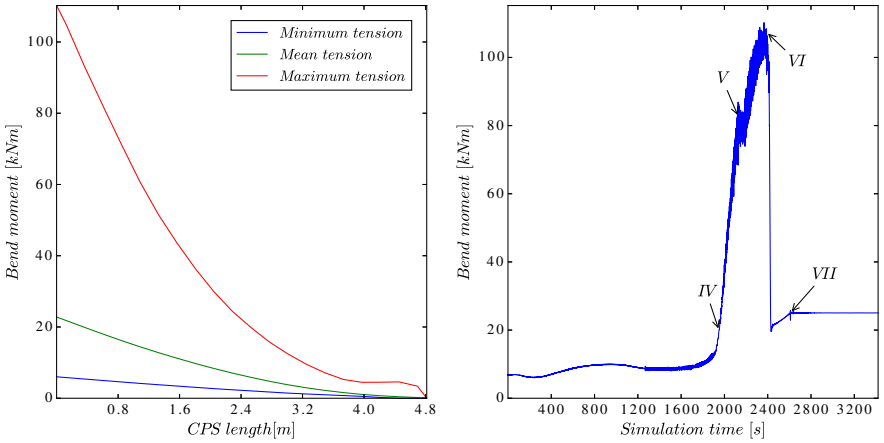

(a) Bend moment over the length (b) Bend moment during simulation

Figure 5.30: Bend moment on the CPS

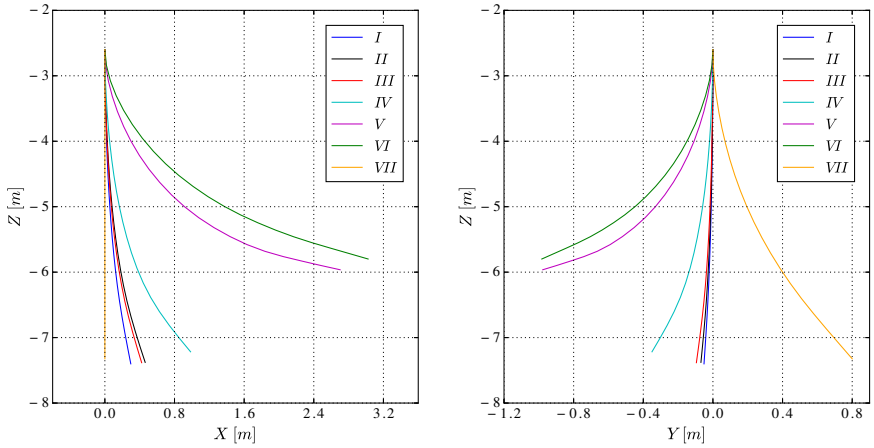

(a) $X-direction$ (b) $Y-direction$

Figure 5.31: CPS shape corresponding to the events

	$H_{max} = 0.93[m]$			$H_{max} = 1.86[m]$			$H_{max} = 2.79[m]$		
Dir/T_s	$3.92[s]$	$5.23[s]$	$6.54[s]$	$4.58[s]$	$5.88[s]$	$7.19[s]$	$5.23[s]$	$6.54[s]$	$7.85[s]$
0°	114.3	111.8	110.7	110.8	109.9	107.6	114.1	114.8	111.7
30°	113.2	114.3	111.4	110.5	108.8	107.1	111.1	99.4	112.5
60°	113.3	111.7	112.0	113.1	117.0	114.2	114.6	118.8	108.2
90°	110.8	113.2	111.4	110.8	105.2	113.0	109.0	105.0	111.4
120°	110.7	109.9	110.1	111.8	111.4	112.7	110.1	106.1	105.2
150°	110.5	113.4	110.8	113.3	107.9	108.8	102.5	107.5	106.9
180°	108.2	110.4	110.0	112.9	108.7	109.7	113.1	111.1	109.9
210°	109.6	111.4	111.6	110.6	111.0	105.4	100.3	98.9	109.6
240°	109.6	110.9	110.5	109.7	107.8	108.6	101.1	107.7	103.3
270°	108.5	111.7	110.4	110.1	110.1	111.1	107.1	108.8	113.3
300°	111.7	110.0	109.7	113.5	113.0	114.3	114.8	110.5	112.0
330°	113.4	113.7	114.4	114.1	109.5	116.6	119.2	106.4	118.8

Table 5.20: Maximum bend moment CPS pull-in method 2 $[kNm]$

5.4 Method 3: Post-lay pull-in via FOWT

In this Section the results of the pull-in method 3 are described. Table 5.21 represents the failure modes for which all cases are tested in method 3. Firstly, the workability is presented to have an indication which failure modes are occurring. Furthermore the minimum, maximum effective tensions and the maximum curvature in the cable for the base case are described in the cable behaviour section. The failure mode cable compression is described afterwards. This Section finishes with the tension in the pull-in winch during the pull-in operation. The results of the limitations which are presented in Table 5.21 and not covered in this Section are added to Appendix F.4.

Number	Limitation
1	Successive sea state
2	Cable compression
3	Exceeding maximum cable tension
4	Exceeding maximum cable curvature
5	Maximum pull-in tension
6	Exceeding maximum bottom tension
7	Maximum bend moment of the CPS
8	Maximum tension in the tether
9	Exceeding maximum cable offset
10	Structure interaction

Table 5.21: Failure modes on which pull-in method 3 is tested

5.4.1 Workability

Similar to Section 5.1 are the results of the workability presented in Table 5.22. The workability of method 3 is 96 percent. The workability indicates that exceeding of the minimum effective cable tension is the only failure mode found for some cases in pull-in method 3.

	$H_{max} = 0.93[m]$			$H_{max} = 1.86[m]$			$H_{max} = 2.79[m]$		
Dir/T_s	$3.92[s]$	$5.23[s]$	$6.54[s]$	$4.58[s]$	$5.88[s]$	$7.19[s]$	$5.23[s]$	$6.54[s]$	$7.85[s]$
0°	1	1	1	1	1	1	1	1	1
30°	1	1	1	1	1	1	2	1	1
60°	1	1	1	1	1	1	1	1	1
90°	1	1	1	1	1	1	2	1	1
120°	1	1	1	1	1	1	1	1	1
150°	1	1	1	1	1	1	1	1	1
180°	1	1	1	1	1	1	1	1	1
210°	1	1	1	1	1	1	2	1	1
240°	1	1	1	1	1	1	1	1	1
270°	1	1	1	1	1	1	2	1	1
300°	1	1	1	1	1	1	1	1	1
330°	1	1	1	1	1	1	2	1	1

Table 5.22: Workability pull-in method 3 [–]

5.4.2 Cable tension and curvature in the base case

A range graph of the effective tension over the cable length in the base case is presented in Figure 5.32a. The upward spike in Figure 5.32a is a result of the weight of the clamp, which is attached on the cable. The difference between the spikes of the minimum, mean and maximum effective tension is smaller compared to the other pull-in methods. An explanation for this small difference is that only the pull-in which is used to perform the pull-in. For this reason no other equipment

adds load to the cable.

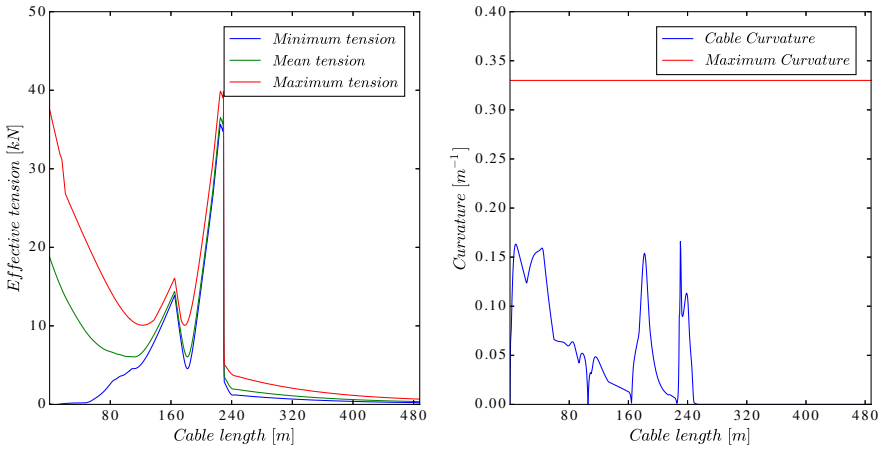

(a) Effective tension of the cable (b) Curvature of the cable

Figure 5.32: Cable behaviour of the pull-in method 3

A range graph of the maximum curvature over the cable length is presented in Figure 5.32b. The first 65 m is curved, since the cable lies on the seabed in a s-shape. The cable section between 160 and 220 m is curved, since this cable section is the buoyant cable section. In addition, the cable is pulled almost vertical into the FOWT. For this reason is the cable bended very limited during the pull-in operation. The maximum effective tension and curvature of the cable are not exceed for the cases with environmental conditions. The results are added to Appendix F.4 for this reason.

5.4.3 Cable compression

The results of the workability in Table 5.22 indicates that cable compression is found in some cases of this pull-in method. An explanation for the cable compression is presented in this Section.

The results of the minimum effective tension for the cases with environmental conditions are presented in Table 5.23. The cable compression found in this pull-in method are relatively low

	$H_{max} = 0.93[m]$			$H_{max} = 1.86[m]$			$H_{max} = 2.79[m]$		
Dir/T_s	$3.92[s]$	$5.23[s]$	$6.54[s]$	$4.58[s]$	$5.88[s]$	$7.19[s]$	$5.23[s]$	$6.54[s]$	$7.85[s]$
0°	0.0	0.0	0.0	0.0	0.0	0.0	0.0	0.0	0.0
30°	0.0	0.0	0.0	0.0	0.0	0.0	-0.4	0.0	0.0
60°	0.0	0.0	0.0	0.0	0.0	0.0	0.0	0.0	0.0
90°	0.0	0.0	0.0	0.0	0.0	0.0	-0.8	0.0	0.0
120°	0.0	0.0	0.0	0.0	0.0	0.0	0.0	0.0	0.0
150°	0.0	0.0	0.0	0.0	0.0	0.0	0.0	0.0	0.0
180°	0.0	0.0	0.0	0.0	0.0	0.0	0.0	0.0	0.0
210°	0.0	0.0	0.0	0.0	0.0	0.0	-0.3	0.0	0.0
240°	0.0	0.0	0.0	0.0	0.0	0.0	0.0	0.0	0.0
270°	0.0	0.0	0.0	0.0	0.0	0.0	-0.3	0.0	0.0
300°	0.0	0.0	0.0	0.0	0.0	0.0	0.0	0.0	0.0
330°	0.0	0.0	0.0	0.0	0.0	0.0	−0.9	0.0	0.0

Table 5.23: Minimum cable tension pull-in method 3 $[kN]$

compared to the values found in the other methods. Nevertheless, the cable compression for the boxed case in Table 5.23, which has the lowest minimum effective tension of -0.9 kN, is investigated in more detail.

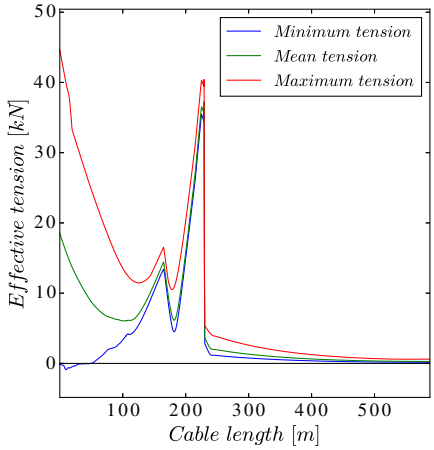

Figure 5.33: Effective tension over cable length of the boxed case

A range graph of the effective tension over the cable length corresponding to the boxed case is presented in Figure 5.33. Cable compression is observed in the front section of the cable. This cable section lies on the seabed at the start of the simulation.

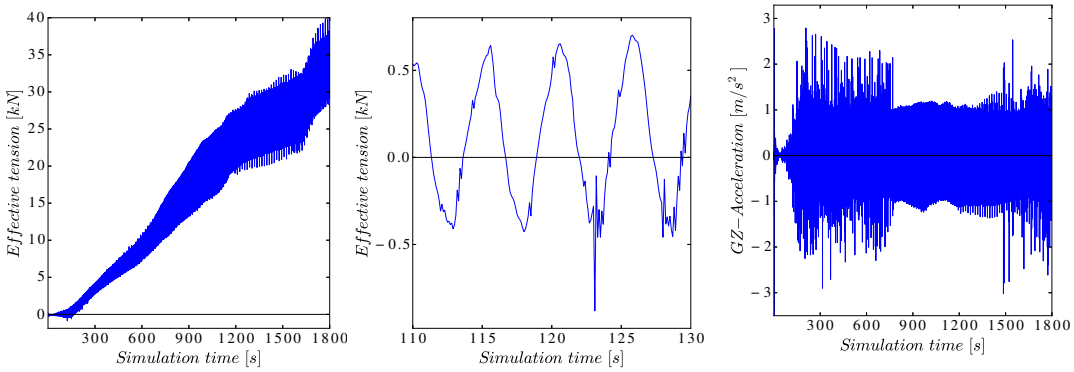

(a) Tension over time

(b) Close-up of spike

(c) GZ-acceleration over time of the boxed case

Figure 5.34: Compression results pull-in method 3

A time series of the effective tension of the corresponding node is presented in Figure 5.34a. Cable compression is observed from the start of the simulation until 150 s, which indicates that cable compression is a result of the interaction of the cable with the seabed.

A close-up of the compression oscillations between 110 s and 130 s is presented in Figure 5.34b. The compression oscillations have a period which is similar to the wave period. The corresponding $GZ - accelerations$ are presented in Figure 5.34c and indicates that the cable has higher accelerations at the start of the simulation. These accelerations of the cable nearby the seabed results in slamming of the cable on the seabed which cause cable compression.

Similar to the free lay model is this method modelled with a maximum time-step of 0.1 s. The influence of decreasing this maximum time-step to 0.01 s is investigated for the boxed case. The results are presented in Figure 5.35.

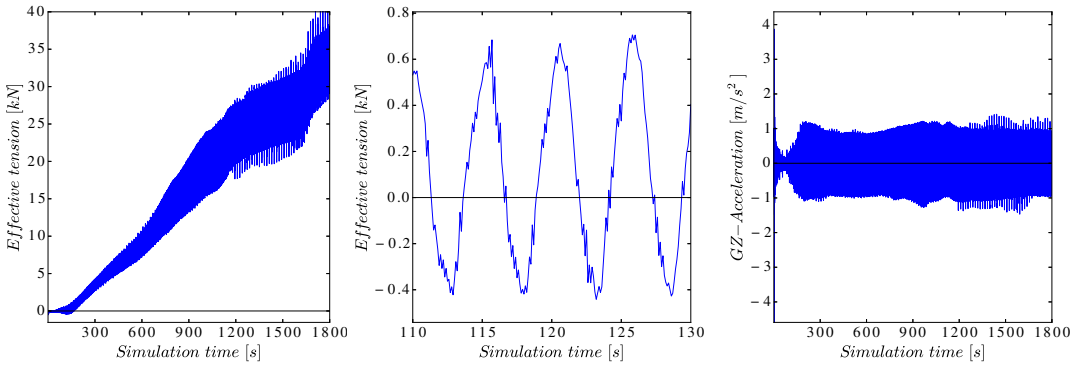

(a) Tension over time (b) Close-up of spike (c) GZ-acceleration over time

Figure 5.35: Compression results pull-in method 3 using a maximum time-step of 0.01 s

A close-up of the effective tension oscillations in Figure 5.35b indicates that the downward spike around 123 s is disappeared, cable compression, however, is still observed. The cable compression found in the cases with environmental conditions are small compared to the other pull-in methods. This is explained by the fact that the pull-in is performed by using the FOWT only. Therefore only the FOWT influences the cable motions, whereas in the other methods also the CLV adds to the dynamic cable behaviour. The FOWT has a more stable motion behaviour in environmental conditions compared to the CLV. For this reason the interaction of the cable with the seabed is reduced and a higher workability is obtained.

5.4.4 Tension equipment

The behaviour of the pull-in winch in method 3 is described in this Section. Similar to the other methods are the events numbered and listed in Table 5.24.

Number	Event
I	First bend of the s-shape wet storage disappeared.
II	Second bend of the s-shape disappeared, cable start sliding towards the centre line.
III	Cable start sliding forward towards the FOWT over the seabed.
IV	Cable contact with the seabed disappeared.
V	The pullhead reaches the entrance of the CPS.
VI	The pullhead reaches the entrance of the FOWT.
VII	The pullhead reaches the hang-off point

Table 5.24: Events explanation

Pull-in of the cable in method 3 is performed by only using a winch installed on the FOWT. For this reason only a time series of the tension of the pull-in winch is presented in Figure 5.36a. No advanced system to control the winches used in pull-in method 3. A constant pull-in velocity is used until the cable reaches the hang-off point. The tension in the pull-in winch increases in time due to the corresponding events. The amount of cable length which is free hanging under the FOWT increases in time. In addition, from II and III the cable slides over the seabed sideways to the cable route and forward towards the FOWT, respectively. Sliding of the cable over the seabed contributes to the tension in the pull-in winch, since friction forces are generated. The corresponding elevation of the sagbend above the seabed is presented in Figure 5.36b.

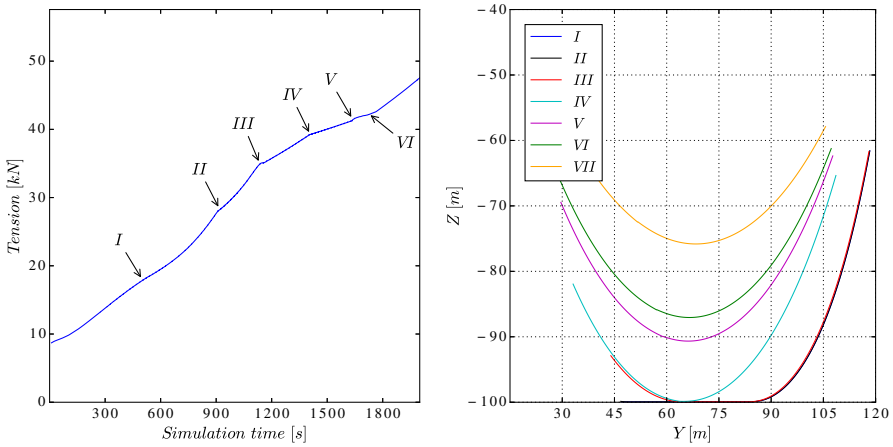

(a) Tension of the pull-in winch in time (b) Sagbend elevation above seabed in time

Figure 5.36: Pull-in winch and elevation of the sagbend

The results of the maximum pull-in tension for this method with environmental conditions are added to Appendix F.4. A maximum pull-in tension of 58.3 kN is found. The required capacity of the pull-in winch for method 3 is significant lower in comparison with the other two pull-in methods. There is no pay-out winch interacting with the pull-in winch in method 3. Interaction of the winches resulted in high bending moments in the CPS which contributed to the tension in the winches. In addition, the absence of a CLV in this method reduces the dynamic cable behaviour.

5.4.5 CPS behaviour

Similar to the other methods is a CPS installed on the FOWT. A range graph of the bending moments over the CPS length is presented in Figure 5.37a. A time series of the bending moments of the fixed end is presented in Figure 5.37b. The bending moments in the CPS in this pull-in method are lower compared to the other methods, since the cable is pulled almost vertical towards the FOWT.

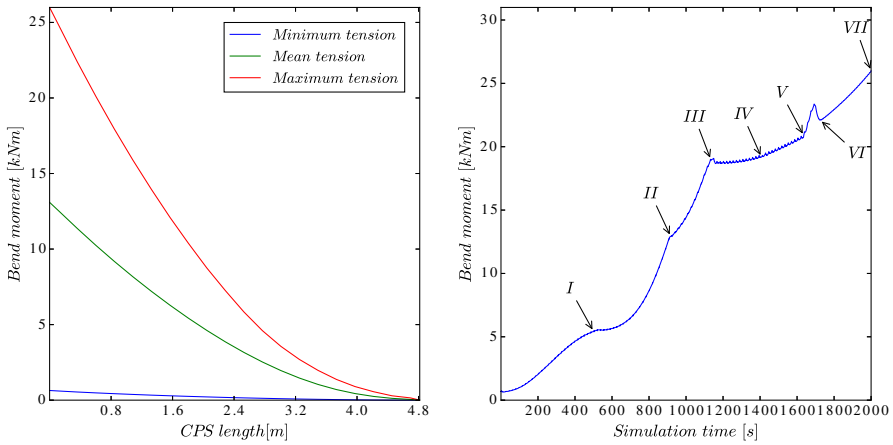

(a) Bend moment over the length (b) Bend moment during simulation

Figure 5.37: Bend moment on the CPS

The CPS is bended in both X and $Y-direction$ during the pull-in operation, presented in Figure 5.38a and 5.38b, respectively. The bending of the CPS in this method is small compared to the other methods, resulting in lower bending moments.

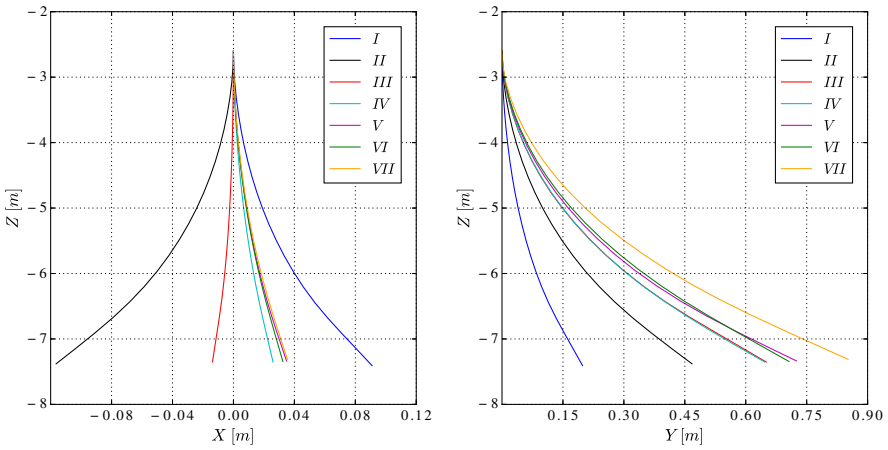

(a) $X-direction$ (b) $Y-direction$

Figure 5.38: CPS shape corresponding to the events

The results of the maximum bending moments of the cases with environmental conditions are added to Appendix F.4. A maximum value of the bending moment of 38.4 kNm is found during the dynamic analyses, which is significantly lower than the other methods.

CHAPTER 6

Conclusion & Recommendations

The goal of this research was to explore multiple installation methods for the pull-in of a dynamic cable into a FOWT and to compare them with respect to workability determined by different limitations. In this Chapter the conclusions of this research are given in Section 6.1. Recommendations for further research are given in Section 6.2.

6.1 Conclusions

Three different pull-in methods are explored and investigated in this research. A free lay model is also created to model the cable installation prior to the pull-in operation. The results show that all pull-in methods are suitable to install the dynamic cable safely into the FOWT. Based on these results pull-in method 3 has the highest workability. This is explained by the fact that the pull-in is performed by using the FOWT only. Therefore only the FOWT influences the cable motions, whereas in the other methods the CLV also adds to the dynamic cable behaviour. The FOWT has a more stable motion behaviour in similar environmental conditions compared to the CLV. For this reason the interaction of the cable with the seabed is reduced and a higher workability is obtained.

Cable compression is a limitation which is a common issue in cable installation analyses. In this research it is the most common failure mechanism for all methods in environmental conditions. The cable compression found in the free lay model is a result of the motions generated by the buoyant section in the splash zone. The compression is decreasing with increasing wave periods. In the splash zone, generally, the particle velocities and accelerations are largest and they decrease for increasing wave periods.

The cable compression in pull-in method 1 is caused in a similar way as in the free lay model. A correlation of the cable compression and high cable accelerations is found. This is related to the buoyant section in the splash zone. The cable compression found in method 1 depends on wave direction, since the wave directions which are pushing the cable towards the CLV show higher cable compression compared to the opposite wave directions, where the cable is pushed away from the CLV. The cable is pushed away from the CLV, since diffraction of the CLV is not included in OrcaFlex.

The dynamic cable is stored on the seabed at the start of the pull-in operation in method 2. The dynamic cable starts interacting with the seabed at the moment the CLV starts recovering the cable from the seabed. This results in cable compression for almost all wave directions for the sea states with the largest waves. The compression oscillates with a period which is similar to the wave period. Compression is only observed in the interval that the cable interacts with the

seabed. There is no compression for the sea states with the waves acting on the bow of the CLV. This means that a higher workability can be realised if the CLV is able to weather vane during recovery of the dynamic cable from the seabed.

Ensuring 10 m seabed clearance is not possible in pull-in method 2, but a minimum seabed clearance of 5.5 m is ensured for the cases with environmental conditions. Changes in the cable configuration, the design of the FOWT, the location of the I-tube and the geometry of the CPS are all influencing the height of the cable above the seabed. All these parameters are unique for every project. Despite the fact that the limitation of ensuring 10 m seabed clearance is not ensured in method 2, it is still considered a suitable pull-in method. The clearance area between the FOWT and the CLV also determines the elevation of the cable above the seabed. The cable comes closer to the seabed when the CLV starts the pull-in too far away from the FOWT. The pull-in would be easier when the CLV would be able to come closer to the FOWT than the 50 m clearance used in this research.

As stated, compression is a common issue in cable analyses. However, in this research it is found that not all values are due to actual physical compression of the cable. Numerical compression is seen quite often in the results. The cases are identified by very short time instances at which compression occurs (typically the length of one time step). Further investigation showed that reducing the maximum time step for the implicit solving scheme in OrcaFlex from 0.1 to 0.01 s resulted in more realistic values for several cases. An explanation for this is found in the variable time step algorithm. This algorithm automatically reduces the time step after the specified maximum amount of iterations per time step is reached. Such systems tend to be prone to generate numerical errors. Cable compression, however, is still present in many cases and the numerical errors are not solved by the same specified time step. It should be noted that reducing the time step significantly increases the total calculation time. Time was unfortunately no longer available.

The cable compression found in this research is due to the buoyant section in the splash zone and interaction of the cable with the seabed. Multiple approaches could solve the compression problems. Firstly, an irregular wave approach instead of a regular wave approach could solve the compression problems which are related to modelling issues, since the cable will be no longer subject to a single frequency. Also, adding structural damping to the models could decrease the compression values. In addition, avoiding of a buoyant cable part in the splash zone should remove the cable compression as was found in the analysis of the free lay model and method 1. For practical purposes, avoiding the floating cable section is desirable, since this section can collide with the stern of the CLV. The buoyant cable part can be removed from the splash zone by adding extra weight to the dynamic cable. This extra weight can be created by using temporary attachments to the cable. As a result, in pull-in method 1 the seabed clearance can no longer be guaranteed and the cable is likely to have temporary interaction with the seabed.

The pull-in tensions of the pull-in winch are higher for pull-in method 1 and 2 compared to pull-in method 3. The tensions are a result of the interaction between the pull-in and pay-out winch performing the pull-in. Both winches are controlled to hold the pullhead in a position above the seabed during the transfer of it towards the FOWT. In addition, the CPS is heavily bended during the transfer of the cable towards the FOWT, resulting in large reaction forces since the CPS tends to go back to its equilibrium position. The system controlling the winches used in pull-in method 1 and 2 worked very well, since the limitations on which it is designed were not exceeded. None of the cases is failed due to failure of the control system. For this reason the system is worthwhile to be developed further to assist during the pull-in operations in reality.

The buoyant part of the cable is modelled with the DBMs uniformly distributed. At the transition point, where the cable diameter changes due to the DBMs, problems with exceeding of the maximum curvature are found, since the cable has no contact with the chute. In reality, this abrupt transition is present at every DBMs, so exceeding of the maximum curvature can occurs multiple

times. This could be solved in practice using a tapered bend restrictor at the end of the DBMs. In addition, avoiding of exceeding of this maximum curvature is possible by introducing a structure which supports the DBMs at the stern of the vessel.

6.2 Recommendations

The system controlling the winches used in this thesis uses instant changes of the winch velocities. Improvement of the system is possible when the velocities of the winches are changed gradually. This means that when the pullhead reaches the limitation that the system is able to let it exceed the limitation for a short period of time and that the winches are taking the pullhead back above the limitation. Another option would be to increase this limitation by the same amount it is allowed to exceed. The downside of this is that the CPS will probably be loaded more heavily. The external script created to control the winches in this research is robust enough for modelling purposes, but is not suitable for use on a CLV. Implementing of such a system requires more research on the elements controlling the equipment on the CLV.

The high tensions in the winches show correlation with the tightness of the pull-in and pay-out winches, resulting in high resistance of the CPS. This tightness is necessary to ensure the minimum seabed clearance. The results show limited movement of the cable sagbend, which indicates that reducing of the minimum seabed clearance should be possible without increasing the risk of cable failure. Lowering of the cable sagbend gives the system more space, resulting in lower tensions. Combination of a control system with a cable monitoring system could increase the workability of the CLV for pull-in operations. In addition, the use of motion compensating winches could also improve the workability.

The pull-in methods are compared on workability. However, the pull-in methods all have their pros and cons on multiple criteria which are not described in this research. A combination of the financial impact, with the pros and cons and the workability of each methods is useful to investigate which method is best in more depth.

The specified maximum time step used for the implicit solving scheme in OrcaFlex is influencing the results of the simulations. A sensitivity analysis on the effect of the size of the time step should be performed looking at all models with environmental conditions. The purpose would be to find the optimum time step for the various combinations of environmental conditions. The explicit solving scheme should also be included in this study.

A regular wave approach is used in this research. A wave approach using irregular waves with snapshots at multiple intervals, could increases the accuracy of the calculations, but also increases the simulation time. This combined with simulation of the models in higher sea states and corresponding sea state for different locations in the world could increase the knowledge of the pull-in methods workability. Also, the cable installation for a smaller and larger water depth, compared to the used water depth in this research, should be investigated. In addition, multiple current profiles and the influence of wind loadings should be investigated.

One specific dynamic cable with corresponding properties and configuration is used. Sensitivity analyses on the influence of changing various parameters which are related to the cable should be part of further research.

The buoys are modelled with a combination of the cable and DBMs properties. A more accurate modelling approach could be used to model the DBMs as attachments to the cable. In addition, to have better understanding of the influence of the DBMs on the fluid behaviour and the drag coefficients, Computational Fluid Dynamics should be used to model the fluid around the cable and DMBs. A sensitivity analysis of varying the total amount of buoyancy, the spacing

and the size of the DBMs should also be part of further research.

The behaviour of the FOWT influences the interaction between the winches performing the pull-in. A smaller investigation within this thesis focussed on a mooring system and its influence on the behaviour of the FOWT. It showed that a mooring system can be neglected if it is stiff enough. However, this may not always be realistic. Therefore the operations should also be investigated with a working mooring system, because a FOWT that moves laterally influences the behaviour of the winch system.

VBMS´ Ndurance is used in this research. Investigation of the pull-in methods with multiple CLVs increases the possibility to compare the CLVs.

The cable clamp used in this research is designed with bellmouts on both ends of it. Addition of dynamic bend stiffeners on both ends of the cable clamp could improve the fatigue lifetime on the cable.

OrcaFlex uses Reynolds number dependent drag coefficients and neglects the Keulegan Carpenter number dependent drag coefficients. A combination of both number to determine the drag coefficients should be part of further research, since this may increase the accuracy of the calculations in the splash zone.

Acknowledgements

Special thanks to Stephan Ingham and James Young from JDR for providing the properties and configuration of a dynamic cable. They also provided the properties of a dynamic bend stiffener. In addition, thanks to John Deasey from Trelleborg for providing the properties of a subsea tether arrangement.

Bibliography

[1] Wind energy council GWEC Global. Global wind energy outlook 2014. *Brussels: GWEC*, 2014.

[2] Kolios AJ. Chahardehi A. Brennan FP. Collu, M. A comparison between the preliminary design studies of a fixed and a floating support structure for a 5 MW offshore wind turbine in the North Sea. pages 21–23, 2010.

[3] L. Holthuijsen. Waves in oceanic and coastal waters. 2007.

[4] Massie W. Journée, J. Offshore Hydromechanics, 2001. *Lecture notes on offshore hydromechanics for Offshore Technology students, code OT4620.*

[5] F. White et al. Fluid mechanics. *McGraw-Hill, New York*, 2003.

[6] Orcina. OrcaFlex Manuel, Version 9.8a, 2014.

[7] Stemat. Equipment sheet Stemat Spirit.

[8] Det Norske Veritas(DNV). DNV-RP-J301: subsea power cables in shallow water renewable energy applications, 2014.

[9] JDR Cable Systems Ltd. (JDR). Technical note: Floating wind turbine-tn-001 created for msc thesis, 2015.

[10] Johanning L. Smith G. H. Thies, P.R. Assessing mechanical loading regimes and fatigue life of marine power cables in marine energy applications. *Journal of Risk and Reliability*, 228 no. 5:469–477, 2014.

[11] Trelleborg Offshore. *Tailored buoyancy solutions.* Trelleborg, 2015.

[12] R. Cochrane. Vertical axis wind turbines. November 17 2011. US Patent App. 10/565,227.

[13] Company Data. *VBMS tender information VAWT.* VBMS, 2015.

[14] Luquiau E. Smadja C. Silvert F. Cahay, M. Use of a vertical wind turbine in an offshore floating wind farm. pages 2–5, 2011.

[15] Company Data. *Equipment drawings.* VBMS, 2015.

[16] Boskalis Royal Westminster. Equipment Sheet Ndurance.

[17] Det Norske Veritas (DNV). DNV-OS-H101: Offshore Standard, Marine Operations, General , 2014.

[18] Trelleborg Offshore. *Tether clamps.* Trelleborg, 2015.

[19] COP. COP21 Paris. 2015.

[20] Feasibility of floating platform systems for wind turbines, author=Musial, W., Butterfield, S., Boone, A., journal=23rd ASME Wind Energy Symposium, Reno, NV, year=2004.

[21] Hasselmann, K., Barnett, TP., Bouws, E., Carlson, H., Cartwright, DE., Enke, K., Ewing, JA., Gienapp, H., Hasselmann, DE., Kruseman, P., and others. Measurements of wind-wave growth and swell decay during the joint north sea wave project (jonswap). Technical report, Deutches Hydrographisches Institut, 1973.

[22] Det Norske Veritas (DNV). DNV-OS-H205: Offshore Standard, Lifting Operations, 2014.

[23] J. Pinkster. *Low frequency second order wave exciting forces on floating structures.* PhD thesis, TU Delft, Delft University of Technology, 1980.

[24] Isaacson M. Wehausen JV. Sarpkaya, T. Mechanics of Wave Forces on Offshore Structures. *Journal of Applied Mechanics*, 1982.

[25] ANSYS Inc. ANSYS AQWA brochure.

[26] Trelleborg Offshore. *Bend protection in dynamic environments.* Trelleborg, 2015.

[27] Collu M. Borg, M. Offshore floating vertical axis wind turbines, dynamics modelling state of the art. Part III: Hydrodynamics and coupled modelling approaches . *Renewable and Sustainable Energy Reviews*, 2014.

[28] International Marine Contractors Association (IMCA). IMCA: Guidelines for The Design and Operation of Dynamically Positioned Vessels, 2007.

[29] Det Norske Veritas (DNV). DNV-RP-H103: Modelling and Analysis of Marine Operations, 2011.

APPENDIX A

Properties FOWT

A.1 Technical drawings

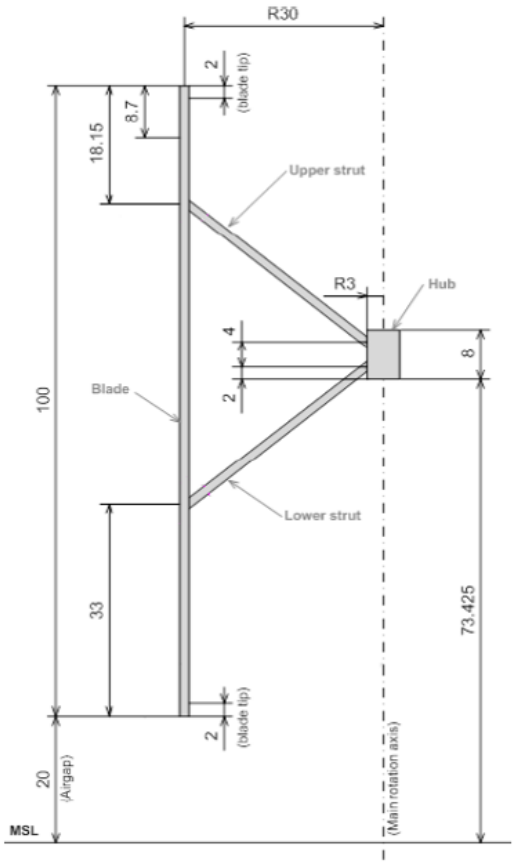

Figure A.1: Technical drawing VAWT [13]

APPENDIX B

Properties Ndurance

B.1 Technical drawings

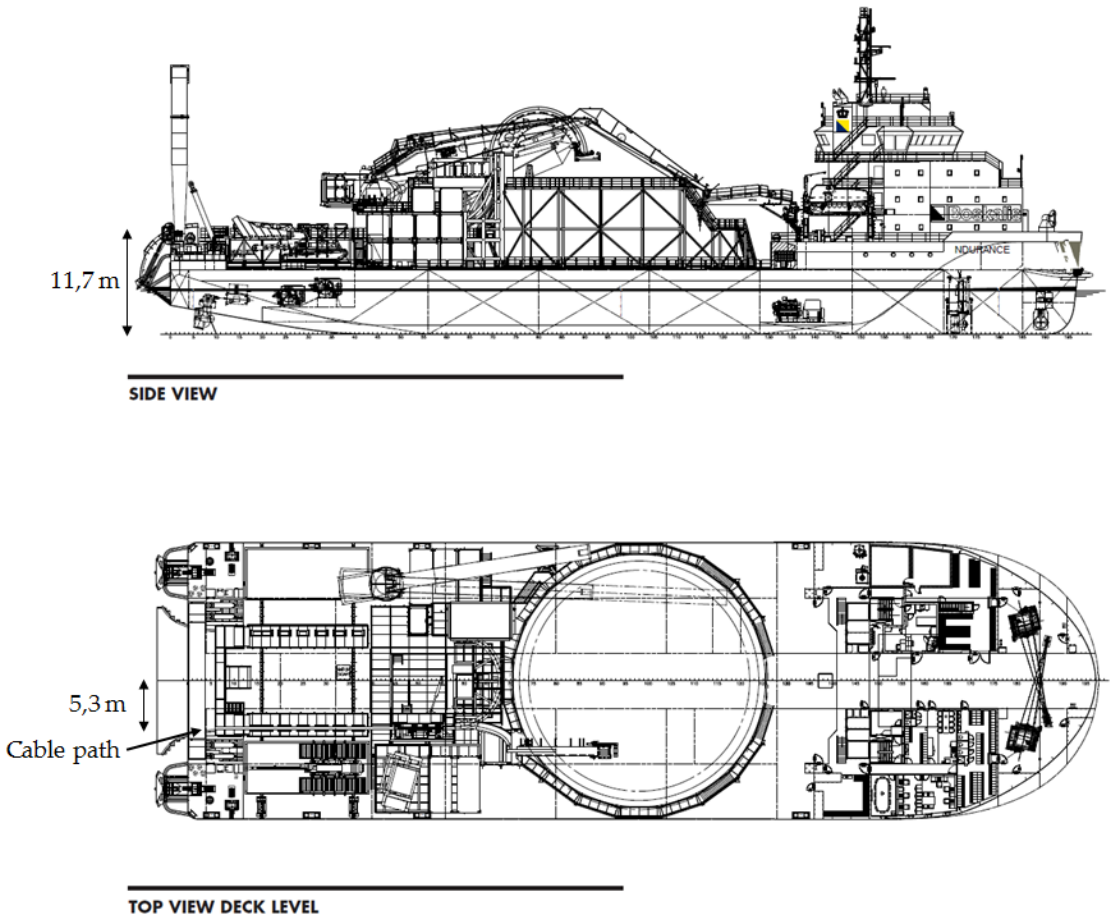

Figure B.1: Ndurance [16]

APPENDIX C

Mooring system investigation

A mooring system is required to keep the FOWT on the right spot during operation. Several options such as a DP system, mooring buoy or mooring lines can provide this mooring solution. A DP system is to expensive for the purpose of thirty years service for a FOWT. So the most common solution is to equip the FOWT with mooring lines. A good design of the mooring lines consist of several parameters of influence. This design is time consuming and out of the scope of this research. Nevertheless a first estimate of the motion behaviour of the FOWT in its mooring system is investigate. The RAOs of the FOWT model can be imported in OrcaFlex as load RAOs or as displacement RAOs, both described in Section 2.4.4. The use of displacement RAOs during numerical analysis of the FOWT are preferred based on the following benefits:

- The model is faster with displacement RAOs because it determines at every time step excursions and rotations of the FOWT, based on the harmonic motion behaviour, with a fixed equilibrium position. Load RAOs calculate at every time step the equilibrium of the hydrodynamic loads and all other forces and loads acting on the FOWT, which is time consuming.

- The use of load RAOs requisite a real design of a mooring system to maintain the position of the FOWT. The introduction of mooring lines in the model increases the risk of line clashes and increases complexity of the simulations.

For this reason a investigation is performed if the use of displacement RAOs instead of load RAOs is possible without introducing errors

C.1 Different mooring set-ups

Four different mooring set-ups are investigated to find the influence of displacement RAOs related to load RAOs. Table **??** presents the different mooring systems which are investigated. Determination of minimum mooring line length (L_{min}) for mooring system No. 1 is based on

No.	Line type	Amount	L_{min}	Diameter	W_{sub}	MBL	Axial stiffness stiffness	Pre-tensions
[–]	[–]	[–]	$[m]$	$[mm]$	$[kN/m]$	$[kN]$	$[MN]$	$[kN]$
1.	Blue Strand	6	1350	48	0.085	1610	107	[50,100-500;100]
2.	Studless Chain	3	750	50	0.424	2740	213	[100-700;100]
3.	Studless Chain	6	750	50	0.424	2740	213	[100-700;100]
4.	Studless Chain	6	450	100	1.696	9864	854	[250,300-700;100]

Table C.1: Mooring systems

Equation C.1, according to DNV standard [17] where h is the waterdepth and W_{sub} is submerged weight in seawater of the mooring line. A waterdepth of 100 m is used in the model.

$$L_{min} = \sqrt{\frac{MBL \cdot h}{W_{sub}}} \tag{C.1}$$

Determination of required length of mooring system No. 2-4 is based on DNV standard [17] to have at least $200m$ chain on the ground in highest tensioned situation.
Figure C.1 presents the mooring system No. 1 modelled in OrcaFlex. The design of the mooring system is symmetric with used mooring line length as calculated in Equation C.1.

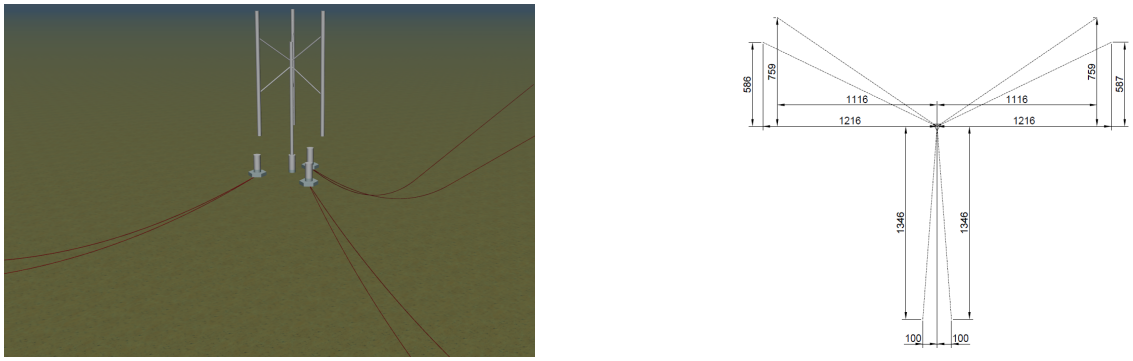

(a) 3D view mooring set-up in OrcaFlex

(b) Top view mooring system

Figure C.1: Modelling mooring system in OrcaFlex

C.1.1 Mooring system characteristics

The characteristics of a mooring system are determined by the properties of the mooring system as described in Section **??**.

Figure C.2 present the simplified schematising of the mooring system, where m is the mass of the FOWT and k the stiffness of the mooring lines. A winch is modelled to generate the force F_w to create a offset u_{FOWT} of the FOWT. This winch pulls the FOWT out of its equilibrium and hold it at a certain offset u_{FOWT} until the force is constant. The springs in Figure C.2 represent the mooring lines, which is a simplification. The lines in the model are modelled based on the OrcaFlex line model, described in Section Line Theory (under construction).
The stiffness of the mooring system k_{ms} can be calculated with the results from the analysis using Equation C.2.

$$k_{ms} = \frac{F_w}{u_{FOWT}} \tag{C.2}$$

Figure C.3 presents the relation between offset and tension on one mooring line with a pre-tension of 10 kN. Figure C.3a clarifies that this relation is non-linear after an offset of approximately 30 meters. So if the offset is lower than 30 meters the relation is assumed to be linear.

The stiffness of the total mooring system is needed to determine the natural frequency of the mooring system. The mooring system is simplified as a mass-spring system, described in Section **??**. Derivation of the natural frequency ω_n is performed in that section and is presented in Equation C.3, where m_{FOWT} the mass of the FOWT is.

$$\omega_n = \sqrt{k_{ms}/m_{FOWT}} \tag{C.3}$$

The stiffness of the mooring system is influenced by the amount of pre-tension of the mooring line. The pre-tension determines the behaviour of the FOWT during operation and is controllable.

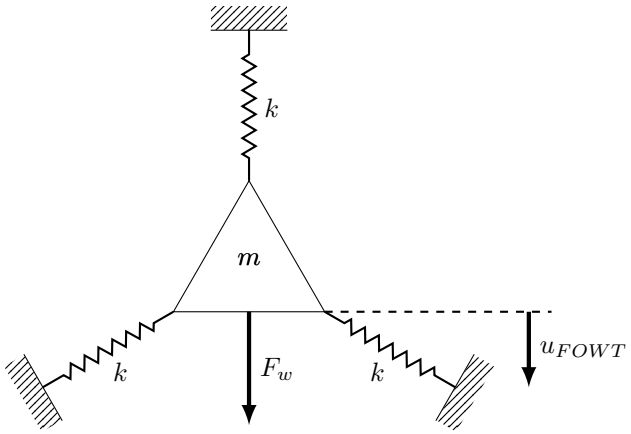

Figure C.2: Schematising mooring system

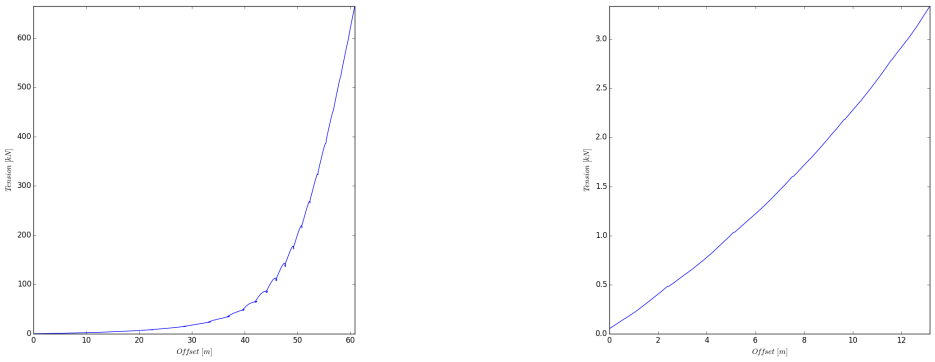

(a) Mooring line tension VS offset

(b) Zoom of linear part

Figure C.3: Tension in one mooring line

A irregular wave approach as described in Section 2.1.2 is used to investigate the behaviour of the different mooring systems in environmental conditions.

C.1.2 Results of the mooring analyses

Results of the mooring investigation are presented in this section.

C.1.3 Load RAOs VS displacement RAOs

First results are related to the investigation of the difference in using load RAOs with a mooring system modelled and displacement RAOs.. It is necessary to remind that second order wave drift forces are only present when load RAOs are used.

Figure C.4 presents the comparison between both types of RAOs for mooring system No. 1 with 50 kN pre-tension in environmental conditions as described in Section **??**. It is clearly visible that the load RAOs include an additional oscillation with a period of approximately 60 seconds. These oscillations are a results of the introduction of second order wave drift forces as described in Section **??**. The oscillations are only present in the non-symmetric motions of the FOWT Surge, Sway and Yaw, respectively, which is in agreement with the theory described in Section 2.4.
A comparison is made for all the mooring systems investigated in this research. Figure C.5 summarises the differences in motions behaviour of load and displacement RAOs. This difference

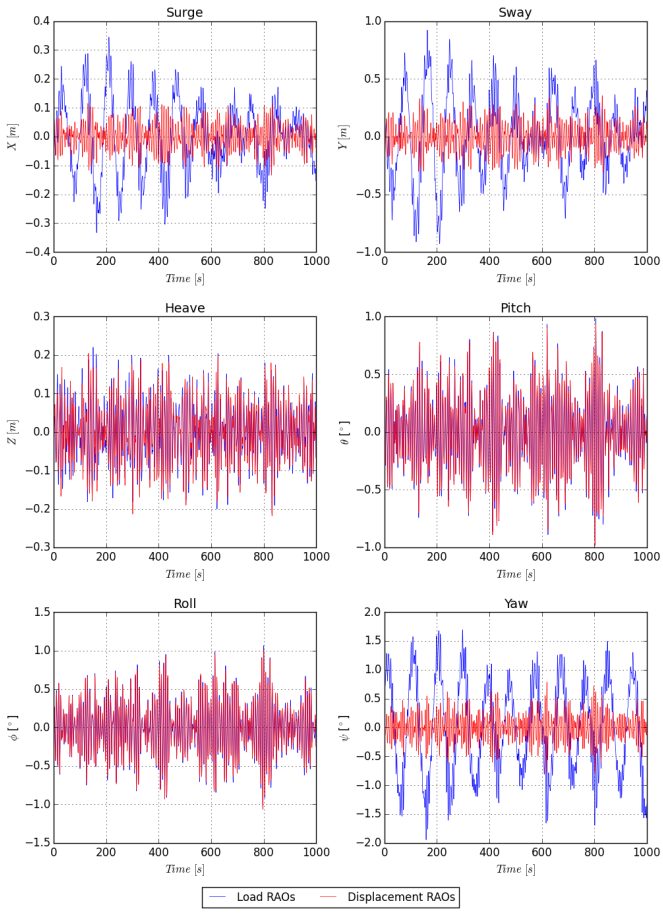

Figure C.4: Comparison load RAOs VS displacement RAOs for mooring system No. 1 with 50 kN pre-tension

is determined with calculation of the moments of the area directly form the time series response and defined as:

$$Difference = \frac{ResponsewithloadRAOs - ResponsewithdisplacementRAOs}{ResponsewithdisplacementRAOs} \tag{C.4}$$

The significant wave amplitude for both load and displacement RAO of every motion direction is calculated and the difference is plotted in Figure C.5. This Figure shows that the difference for the harmonic motions is decreasing over increasing pre-tension. An explanation for this phenomena is given in Section C.1.3.1. This Figure also shows that the difference for the non-symmetric motions is increasing. An explanation for this phenomena is that higher pre-tension results in higher reaction force in the mooring lines. For example when the FOWT is pitching in one direction, the cables on the other side are given a hugh reaction force. The Figure also shows that the smallest difference between load an displacement RAOs is reached with mooring system No. 1. The other systems are probably to heavy for this FOWT.

C.1.3.1 Influence of pre-tension on the natural frequency

In order to give an explanation for the phenomena that higher pre-tension results in less second order wave drift motions, an small investigation is performed. This Section describes the results of this investigation that is performed according to the description presented in Section **??**.

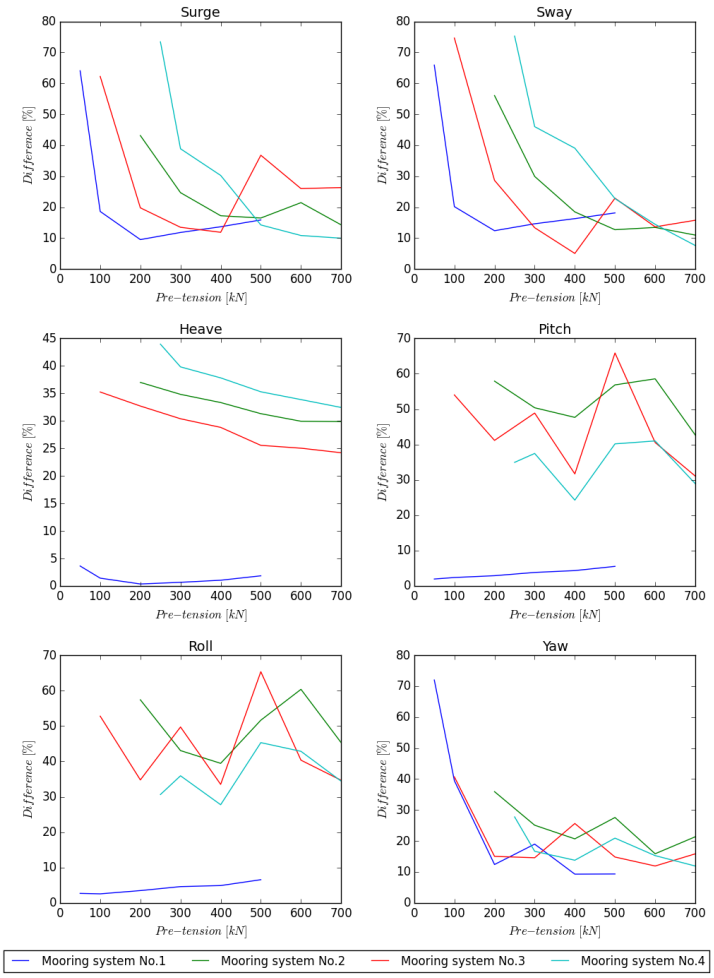

Figure C.5: Moorings stiffness comparison different systems

Figure C.6a presents the relation between the amount of pre-tension and the stiffness of the mooring system. The non-linearity of cable dynamics is visible in this figure. First of all the amount of tension as a result of excitation is non-linear for big excitations. Besides that the departure angle of the mooring lines changes if the pre-tension of the line changes. For this reason a small excitation is chosen to stay in the linear part of the catenary of mooring lines. An excitation of 1.5 meter is taken according to the maximum amplitude of the oscillations presented in Figure C.4.

The natural frequency of the mooring system with increasing pre-tensions is calculated after determination of the mooring stiffness. Figure C.6b present the results of the natural frequency related to the pre-tension. The natural frequency increases when the pre-tension increases. The energy density spectrum of the low frequency part of the wave drift force $S_f(\mu)$ for the JONSWAP spectrum $S(\omega)$ described in Section **??** are also plotted. Increasing pre-tension results in a higher natural frequency of the mooring system.

Figure C.7 presents the results of the investigation of the mooring stiffness influenced by pre-tension of all the mooring system investigated in this research. The Figure shows that the relation is increasing for all mooring system investigated.

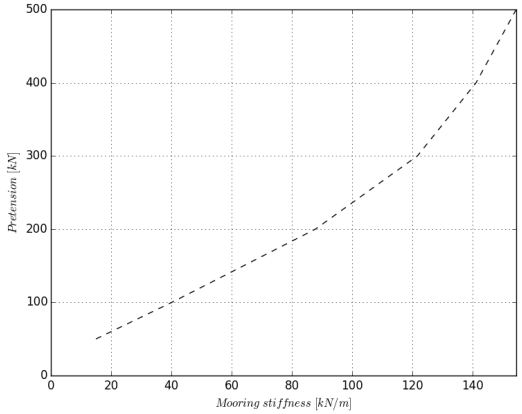

(a) Relation mooring stiffness VS pre-tension

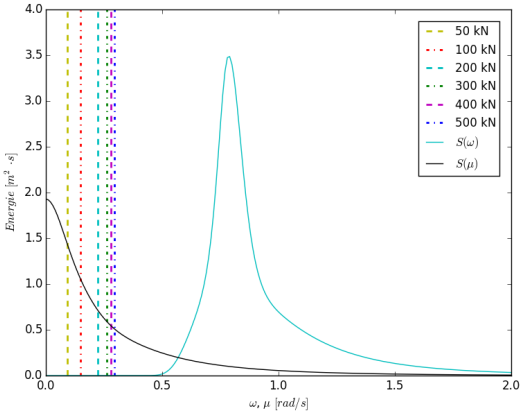

(b) Natural frequency per pre-tension

Figure C.6: Mooring system No. 1 Characteristics

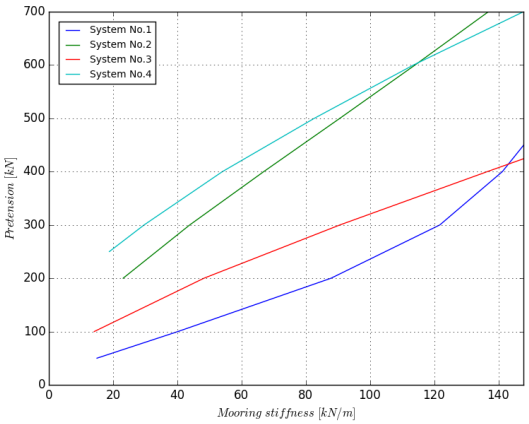

Figure C.7: Moorings stiffness comparison different systems

C.1.4 Conclusion

Figure C.4 presents that the second order wave drift forces are significant for the used sea state and low pre-tension, which is the case for all investigated mooring systems. Increasing the stiffness of the mooring system results in a shift of the mooring system natural frequency. Shifting of the natural frequency takes it to a region where the spectral density of the second order wave drift forces is lower, resulting in less second order motions. Designing of a mooring system that can operate for 30 years, which fulfils all the requirements, is time consuming and an investigation by itself. Modelling the pull-in of the power cable with an mooring system also increases the simulation time and increases the probability of modelling issues, when the design is not representative, with errors following. For these reasons the decision is made to model the FOWT during this research with displacement RAOs under the assumption that the motions of a project specific design of a mooring system of a FOWT, are equal using displacement RAOs in stead of load RAOs.

APPENDIX D

Python scripts

Confidential

APPENDIX E

Wave parameters

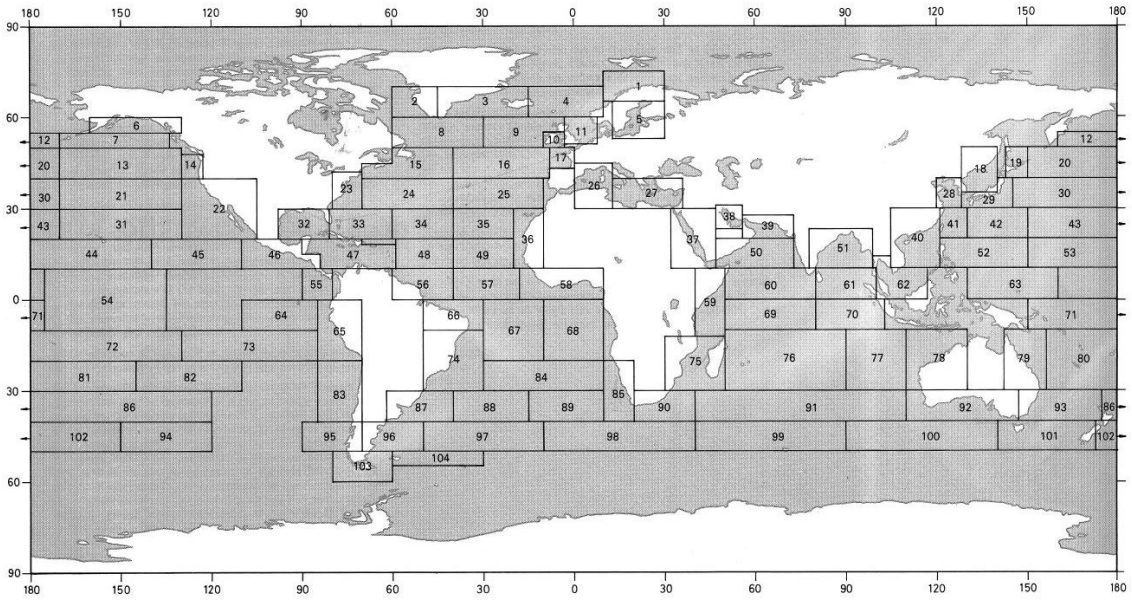

Figure E.1: Definition of nautical zones for estimation of long term wave distribution parameters [17]

	T_z $[s]$																	
H_s $[m]$	**1.5**	**2.0**	**2.5**	**3.0**	**3.5**	**4.0**	**4.5**	**5.0**	**5.5**	**6.0**	**6.5**	**7.0**	**7.5**	**8.0**	**8.5**	**9.0**	**Total**	**%**
0.25	16	292	**1238**	**2362**	**2804**	**2466**	**1777**	**1119**	**641**	**344**	176	87	42	20	10	4	13399	13.4
0.5	3	103	**646**	**1674**	**2557**	**2783**	**2412**	**1785**	**1181**	**721**	**415**	229	122	64	33	17	14742	14.75
0.75	1	42	**344**	**1109**	**2022**	**2552**	**2510**	**2074**	**1512**	**1006**	**626**	**370**	211	117	63	34	14594	14.6
1.0	0	18	186	**717**	**1510**	**2148**	**2338**	**2109**	**1660**	**1182**	**781**	**488**	292	169	95	53	13745	13.7
1.25	0	8	101	**457**	**1091**	**1721**	**2044**	**1986**	**1668**	**1258**	**874**	**571**	**356**	214	125	71	12546	12.5
1.5	0	4	55	288	**771**	**1334**	**1713**	**1779**	**1583**	**1254**	**911**	**619**	**400**	248	149	88	11197	11.2
2.0	0	1	16	111	**366**	**749**	**1105**	**1290**	**1269**	**1098**	**861**	**626**	**429**	281	177	109	8490	8.5
2.5	0	0	5	41	165	**392**	**657**	**852**	**917**	**856**	**718**	**554**	**400**	274	180	115	6126	6.1
3.5	0	0	0	5	29	93	196	**307**	**389**	**417**	**394**	**337**	266	197	139	94	2863	2.9
4.5	0	0	0	1	4	19	49	92	136	166	174	164	140	111	83	59	1199	1.2
5.5	0	0	0	0	1	3	11	24	41	56	66	68	63	53	42	32	460	0.5
6.0	0	0	0	0	0	1	5	12	21	31	39	42	40	35	29	22	277	0.3
6.5	0	0	0	0	0	0	2	5	11	17	22	25	25	23	19	15	164	0.2
7.0	0	0	0	0	0	0	1	2	5	9	12	14	15	14	12	10	95	0.1
7.5	0	0	0	0	0	0	0	1	3	5	7	8	9	9	8	6	55	0.1
8.0	0	0	0	0	0	0	0	0	1	2	3	5	5	5	5	4	31	0
8.5	0	0	0	0	0	0	0	0	1	1	2	2	3	3	3	2	17	0
Total	20	467	2592	6765	11321	14262	14819	13439	11038	8424	6083	4209	2818	1837	1172	735	100000	
%	0	0.5	2.6	6.8	11.3	14.3	14.8	13.4	11.0	8.4	6.1	4.2	2.8	1.8	1.2	0.7	0	

Table E.1: Wave scatter area 26

APPENDIX F

Result tables

F.1 Free lay

	$H_{max} = 0.93[m]$			$H_{max} = 1.86[m]$			$H_{max} = 2.79[m]$		
Dir/T_s	$3.92[s]$	$5.23[s]$	$6.54[s]$	$4.58[s]$	$5.88[s]$	$7.19[s]$	$5.23[s]$	$6.54[s]$	$7.85[s]$
0°	50.8	51.9	60.6	57.9	63.0	73.8	65.3	76.9	70.8
30°	48.7	57.4	61.0	53.3	64.4	68.0	68.5	84.4	71.2
60°	48.1	56.0	49.2	54.3	55.1	53.9	62.6	57.3	65.8
90°	47.9	48.2	53.9	59.5	52.2	52.5	59.2	54.1	57.2
120°	48.2	48.9	50.9	50.0	55.9	53.7	61.9	61.0	59.4
150°	48.2	52.3	60.5	49.8	61.4	69.1	66.8	82.3	77.5
180°	52.6	51.1	52.8	55.9	55.9	70.3	60.8	62.2	73.6
210°	48.3	51.6	54.2	50.1	63.5	57.6	59.6	73.5	63.3
240°	48.8	57.1	51.3	53.7	61.7	60.9	63.1	68.2	65.8
270°	49.6	52.2	57.3	53.6	63.5	55.8	63.3	62.1	65.5
300°	49.2	52.0	56.9	54.1	59.5	64.4	70.5	74.3	68.1
330°	48.5	53.7	57.4	62.5	70.1	70.7	66.9	84.1	72.7

Table F.1: Maximum cable tension free lay $[kN]$

	$H_{max} = 0.93[m]$			$H_{max} = 1.86[m]$			$H_{max} = 2.79[m]$		
Dir/T_s	$3.92[s]$	$5.23[s]$	$6.54[s]$	$4.58[s]$	$5.88[s]$	$7.19[s]$	$5.23[s]$	$6.54[s]$	$7.85[s]$
0°	No	No	No	No	No	No	No	No	No
30°	No	No	No	No	No	No	No	No	No
60°	No	No	No	No	No	No	No	No	No
90°	No	No	No	No	No	No	No	No	No
120°	No	No	No	No	No	No	No	No	No
150°	No	No	No	No	No	No	No	No	No
180°	No	No	No	No	No	No	No	No	No
210°	No	No	No	No	No	No	No	No	No
240°	No	No	No	No	No	No	No	No	No
270°	No	No	No	No	No	No	No	No	No
300°	No	No	No	No	No	No	No	No	No
330°	No	No	No	No	No	No	No	No	No

Table F.2: Structure interaction free lay [–]

F.2 Direct pull-in method

	$H_{max} = 0.93[m]$			$H_{max} = 1.86[m]$			$H_{max} = 2.79[m]$		
Dir/T_s	$3.92[s]$	$5.23[s]$	$6.54[s]$	$4.58[s]$	$5.88[s]$	$7.19[s]$	$5.23[s]$	$6.54[s]$	$7.85[s]$
0°	39.3	39.0	38.8	39.9	39.6	39.4	40.8	40.1	39.9
30°	39.1	39.5	45.3	40.6	50.3	39.3	49.5	51.7	46.5
60°	38.6	38.5	38.7	40.7	52.1	47.9	53.2	53.5	49.6
90°	38.8	40.3	50.4	52.9	49.9	52.1	63.8	54.4	47.6
120°	38.7	38.4	48.0	51.2	51.8	53.3	59.1	52.8	50.2
150°	39.0	39.5	38.9	40.9	49.7	52.1	55.0	51.3	48.7
180°	39.4	39.0	38.9	39.9	52.0	39.4	45.9	49.6	39.8
210°	39.4	39.1	39.0	40.2	39.7	39.6	43.0	40.3	40.2
240°	39.3	39.3	39.1	40.3	49.3	39.9	41.2	41.0	40.4
270°	39.2	39.4	39.1	40.0	40.0	40.8	43.0	40.5	40.5
300°	39.3	39.3	38.9	40.1	49.2	39.7	46.7	40.1	40.5
330°	39.3	39.2	39.0	40.3	40.0	39.8	42.6	40.5	40.2

Table F.3: Maximum cable tension pull-in method 1 [kN]

	$H_{max} = 0.93[m]$			$H_{max} = 1.86[m]$			$H_{max} = 2.79[m]$		
Dir/T_s	$3.92[s]$	$5.23[s]$	$6.54[s]$	$4.58[s]$	$5.88[s]$	$7.19[s]$	$5.23[s]$	$6.54[s]$	$7.85[s]$
0°	0.19	0.19	0.19	0.19	0.19	0.19	0.23	0.19	0.19
30°	0.19	0.19	0.19	0.20	0.19	0.19	0.22	0.19	0.19
60°	0.19	0.19	0.19	0.21	0.19	0.19	0.23	0.23	0.20
90°	0.19	0.19	0.19	0.21	0.19	0.20	0.21	0.23	0.21
120°	0.19	0.19	0.19	0.20	0.19	0.19	0.21	0.23	0.22
150°	0.19	0.19	0.19	0.21	0.19	0.19	0.21	0.19	0.20
180°	0.19	0.19	0.19	0.19	0.19	0.19	0.22	0.19	0.19
210°	0.19	0.20	0.20	0.21	0.20	0.20	0.22	0.20	0.20
240°	0.20	0.20	0.20	0.21	0.20	0.20	0.22	0.20	0.20
270°	0.20	0.20	0.20	0.21	0.20	0.20	0.22	0.20	0.20
300°	0.20	0.20	0.20	0.21	0.20	0.20	0.22	0.20	0.20
330°	0.19	0.19	0.19	0.21	0.20	0.20	0.23	0.20	0.20

Table F.4: Maximum curvature pull-in method 1 $[m^{-1}]$

	$H_{max} = 0.93[m]$			$H_{max} = 1.86[m]$			$H_{max} = 2.79[m]$		
Dir/T_s	$3.92[s]$	$5.23[s]$	$6.54[s]$	$4.58[s]$	$5.88[s]$	$7.19[s]$	$5.23[s]$	$6.54[s]$	$7.85[s]$
0°	79.9	76.9	78.9	81.6	84.5	78.3	84.6	83.8	80.4
30°	80.2	83.9	77.0	82.2	79.5	83.9	89.6	82.8	86.3
60°	79.8	77.5	76.8	82.0	84.4	81.7	83.6	91.4	85.5
90°	80.0	81.1	80.6	80.8	82.0	82.1	90.0	95.6	85.0
120°	80.3	76.7	79.1	81.4	82.9	83.5	83.0	81.6	84.0
150°	75.6	74.4	75.7	77.2	74.3	84.6	76.2	82.3	86.7
180°	76.5	75.5	78.4	77.5	81.8	83.7	88.7	83.0	81.9
210°	78.1	85.1	84.2	85.7	93.7	79.0	100.8	83.1	92.9
240°	87.3	76.2	83.3	81.1	86.2	74.8	87.0	107.5	89.5
270°	87.6	88.2	86.6	90.0	86.2	89.0	111.3	118.2	89.7
300°	78.7	75.7	79.8	80.6	91.8	82.6	89.8	92.0	90.2
330°	78.2	76.2	76.1	76.3	75.8	78.1	76.9	76.7	81.3

Table F.5: Maximum pull-in tension pull-in method 1 $[kN]$

	$H_{max} = 0.93[m]$			$H_{max} = 1.86[m]$			$H_{max} = 2.79[m]$		
Dir/T_s	$3.92[s]$	$5.23[s]$	$6.54[s]$	$4.58[s]$	$5.88[s]$	$7.19[s]$	$5.23[s]$	$6.54[s]$	$7.85[s]$
0°	35.6	33.5	34.3	35.7	37.9	34.6	39.3	40.6	34.3
30°	37.3	36.2	32.8	38.3	33.4	36.2	53.2	35.2	37.4
60°	38.5	32.8	33.2	40.2	39.7	35.2	39.2	38.4	37.4
90°	37.2	34.3	34.4	36.0	43.7	36.4	44.4	45.5	36.8
120°	35.7	33.5	34.9	35.3	38.0	37.2	37.3	44.5	36.6
150°	33.6	32.7	33.5	32.6	33.4	38.2	32.4	37.6	40.5
180°	33.7	33.1	35.1	34.0	37.4	38.1	37.3	44.5	37.6
210°	35.2	34.4	34.2	35.3	38.0	35.8	40.2	34.5	40.5
240°	37.9	33.7	33.9	39.0	35.8	33.5	35.3	39.0	38.3
270°	37.6	37.4	35.1	38.6	35.3	37.3	54.3	44.4	37.6
300°	36.1	32.9	35.2	35.0	39.6	37.3	38.6	46.3	39.2
330°	33.9	33.2	32.7	33.1	32.6	35.1	32.1	34.2	35.8

Table F.6: Maximum pay-out tension pull-in method 1 $[kN]$

	$H_{max} = 0.93[m]$			$H_{max} = 1.86[m]$			$H_{max} = 2.79[m]$		
Dir/T_s	$3.92[s]$	$5.23[s]$	$6.54[s]$	$4.58[s]$	$5.88[s]$	$7.19[s]$	$5.23[s]$	$6.54[s]$	$7.85[s]$
0°	8.0	8.1	8.1	8.0	8.0	8.1	8.0	8.1	8.1
30°	7.9	7.9	8.0	7.8	7.9	7.9	7.8	7.8	7.9
60°	7.8	7.8	7.9	7.7	7.7	7.8	7.6	7.6	7.7
90°	7.9	7.9	7.9	7.7	7.7	7.8	7.5	7.6	7.7
120°	8.0	8.0	8.0	7.9	7.9	7.9	7.7	7.8	7.8
150°	8.1	8.1	8.1	8.0	8.1	8.1	7.9	8.0	8.0
180°	8.2	8.2	8.2	8.2	8.2	8.2	8.2	8.2	8.2
210°	8.3	8.3	8.3	8.4	8.4	8.4	8.4	8.4	8.4
240°	8.4	8.4	8.4	8.5	8.5	8.5	8.6	8.5	8.6
270°	8.4	8.4	8.4	8.5	8.5	8.4	8.6	8.5	8.6
300°	8.3	8.3	8.3	8.4	8.4	8.3	8.5	8.4	8.4
330°	8.2	8.2	8.2	8.2	8.2	8.2	8.3	8.3	8.3

Table F.7: Maximum bottom tension pull-in method 1 $[kN]$

	$H_{max} = 0.93[m]$			$H_{max} = 1.86[m]$			$H_{max} = 2.79[m]$		
Dir/T_s	$3.92[s]$	$5.23[s]$	$6.54[s]$	$4.58[s]$	$5.88[s]$	$7.19[s]$	$5.23[s]$	$6.54[s]$	$7.85[s]$
0°	3.1	3.0	2.8	3.5	3.5	3.2	4.4	3.9	3.8
30°	3.4	3.0	2.6	4.0	3.5	2.8	4.9	3.6	3.4
60°	2.5	2.4	2.0	3.0	2.6	2.0	3.5	2.5	2.5
90°	1.4	1.3	1.2	1.1	1.1	1.0	1.0	0.9	0.8
120°	0.5	0.5	0.6	0.1	0.1	0.3	0.0	0.0	0.2
150°	0.0	0.0	0.2	0.0	0.0	0.0	0.0	0.0	0.0
180°	0.1	0.1	0.2	0.0	0.0	0.0	0.0	0.0	0.0
210°	0.3	0.3	0.4	0.0	0.0	0.1	0.0	0.0	0.0
240°	0.7	0.7	0.8	0.5	0.5	0.6	0.2	0.4	0.5
270°	1.4	1.3	1.3	1.4	1.4	1.4	1.4	1.5	1.4
300°	2.1	2.0	1.9	2.6	2.3	2.2	2.8	2.5	2.6
330°	3.0	2.7	2.6	4.0	3.1	3.3	4.3	3.9	3.8

Table F.8: Maximum offset pull-in method 1 $[m]$

	$H_{max} = 0.93[m]$			$H_{max} = 1.86[m]$			$H_{max} = 2.79[m]$		
Dir/T_s	$3.92[s]$	$5.23[s]$	$6.54[s]$	$4.58[s]$	$5.88[s]$	$7.19[s]$	$5.23[s]$	$6.54[s]$	$7.85[s]$
0°	No	No	No	No	No	No	No	No	No
30°	No	No	No	No	No	No	No	No	No
60°	No	No	No	No	No	No	No	No	No
90°	No	No	No	No	No	No	No	No	No
120°	No	No	No	No	No	No	No	No	No
150°	No	No	No	No	No	No	No	No	No
180°	No	No	No	No	No	No	No	No	No
210°	No	No	No	No	No	No	No	No	No
240°	No	No	No	No	No	No	No	No	No
270°	No	No	No	No	No	No	No	No	No
300°	No	No	No	No	No	No	No	No	No
330°	No	No	No	No	No	No	No	No	No

Table F.9: Structure interaction pull-in method 1 $[-]$

	$H_{max} = 0.93[m]$			$H_{max} = 1.86[m]$			$H_{max} = 2.79[m]$		
Dir/T_s	$3.92[s]$	$5.23[s]$	$6.54[s]$	$4.58[s]$	$5.88[s]$	$7.19[s]$	$5.23[s]$	$6.54[s]$	$7.85[s]$
0°	Yes	Yes	Yes	Yes	Yes	Yes	Yes	Yes	Yes
30°	Yes	Yes	Yes	Yes	Yes	Yes	Yes	Yes	Yes
60°	Yes	Yes	Yes	Yes	Yes	Yes	Yes	Yes	Yes
90°	Yes	Yes	Yes	Yes	Yes	Yes	Yes	Yes	Yes
120°	Yes	Yes	Yes	Yes	Yes	Yes	Yes	Yes	Yes
150°	Yes	Yes	Yes	Yes	Yes	Yes	Yes	Yes	Yes
180°	Yes	Yes	Yes	Yes	Yes	Yes	Yes	Yes	Yes
210°	Yes	Yes	Yes	Yes	Yes	Yes	Yes	Yes	Yes
240°	Yes	Yes	Yes	Yes	Yes	Yes	Yes	Yes	Yes
270°	Yes	Yes	Yes	Yes	Yes	Yes	Yes	Yes	Yes
300°	Yes	Yes	Yes	Yes	Yes	Yes	Yes	Yes	Yes
330°	Yes	Yes	Yes	Yes	Yes	Yes	Yes	Yes	Yes

Table F.10: 10 m seabed clearance ensured in pull-in method 1 [–]

F.3 Post-lay pull-in

	$H_{max} = 0.93[m]$			$H_{max} = 1.86[m]$			$H_{max} = 2.79[m]$		
Dir/T_s	$3.92[s]$	$5.23[s]$	$6.54[s]$	$4.58[s]$	$5.88[s]$	$7.19[s]$	$5.23[s]$	$6.54[s]$	$7.85[s]$
0°	48.3	46.6	46.6	46.9	45.2	45.6	46.5	47.6	43.9
30°	47.4	46.7	46.7	47.1	45.9	44.3	47.0	49.8	44.9
60°	46.5	46.7	46.2	45.9	43.9	46.5	45.5	47.0	45.6
90°	40.7	46.2	47.0	46.0	44.5	46.9	49.1	46.4	45.0
120°	44.9	47.1	46.9	46.9	45.7	44.7	46.7	43.2	42.4
150°	42.7	47.9	47.5	46.9	45.0	44.9	46.8	46.9	43.5
180°	43.3	47.2	48.3	47.0	46.7	46.2	45.5	46.8	44.7
210°	43.7	46.8	46.9	47.8	46.1	45.5	46.2	47.8	44.5
240°	46.4	46.0	46.4	47.1	45.7	45.1	47.7	45.9	61.5
270°	47.1	45.6	47.5	47.8	45.4	47.3	49.0	45.6	45.9
300°	43.9	46.2	47.0	47.1	45.5	45.4	45.5	45.0	44.1
330°	47.6	46.3	46.9	48.0	45.6	45.9	46.5	45.3	45.0

Table F.11: Maximum cable tension pull-in method 2 [kN]

	$H_{max} = 0.93[m]$			$H_{max} = 1.86[m]$			$H_{max} = 2.79[m]$		
Dir/T_s	$3.92[s]$	$5.23[s]$	$6.54[s]$	$4.58[s]$	$5.88[s]$	$7.19[s]$	$5.23[s]$	$6.54[s]$	$7.85[s]$
0°	0.18	0.18	0.18	0.18	0.18	0.18	0.18	0.18	0.18
30°	0.18	0.18	0.18	0.18	0.18	0.18	0.18	0.18	0.18
60°	0.18	0.18	0.18	0.18	0.18	0.18	0.18	0.18	0.19
90°	0.18	0.18	0.18	0.18	0.18	0.18	0.18	0.19	0.18
120°	0.18	0.18	0.18	0.18	0.18	0.18	0.18	0.18	0.18
150°	0.18	0.18	0.18	0.18	0.18	0.18	0.18	0.18	0.18
180°	0.18	0.18	0.18	0.18	0.18	0.18	0.18	0.18	0.18
210°	0.18	0.18	0.18	0.18	0.18	0.18	0.18	0.18	0.18
240°	0.18	0.18	0.18	0.18	0.18	0.18	0.18	0.18	0.18
270°	0.18	0.18	0.18	0.18	0.18	0.18	0.18	0.18	0.18
300°	0.18	0.18	0.18	0.18	0.18	0.18	0.18	0.18	0.18
330°	0.18	0.18	0.18	0.18	0.18	0.18	0.18	0.18	0.18

Table F.12: Maximum curvature pull-in method 2 $[m^{-1}]$

	$H_{max} = 0.93[m]$			$H_{max} = 1.86[m]$			$H_{max} = 2.79[m]$		
Dir/T_s	$3.92[s]$	$5.23[s]$	$6.54[s]$	$4.58[s]$	$5.88[s]$	$7.19[s]$	$5.23[s]$	$6.54[s]$	$7.85[s]$
0°	100.3	98.4	96.1	98.1	96.1	91.1	100.6	101.6	95.0
30°	100.7	101.3	98.7	97.1	94.2	91.4	90.6	80.7	97.8
60°	100.6	96.7	97.2	101.6	102.7	99.3	101.9	104.2	92.4
90°	97.7	99.8	97.6	98.0	90.2	100.7	88.7	88.0	97.4
120°	96.9	95.9	95.7	98.0	98.0	99.0	97.4	93.4	91.5
150°	95.9	98.3	96.4	97.6	92.9	93.9	86.3	94.8	91.6
180°	94.8	95.6	95.0	97.6	96.7	95.2	98.2	96.2	93.7
210°	95.8	98.3	96.2	98.7	99.1	88.6	83.0	81.1	92.2
240°	94.8	96.7	94.9	96.5	92.6	92.6	85.8	91.3	87.1
270°	94.3	98.3	97.4	97.0	96.5	97.3	83.7	94.8	100.4
300°	98.9	96.7	95.4	100.8	99.0	96.2	100.6	98.0	94.2
330°	101.7	98.3	101.3	100.2	91.5	102.9	97.3	85.5	102.0

Table F.13: Maximum pull-in tension pull-in method 2 $[kN]$

	$H_{max} = 0.93[m]$			$H_{max} = 1.86[m]$			$H_{max} = 2.79[m]$		
Dir/T_s	$3.92[s]$	$5.23[s]$	$6.54[s]$	$4.58[s]$	$5.88[s]$	$7.19[s]$	$5.23[s]$	$6.54[s]$	$7.85[s]$
0°	60.0	58.4	58.3	61.7	54.6	52.5	56.5	56.2	55.5
30°	58.1	60.2	52.5	60.9	54.6	55.4	54.8	59.5	57.1
60°	60.6	59.6	59.9	61.4	55.1	52.7	55.9	56.0	55.3
90°	59.0	59.9	59.2	58.3	54.9	55.4	56.5	56.9	53.9
120°	57.9	59.2	59.9	59.1	59.3	53.9	60.0	54.4	54.0
150°	59.1	59.5	58.7	60.9	54.0	56.8	51.3	57.1	52.5
180°	57.1	59.2	59.6	59.5	57.9	57.0	60.2	60.1	52.8
210°	57.6	59.8	58.6	58.6	58.4	52.9	59.5	55.8	53.7
240°	57.5	58.1	58.4	58.2	55.5	52.1	58.4	57.3	61.9
270°	56.7	59.3	57.0	57.4	55.3	57.7	58.8	53.2	51.3
300°	58.2	57.5	58.4	59.0	53.7	53.5	58.1	57.1	53.3
330°	58.9	58.8	59.0	58.4	53.9	52.4	56.1	53.5	54.4

Table F.14: Maximum pay-out tension pull-in method 2 $[kN]$

	$H_{max} = 0.93[m]$			$H_{max} = 1.86[m]$			$H_{max} = 2.79[m]$		
Dir/T_s	$3.92[s]$	$5.23[s]$	$6.54[s]$	$4.58[s]$	$5.88[s]$	$7.19[s]$	$5.23[s]$	$6.54[s]$	$7.85[s]$
0°	3.8	3.8	3.9	3.9	4.0	3.9	4.0	4.2	4.3
30°	3.8	3.8	3.9	3.8	4.0	4.1	4.0	4.2	4.2
60°	3.7	3.7	3.8	3.7	4.0	4.1	3.9	4.1	4.2
90°	3.7	3.7	4.0	3.7	3.6	4.1	3.8	3.8	4.1
120°	3.7	3.7	3.8	3.7	3.8	4.1	3.7	3.8	3.9
150°	3.8	3.8	3.8	3.8	3.7	3.7	3.6	3.8	3.9
180°	3.8	3.8	3.8	3.8	3.9	3.9	3.9	3.9	4.2
210°	3.9	3.9	4.0	3.9	4.0	4.2	3.9	4.4	4.5
240°	3.9	4.0	4.2	4.0	4.3	4.3	4.3	4.5	4.6
270°	3.9	4.0	4.0	4.0	4.3	4.1	4.4	4.1	4.4
300°	3.9	3.9	4.0	3.9	4.1	4.2	4.0	4.5	4.1
330°	3.8	3.9	3.9	3.9	4.1	4.1	4.2	3.9	4.4

Table F.15: Maximum bottom tension pull-in method 2 $[kN]$

	$H_{max} = 0.93[m]$			$H_{max} = 1.86[m]$			$H_{max} = 2.79[m]$		
Dir/T_s	$3.92[s]$	$5.23[s]$	$6.54[s]$	$4.58[s]$	$5.88[s]$	$7.19[s]$	$5.23[s]$	$6.54[s]$	$7.85[s]$
0°	17.7	17.8	18.1	17.9	17.9	17.9	18.0	17.8	17.8
30°	17.9	17.9	17.9	17.9	18.2	18.1	18.2	17.5	18.0
60°	17.8	18.0	18.4	17.9	18.0	17.8	18.0	18.0	17.5
90°	17.8	18.0	17.8	17.6	18.2	18.1	18.4	17.9	17.3
120°	17.8	17.7	17.7	17.9	17.8	18.3	17.8	17.9	18.3
150°	17.6	17.9	17.7	17.9	17.9	17.8	18.1	17.8	17.8
180°	17.7	17.7	17.7	17.9	17.9	17.8	17.8	17.8	18.0
210°	18.0	17.9	17.9	18.2	18.1	17.8	18.2	18.0	17.7
240°	17.9	17.9	17.9	18.0	17.8	17.6	17.8	17.8	19.3
270°	17.7	17.8	17.7	17.8	18.0	18.1	18.1	18.1	17.9
300°	17.8	17.8	17.8	18.1	17.7	17.8	17.8	17.9	17.8
330°	17.6	17.9	17.9	17.9	18.1	17.8	18.2	18.2	17.9

Table F.16: Maximum tether tension pull-in method 2 $[kN]$

	$H_{max} = 0.93[m]$			$H_{max} = 1.86[m]$			$H_{max} = 2.79[m]$		
Dir/T_s	$3.92[s]$	$5.23[s]$	$6.54[s]$	$4.58[s]$	$5.88[s]$	$7.19[s]$	$5.23[s]$	$6.54[s]$	$7.85[s]$
0°	0.0	0.0	0.0	0.0	0.0	0.0	0.0	0.0	0.0
30°	0.0	0.0	0.0	0.0	0.0	0.0	0.0	0.0	0.0
60°	0.0	0.0	0.0	0.0	0.0	0.0	0.0	0.0	0.0
90°	0.0	0.0	0.0	0.0	0.0	0.0	0.0	0.0	0.0
120°	0.0	0.0	0.0	0.0	0.0	0.0	0.0	0.0	0.0
150°	0.0	0.0	0.0	0.0	0.0	0.0	0.0	0.0	0.0
180°	0.0	0.0	0.0	0.0	0.0	0.0	0.0	0.0	0.0
210°	0.0	0.0	0.0	0.0	0.0	0.0	0.0	0.0	0.0
240°	0.0	0.0	0.0	0.0	0.0	0.0	0.0	0.0	0.0
270°	0.0	0.0	0.0	0.0	0.0	0.0	0.0	0.0	0.0
300°	0.0	0.0	0.0	0.0	0.0	0.0	0.0	0.0	0.0
330°	0.0	0.0	0.0	0.0	0.0	0.0	0.0	0.0	0.0

Table F.17: Maximum offset pull-in method 2 $[m]$

	$H_{max} = 0.93[m]$			$H_{max} = 1.86[m]$			$H_{max} = 2.79[m]$		
Dir/T_s	$3.92[s]$	$5.23[s]$	$6.54[s]$	$4.58[s]$	$5.88[s]$	$7.19[s]$	$5.23[s]$	$6.54[s]$	$7.85[s]$
0°	No	No	No	No	No	No	No	No	No
30°	No	No	No	No	No	No	No	No	No
60°	No	No	No	No	No	No	No	No	No
90°	No	No	No	No	No	No	No	No	No
120°	No	No	No	No	No	No	No	No	No
150°	No	No	No	No	No	No	No	No	No
180°	No	No	No	No	No	No	No	No	No
210°	No	No	No	No	No	No	No	No	No
240°	No	No	No	No	No	No	No	No	No
270°	No	No	No	No	No	No	No	No	No
300°	No	No	No	No	No	No	No	No	No
330°	No	No	No	No	No	No	No	No	No

Table F.18: Structure interaction pull-in method 2 [–]

F.4 Pull-in via FOWT

	$H_{max} = 0.93[m]$			$H_{max} = 1.86[m]$			$H_{max} = 2.79[m]$		
Dir/T_s	$3.92[s]$	$5.23[s]$	$6.54[s]$	$4.58[s]$	$5.88[s]$	$7.19[s]$	$5.23[s]$	$6.54[s]$	$7.85[s]$
0°	40.4	40.3	40.4	41.0	40.5	40.4	40.4	40.4	40.4
30°	40.1	40.3	40.3	41.3	41.7	40.2	43.9	41.9	40.9
60°	40.9	40.1	40.2	41.7	40.9	40.2	40.3	40.8	40.1
90°	40.3	41.4	40.1	40.1	42.2	40.1	46.3	42.1	40.1
120°	41.0	39.9	39.9	41.6	40.5	39.9	40.3	40.9	40.0
150°	40.0	40.3	39.9	41.2	42.3	40.1	44.1	43.5	40.5
180°	40.1	40.0	39.9	41.2	40.8	40.0	40.0	40.3	40.0
210°	40.2	40.5	40.2	40.2	40.6	40.2	44.4	41.1	40.3
240°	40.1	40.1	40.1	40.7	40.1	40.1	40.2	40.1	40.0
270°	40.4	40.4	40.4	40.5	40.5	40.5	40.7	41.4	40.4
300°	40.0	40.2	40.0	40.6	40.0	40.3	40.5	40.1	40.2
330°	40.3	40.4	40.3	40.2	40.5	40.2	44.6	41.5	40.3

Table F.19: Maximum cable tension pull-in method 3 [kN]

	$H_{max} = 0.93[m]$			$H_{max} = 1.86[m]$			$H_{max} = 2.79[m]$		
Dir/T_s	$3.92[s]$	$5.23[s]$	$6.54[s]$	$4.58[s]$	$5.88[s]$	$7.19[s]$	$5.23[s]$	$6.54[s]$	$7.85[s]$
0°	0.17	0.16	0.16	0.17	0.17	0.16	0.17	0.17	0.17
30°	0.17	0.17	0.17	0.18	0.17	0.17	0.19	0.18	0.17
60°	0.17	0.16	0.16	0.17	0.17	0.16	0.17	0.17	0.17
90°	0.17	0.17	0.17	0.17	0.17	0.17	0.19	0.17	0.17
120°	0.17	0.16	0.16	0.17	0.17	0.16	0.17	0.17	0.17
150°	0.16	0.17	0.16	0.17	0.17	0.16	0.18	0.17	0.16
180°	0.16	0.16	0.16	0.17	0.16	0.16	0.16	0.16	0.16
210°	0.16	0.16	0.16	0.16	0.17	0.16	0.18	0.17	0.16
240°	0.16	0.16	0.16	0.16	0.16	0.16	0.16	0.16	0.16
270°	0.16	0.16	0.16	0.16	0.17	0.16	0.17	0.17	0.16
300°	0.16	0.16	0.16	0.17	0.16	0.16	0.17	0.16	0.16
330°	0.16	0.17	0.16	0.17	0.17	0.16	0.19	0.17	0.17

Table F.20: Maximum curvature pull-in method 3 $[m^{-1}]$

	$H_{max} = 0.93[m]$			$H_{max} = 1.86[m]$			$H_{max} = 2.79[m]$		
Dir/T_s	$3.92[s]$	$5.23[s]$	$6.54[s]$	$4.58[s]$	$5.88[s]$	$7.19[s]$	$5.23[s]$	$6.54[s]$	$7.85[s]$
0°	50.3	49.7	50.0	51.1	51.0	49.6	49.7	50.8	50.0
30°	50.5	50.6	50.5	52.5	52.2	51.0	55.2	52.8	50.8
60°	51.1	49.7	50.0	52.1	51.6	49.8	50.4	51.1	49.8
90°	51.0	52.5	50.6	50.7	53.1	50.9	58.2	52.7	51.0
120°	51.1	49.4	50.1	52.0	51.4	49.8	50.5	51.2	49.8
150°	50.5	50.6	50.5	52.3	52.3	50.9	55.2	52.7	50.8
180°	50.2	49.6	49.9	51.2	51.0	49.6	49.7	50.6	50.0
210°	50.3	51.6	50.4	50.0	51.9	50.0	55.2	52.4	50.8
240°	49.7	49.4	49.8	51.2	50.4	49.6	49.6	50.0	50.1
270°	49.9	49.8	50.5	50.9	51.4	50.1	52.4	52.1	49.8
300°	49.8	49.5	49.8	51.2	50.3	49.6	49.6	50.0	50.1
330°	50.3	51.5	50.5	50.0	51.8	50.1	55.1	52.2	50.8

Table F.21: Maximum pull-in tension pull-in method 3 $[kN]$

	$H_{max} = 0.93[m]$			$H_{max} = 1.86[m]$			$H_{max} = 2.79[m]$		
Dir/T_s	$3.92[s]$	$5.23[s]$	$6.54[s]$	$4.58[s]$	$5.88[s]$	$7.19[s]$	$5.23[s]$	$6.54[s]$	$7.85[s]$
0°	1.9	1.9	1.9	1.9	1.9	1.9	1.9	1.9	1.9
30°	1.9	1.9	1.9	1.9	1.9	1.9	1.9	1.9	1.9
60°	1.9	1.9	1.9	1.9	1.9	1.9	1.9	1.9	1.9
90°	1.9	1.9	1.9	1.9	1.9	1.9	1.9	1.9	1.9
120°	1.9	1.9	1.9	1.9	1.9	1.9	1.9	1.9	1.9
150°	1.9	1.9	1.9	1.9	1.9	1.9	1.9	1.9	1.9
180°	2.0	2.0	2.0	2.0	2.0	2.0	2.0	2.0	2.0
210°	1.9	2.0	2.0	2.0	2.0	2.0	2.0	2.0	2.0
240°	2.0	2.0	2.0	2.0	2.0	2.0	2.0	2.0	2.0
270°	2.0	2.0	2.0	2.0	2.0	2.0	2.0	2.0	2.0
300°	2.0	2.0	2.0	2.0	2.0	2.0	2.0	2.0	2.0
330°	2.0	2.0	2.0	2.0	2.0	2.0	2.0	2.0	2.0

Table F.22: Maximum bottom tension pull-in method 3T $[kN]$

	$H_{max} = 0.93[m]$			$H_{max} = 1.86[m]$			$H_{max} = 2.79[m]$		
Dir/T_s	$3.92[s]$	$5.23[s]$	$6.54[s]$	$4.58[s]$	$5.88[s]$	$7.19[s]$	$5.23[s]$	$6.54[s]$	$7.85[s]$
0°	27.2	26.8	27.1	27.1	27.9	27.5	28.0	28.9	27.7
30°	27.6	28.4	27.7	28.6	30.3	27.6	33.3	30.3	27.5
60°	28.5	27.7	27.8	29.5	29.5	28.1	30.0	30.0	29.2
90°	28.1	30.7	29.5	30.5	33.4	30.2	38.4	34.1	31.3
120°	28.5	27.6	27.9	29.5	29.3	28.2	29.8	30.1	29.1
150°	27.6	28.4	27.7	28.7	30.5	27.7	33.3	30.4	27.5
180°	27.0	26.8	27.0	27.2	27.8	27.6	28.0	28.9	27.6
210°	26.0	25.8	26.0	26.8	25.7	26.1	26.4	26.1	26.2
240°	26.0	25.9	26.3	25.6	26.6	26.9	26.6	27.9	27.5
270°	26.3	26.1	26.1	25.2	26.4	26.6	27.4	27.2	27.2
300°	26.0	25.8	26.4	25.6	26.6	26.9	26.6	28.0	27.4
330°	26.1	25.9	26.0	26.9	25.8	26.1	26.4	26.0	26.4

Table F.23: Maximum bend moment CPS pull-in method 3 $[kNm]$

	$H_{max} = 0.93[m]$			$H_{max} = 1.86[m]$			$H_{max} = 2.79[m]$		
Dir/T_s	$3.92[s]$	$5.23[s]$	$6.54[s]$	$4.58[s]$	$5.88[s]$	$7.19[s]$	$5.23[s]$	$6.54[s]$	$7.85[s]$
0°	18.1	18.0	18.1	18.3	18.1	18.1	18.1	18.1	18.2
30°	18.1	18.2	18.0	18.2	18.2	18.2	18.5	18.1	18.3
60°	18.2	18.1	18.1	18.2	18.2	18.1	18.2	18.1	18.2
90°	18.1	18.3	18.1	18.0	18.4	18.1	18.6	18.1	18.2
120°	18.1	18.0	18.0	18.2	18.2	18.1	18.3	18.1	18.2
150°	18.0	18.1	18.0	18.1	18.3	18.1	18.5	18.1	18.2
180°	18.0	18.0	18.0	18.3	18.1	18.1	18.1	18.1	18.1
210°	18.0	18.1	18.1	18.1	18.2	18.1	18.4	18.1	18.1
240°	18.0	18.1	18.1	18.3	18.2	18.0	18.2	18.2	18.1
270°	18.1	18.0	18.1	18.2	18.3	18.2	18.2	18.3	18.1
300°	18.0	18.0	18.1	18.3	18.1	18.0	18.2	18.2	18.0
330°	18.0	18.1	18.1	18.2	18.1	18.0	18.4	18.2	18.2

Table F.24: Maximum tether tension post-lay pull-in method 3 $[kN]$

	$H_{max} = 0.93[m]$			$H_{max} = 1.86[m]$			$H_{max} = 2.79[m]$		
Dir/T_s	$3.92[s]$	$5.23[s]$	$6.54[s]$	$4.58[s]$	$5.88[s]$	$7.19[s]$	$5.23[s]$	$6.54[s]$	$7.85[s]$
0°	0.0	0.0	0.0	0.0	0.0	0.0	0.0	0.0	0.0
30°	0.0	0.0	0.0	0.0	0.0	0.0	0.0	0.0	0.0
60°	0.0	0.0	0.0	0.0	0.0	0.0	0.0	0.0	0.0
90°	0.0	0.0	0.0	0.0	0.0	0.0	0.0	0.0	0.0
120°	0.0	0.0	0.0	0.0	0.0	0.0	0.0	0.0	0.0
150°	0.0	0.0	0.0	0.0	0.0	0.0	0.0	0.0	0.0
180°	0.0	0.0	0.0	0.0	0.0	0.0	0.0	0.0	0.0
210°	0.0	0.0	0.0	0.0	0.0	0.0	0.0	0.0	0.0
240°	0.0	0.0	0.0	0.0	0.0	0.0	0.0	0.0	0.0
270°	0.0	0.0	0.0	0.0	0.0	0.0	0.0	0.0	0.0
300°	0.0	0.0	0.0	0.0	0.0	0.0	0.0	0.0	0.0
330°	0.0	0.0	0.0	0.0	0.0	0.0	0.0	0.0	0.0

Table F.25: Maximum offset pull-in method 3 $[m]$

	$H_{max} = 0.93[m]$			$H_{max} = 1.86[m]$			$H_{max} = 2.79[m]$		
Dir/T_s	$3.92[s]$	$5.23[s]$	$6.54[s]$	$4.58[s]$	$5.88[s]$	$7.19[s]$	$5.23[s]$	$6.54[s]$	$7.85[s]$
0°	No	No	No	No	No	No	No	No	No
30°	No	No	No	No	No	No	No	No	No
60°	No	No	No	No	No	No	No	No	No
90°	No	No	No	No	No	No	No	No	No
120°	No	No	No	No	No	No	No	No	No
150°	No	No	No	No	No	No	No	No	No
180°	No	No	No	No	No	No	No	No	No
210°	No	No	No	No	No	No	No	No	No
240°	No	No	No	No	No	No	No	No	No
270°	No	No	No	No	No	No	No	No	No
300°	No	No	No	No	No	No	No	No	No
330°	No	No	No	No	No	No	No	No	No

Table F.26: Structure interaction pull-in method 3 [–]